Optimization of an antibody microarray platform for exosome proteomics

Rosalie Martel

Program of Biological & Biomedical Engineering

McGill University, Montreal

August 2018

A thesis submitted to McGill University in partial fulfillment of the requirements of the degree of Master of Engineering

Table of Contents

List of Figures

List of Tables

Abstract

Extracellular vesicles (EVs) are a heterogeneous ensemble of membrane bodies released by all cell types into their environment. Initially dismissed as cell debris, they have since been shown to play a central role in intercellular communication. Specifically, the proteins expressed at the surface of exosomes —EVs sized between 30 and 100 nm—have been identified as biomolecular zip codes and biomarkers. Exosome protein expression and cargo have been probed using various technologies—from mass spectrometry to integrated microfluidic chips—and shown to be linked to the pathogenesis and progression of several conditions, from cancer to neurodegenerative diseases. Antibody microarrays are a powerful and high-throughput technology that has been adapted to multiplexed EV protein expression analysis. However, the microarray platform and its protocol need to be characterized and optimized specially for exosome protein analysis to ensure data quality and reliability. In this work, we optimized an antibody microarray to capture exosomes and probe the membrane protein content of cancer-cell derived exosomes with high intensity and reproducibility. We separately optimized the (i) capture and (ii) detection of exosomes from CD63-GFP-expressing A431 epidermoid carcinoma cells, and combined them into an optimal exosome capture and detection microarray protocol. Microarrays of IgGs targeting exosome protein markers were inkjet-spotted using 29 different printing buffers and successively incubated with exosomes and detection antibodies. Different combinations of capture and detection antibodies targeting surface proteins CD63, CD9, CD81 and EGFR were tested and the fluorescence intensity and coefficient of variation of the intrinsic GFP and detection antibody compared based on the printing buffer used and the proteins targeted. Using the optimized assay protocol, 4 different cancer cell lines were profiled for 15 targets, including exosome marker CD63; integrins αVβ5, α2, α6, β1, and β4; receptors EGFR, CCR5, and PD-1; and transmembrane proteins ADAM10, EpCAM, PD-L1, CD44, CD82 and CD133. Our proposed antibody microarray platform, termed ExAM (**Ex**osome **A**ntibody **M**icroarray), which we showed can phenotype vesicles with strong signal intensity and high reproducibility, may be useful in analyzing exosomes in the context of disease diagnosis and treatment.

Résumé

Les vésicules extracellulaires (EV) constituent un ensemble hétérogène de corps membraneux relâchés dans l'espace extracellulaire par toutes les cellules, peu importe leur type. Initialement considérés comme de simples débris, ils se sont depuis avérés jouer un rôle important dans la communication intercellulaire. Plus précisément, les protéines présentes à la surface des exosomes – une sous-catégorie d'EV dont la taille est comprise entre 30 et 100 nm – sont considérées comme des biomarqueurs ou codes postaux biomoléculaires. L'expression protéique et le contenu en biomolécules des exosomes ont été sondés au moyen de technologies variées — de la spectrométrie de masse aux puces microfluidiques intégrées — et des liens avec la pathogenèse et la progression de plusieurs conditions, du cancer aux maladies neurodégénératives, ont été établis. Les biopuces d'anticorps représentent une puissante technologie à haut criblage pouvant effectuer l'analyse multiplexée de la cargaison protéique des EV. Cependant, pour assurer la qualité et la fiabilité des données, la micropuce et le protocole régissant son utilisation doivent être caractérisés et optimisés spécialement pour l'analyse des protéines exosomales. Nous avons donc optimisé une biopuce d'anticorps pour capturer des exosomes issus de cellules cancéreuses et sonder les protéines que contient leur membrane, et ce, de manière claire et reproductible. Nous avons séparément optimisé (i) la capture et (ii) la détection d'exosomes provenant de cellules de carcinome épidermoïde (type A431, modifiées pour exprimer la protéine de fusion CD63-GFP), puis les avons combinés pour obtenir un protocole de micropuce optimisé pour la capture et la détection d'exosomes. Des micropuces d'IgG ciblant les marqueurs protéiques à la surface des exosomes ont été produites à l'aide d'une bioimprimante à jet d'encre et de vingt-neuf solutions d'impression différentes. Les biopuces résultantes ont ensuite été successivement incubées avec des échantillons d'exosomes et différents anticorps de détection. Différentes combinaisons d'anticorps de capture et de détection ciblant les protéines de surface CD63, CD9, CD81 et EGFR ont été testées et comparées sur la base de l'intensité et du coefficient de variation des signaux fluorescents dus au GFP intrinsèque et aux fluorophores utilisés pour la détection, en fonction de la solution d'impression utilisée et des protéines ciblées par les anticorps. La puce optimisée a ensuite été validée via l'analyse ciblée de quatre lignées cellulaires cancéreuses pour détecter 15 protéines, incluant le marqueur exosomal CD63; les intégrines αVβ5, α2, α6, β1, et β4; les récepteurs EGFR, CCR5, et PD-1; et les protéines transmembranaires ADAM10, EpCAM, PD-L1, CD44, CD82 et CD133. Notre plateforme d'analyse, capable de détecter des cibles protéiques de manière claire et reproductible, pourrait être utile pour analyser des exosomes de différentes sources, contribuant au développement de nouvelles modalités de diagnostic et de traitement.

Acknowledgements

First and foremost, I would like to thank my supervisor, Prof. David Juncker, for the guidance and invaluable feedback he provided throughout my degree, which largely contributed to make this research a success. I also wish to acknowledge Frédéric Normandeau for providing antibody microarray foundations on which to build the ExAM platform, as well as for our many fruitful discussions about experiments, data analysis, thesis writing, and graduate student life; Philippe DeCorwin-Martin for sharing his theoretical and empirical knowledge of EVs when I first started, for his continuing help and input, and for reading and commenting the literature review section of the present thesis; Dr. Grace Oh for her suggestions, precious advice, and moral support; Dr. Andy Ng for answering many of my questions; and everyone at Juncker Lab for providing continuous feedback and moral support, and for making the last two years unforgettable.

I also would like to thank our collaborators from the Rak Lab at McGill University, and more specifically Prof. Janusz Rak and Laura Montermini, for providing the A431-GFP cell line used in this research, and for teaching us how to purify exosomes from cell supernatant using size-exclusion chromatography. Furthermore, their knowledge of exosome biology and advice was instrumental in troubleshooting the platform and the assay protocol to shape them into what they are today.

Finally, I wish to acknowledge financial support from the Biomedical Engineering Department at McGill University though the Recruitment Award, from NSERC through the CSGM Award, and from FRQNT through the Master's Research Scholarship.

1. Project Description

1.1 Motivation

Extracellular vesicles, and especially exosomes, are increasingly studied for their role in intercellular communication, and consequently in health and disease. Exosome proteins, notably, have been shown to play a role in cancer metastasis formation[1] and to have potential cancer diagnosis implications[2,3]. They have also been catalogued and analyzed in a growing number of exosome phenotyping studies, some of which were performed using antibody microarrays[4-6]. Antibody microarray platforms have important advantages for targeted exosome protein analysis, including small sample requirements, high throughput and high sensitivity[4,7]. The motivation for this work is to understand how different aspects of antibody microarray fabrication and experimental handling affect exosome proteomics results, and to leverage that knowledge to build an optimized antibody microarray platform for exosome protein analysis. The resulting platform could be instrumental to the identification of new exosome biomarkers useful in clinical applications.

1.2 Project Goals

The overall goal of this project was to optimize and test an antibody microarray platform for the capture and detection of cancer cell exosomes with high precision and reproducibility. More specifically, the two aims were (i) the optimization of exosome capture and detection on inkjet-printed microarrays and (ii) the validation of the optimized platform through the assessment of the protein content of exosomes from different cancer cell lines.

1.3 Contribution of Authors

For the present thesis, Rosalie Martel performed almost all of the experimental work and data analysis. The procedure followed for the optimization of the antibody printing buffer, including the algorithm used for the spatial randomization of the antibody spots, was adapted for exosome analysis from previous antibody microarray work by Frédéric Normandeau. The validation exosome phenotyping experiment was designed, performed and analyzed in collaboration with Philippe DeCorwin-Martin. Prof. Janusz Rak provided the A431-GFP cells used in the reported experiments. Prof. David Juncker supervised this project and provided continued guidance throughout its development. The thesis and accompanying figures were prepared by Rosalie Martel and edited with the help of Prof. David Juncker.

1.4 Declaration of Novelty

To the best of our knowledge, this work represents the first detailed characterization of how the fabrication of an antibody microarray platform and the particularities of its accompanying assay protocol impact data quality and reliability in the context of exosome proteomics. We also believe this study to be the first to compare exosomes from MDA-MB-231 (metastatic adenocarcinoma), A431 (epidermoid carcinoma), SK-BR-3 (metastatic adenocarcinoma), and BT-474 (ductal carcinoma) cells for the 15 proteins included in the panel.

2. Introduction

Extracellular vesicles (EVs) is an umbrella term referring to various types of membrane-shed vesicles released by cells in the extracellular environment[8]. Despite their existence being known for decades and their presence being regularly witnessed in micrographs[9], EVs were typically dismissed as cell debris—products of necrosis[9] or vehicles used by cells to rid themselves of unneeded membrane proteins[8,10]. As such, they did not attract widespread scientific interest until recently, when it became increasingly clear that these vesicles were integral components of intercellular communication[11,12], thus fulfilling many complex physiological and pathological functions.

2.1 Extracellular Vesicles (EVs): a Heterogeneous Mixture of Biologically Potent Vehicles

Increased research efforts in the last decade highlighted that cells release membrane bodies of different sizes and biomolecular compositions, both to maintain homoeostasis and react to changes[8]. Consequently, EVs are highly heterogeneous in nature, and can be divided in subtypes that either reflect their biogenesis, their function, or the tissue from which they are released[13]. For instance, while the terms *exosomes* and *ectosomes* refer to the subcellular site of origin of the vesicles (the late endosome and the plasma membrane [PM], respectively), oncosomes are large EVs that carry biological material involved in the development of malignancy[14], and prostasomes are vesicles secreted by the prostate epithelium[15]. Since definitions of EV subtypes often overlap, we will focus on the three most conventionally used categories, based on the underlying biogenetic processes: apoptotic bodies (apoptosis), microvesicles/ectosomes (membrane blebbing) and exosomes (modified endocytosis)[14]. Table 1 presents a summary of the main distinctive physical, biomolecular and physiological characteristics of each EV subtype, as discussed in the next sections.

EV SUBTYPE	SIZE	DENSITY	BIOGENETIC PROCESS	COMMON MARKERS	EXAMPLES OF PHYSIOLOGICAL OR PATHOLOGICAL PROCESSES
APOPTOTIC BODIES	50 nm – 5 μm[16-18]	1.16 – 1.28 g/mL[7,17]	Apoptosis[14]	PtdSer[16], annexin V[17,19], phosphatidyl serine[17,19]	Inflammation[16], autoimmune diseases[16], atherosclerosis[20]
MICROVESICLES	50 – 1000 nm[17]	1.04 – 1.07 g/mL[17]	Plasma membrane blebbing[14]	No recognized markers; integrins, selectins, flotillin-2, CD40, metalloproteinase can help identification[17,21]	Coagulation[22,23], tumour progression[9,13,22,24],
EXOSOMES	30 – 100 nm[25,26]	1.13 – 1.19 g/mL[25,26]	Modified endocytosis[14]	CD63, CD9, CD81, TSG101, alix, flo-tillin[17]	Immune synapse[27], tumour progression[28-30], pre-metastatic niche formation[1,31], neurodegenerative diseases[32,33]

Table 1 Key characteristics of the three main EV subtypes

2.1.1 Apoptotic Bodies

Also called apoptosomes, apoptotic bodies (ABs) are specialized vesicles that are exclusively released by cells undergoing programmed cell death, or apoptosis[18]. They are generally the largest out of the three main categories of EVs[16,18], but their wide size range of 50 nm to 5 μm[16-18] overlaps with that of other EVs, namely microvesicles (50–1000 nm[8,18]) and exosomes (30-100 nm[18]). ABs are formed during the first two stages of the apoptotic cell disassembly process (figure 1A), PM blebbing and protrusion formation, although they are not released until the third and last step, fragmentation[16,22]. Given their involvement with cell death, their release and clearing are tightly regulated: leakage of their contents (biomolecules, organelles and other remains of the dying cell) could have serious consequences, including inflammation and autoimmune reactions[16,22].

AB formation requires substantial membrane rearrangements, which are put into motion by caspases—cysteine proteases involved in the cascade activation of important

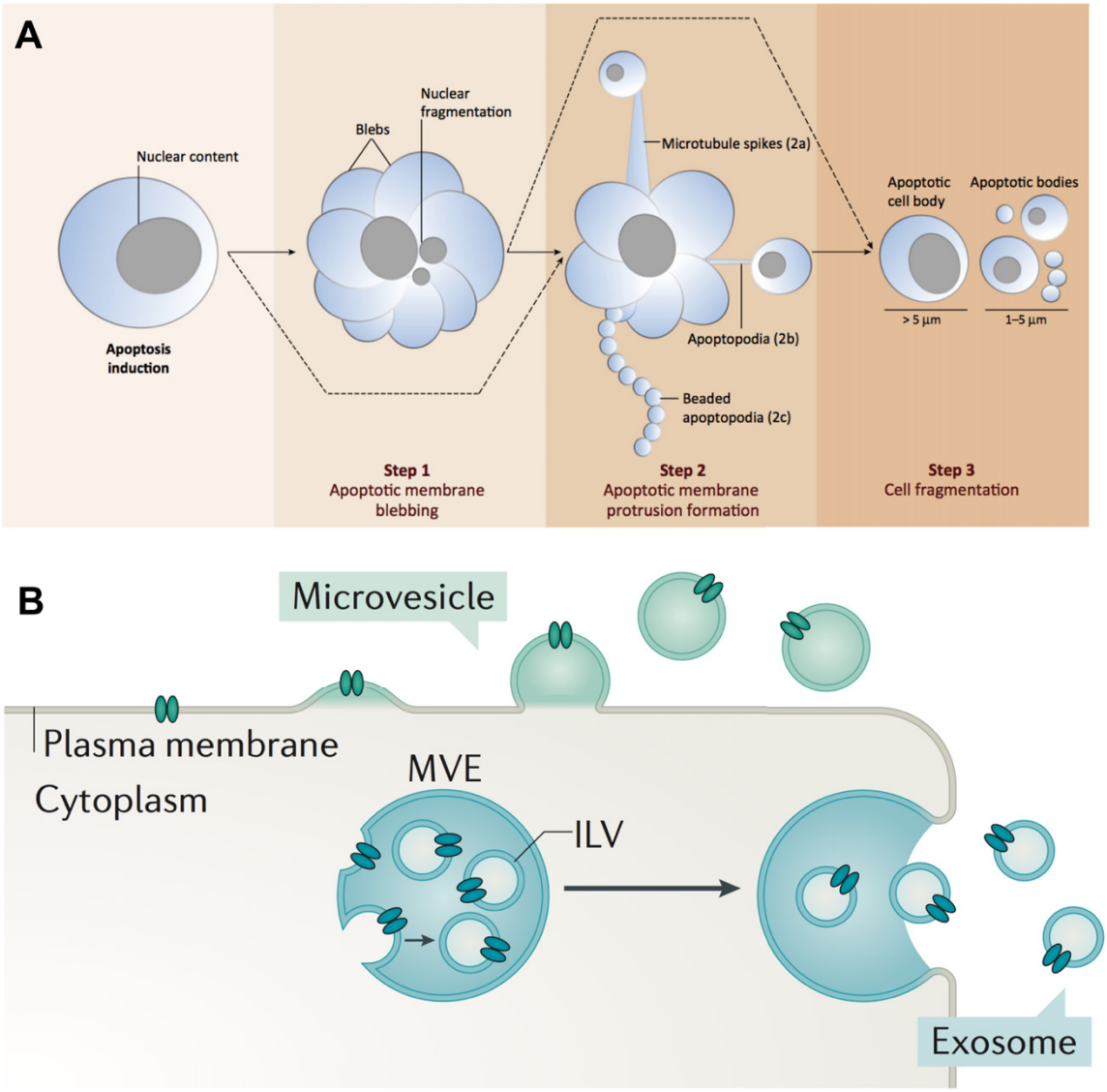

Figure 1 Origin of apoptotic bodies, microvesicles and exosomes (**A**) Morphological stages of the cell disassembly process and ensuing release of ABs[16]: *1)* cyclic PM blebbing and packing of specific contents into forming ABs, *2)* protrusion of the apoptotic membrane to form microtubule spikes, apoptopodia or beaded apoptopodia, and *3)* cell fragmentation and AB release. Of note, PM blebbing and protrusion formation can occur independently and individually, and AB generation can be a direct result of either, or both. Reused from [16], Copyright 2017, with permission from Elsevier. (**B**) Despite their resemblances, microvesicles and exosomes originate from different subcellular compartments: microvesicles bud directly from the plasma membrane, while exosomes first form as ILV by inward budding of the endosomal membrane, before being released as exosomes in the extracellular space when the resulting MVBs fuse with the PM[8]. Reused from [8], Copyright 2018, with permission from Springer Nature.

effectors and processes[22]. These membrane changes include phospholipid phosphatidylserine (PS) externalization, which contributes to bleb formation and tagging

of ABs for consumption by phagocytes and macrophages[16], but most importantly actomyosin contraction, one of the main governing forces behind PM blebbing[16,18,22]. PM blebbing (figure 1A)—the formation of bulges that swell and retract at the cell surface[16]—is cyclic in nature and said to help pack specific contents into ABs[22]. It was long credited with AB generation, but it was recently uncovered that the second stage of programmed cell death, protrusion formation, can also result in the release of ABs[16,22]. During fragmentation, ABs detach from the cell periphery and/or membrane protrusions. Mechanical influence from the extracellular environment, cell-cell interactions, and cytoskeletal rearrangements are believed to be involved[16].

The main function of the cell disassembly process and release of ABs is to ensure the safe and efficient disposal of cell contents during apoptosis[22]. This role in itself imparts them with notable significance in pathology. Indeed, perturbations of this orderly process result in inflammatory and immunological problems[16,22]. For example, inadequate apoptotic clearance has been linked to atherosclerosis, an inflammatory condition, and systemic lupus erythematosus (SLE), an autoimmune disease[16]. Recent findings, however, have brought to light an additional role category for ABs: their involvement in intercellular communication. Since ABs are membrane bodies with a diversified cargo composed of lipids, proteins and nucleic acids, they can potentially transport these biomolecules to a cell target and thus fulfill a physiological signalling role[16,18]. Examples of such behaviour are increasingly reported in the literature. For instance, in the context of atherosclerosis, ABs released by endothelial cells have been shown to be enriched in miRNA-126[20]. miRNA-126 mediates the production by vascular cells of CXCL12, a chemokine involved in apoptosis control and progenitor cell recruitment[20]. In mouse models of atherosclerosis, these miRNA-126-enriched vesicles have been shown to grant some vascular protection[20].

2.1.2 Microvesicles

Despite having been studied extensively in the last decade, microvesicles—membrane bodies sized between 50 and 1000 nm generated through outward budding of the PM[17] (figure 1B)—still lack a well-defined nomenclature. Depending on the perspective, they can also be referred to as ectosomes, shedding vesicles, shedding bodies, microparticles, or exovesicles[9,34]. Given the general nature of the following discussion, the term *microvesicle* (MV), which is gaining ground when designating PM-derived vesicles independently of the cell type of origin or specific biological context, will be used herein.

Many processes and effectors are believed to contribute to MV biogenesis, some of which might not have been uncovered yet, as it appears likely that MV secretion is function- and cell-type-dependent[9,13,22]. Nevertheless, membrane rearrangements, cytoskeleton remodeling, Ca^{2+}, and specific proteins related to membrane trafficking, budding and fission have been found to be involved[8,9,22] (figure 2). Membrane-related changes include the formation of PM microdomains in which specific lipids (cholesterol, sphingomyelin, but not phosphatidylcholine or phosphatidylethanolamine) and proteins (tetraspanins, glycosylphosphatidylinositol-anchored proteins, flotillin) are enriched[8,15,18,35]. These microdomains participate actively in the sorting of cytosolic/luminal cargo into MVs through anchoring to or affinity for proteins or lipids[8]. Ca^{2+}-dependent proteins and enzymes act in parallel to induce changes in PM phospholipids asymmetry[8]—the non-arbitrary way lipids are distributed in the membrane bilayer[36]—and control the phospholipid content of the inner and outer leaflets[8]. In the case of MV formation, these proteins and enzymes enrich PS in the outer leaflet, similarly to what happens during AB generation[8,17,22]. PS enrichment, along with the ensuing reorganization of the subjacent actin network, leads to bending of the membrane and vesicle formation[8,18,22,35]. Of note, although it is possible that PS-induced

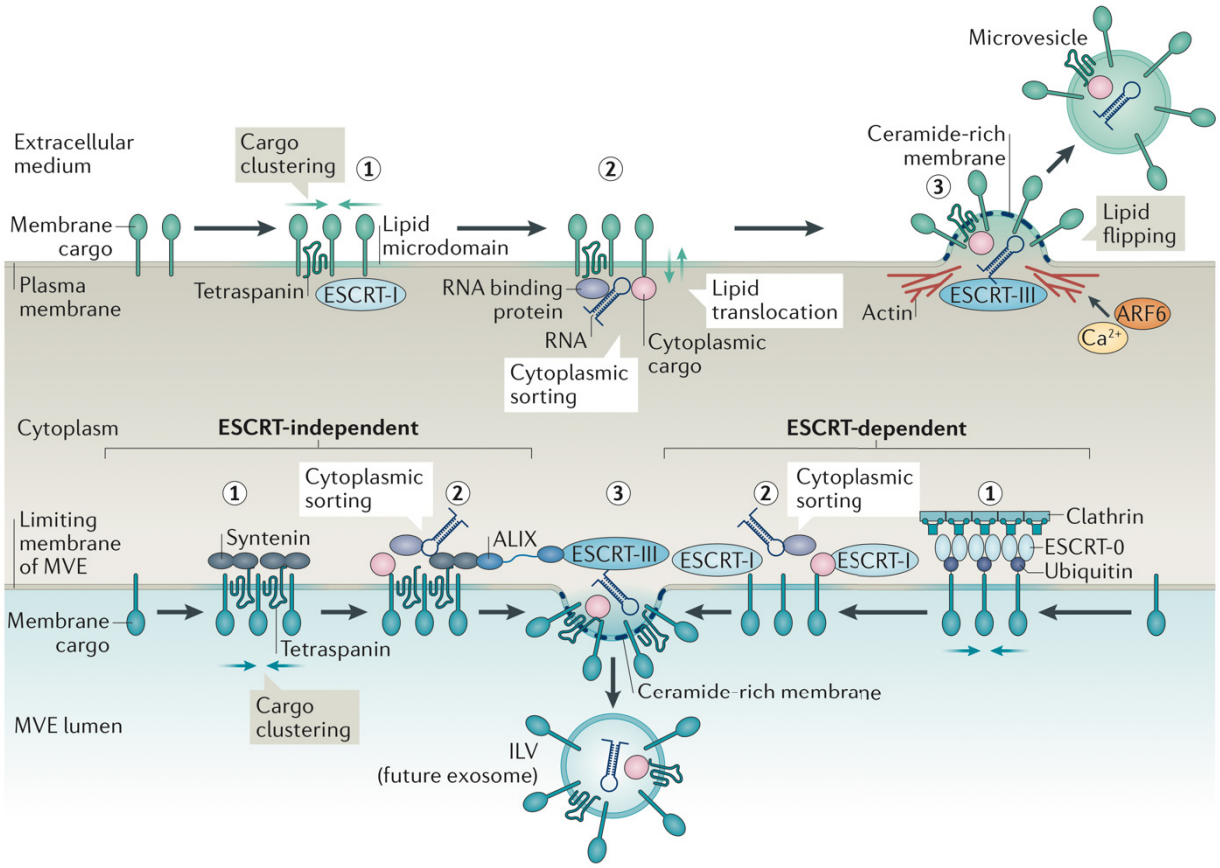

Figure 2 Comparison of microvesicle and exosome biogenesis[8]. Microvesicle (*top*) and exosome (*bottom*) formation share some effectors but occur differently. In the case of microvesicles, cargoes are clustered in membrane microdomains which also help recruit cytosolic biomolecules[8,15,18,35]; budding and scission occur through membrane rearrangements, cytoskeleton changes and the involvement of select ESCRT proteins[8,9,22]. As for exosomes, there are two main formation pathways: ESCRT-dependent and ESCRT-independent. In the former, members of the ESCRT machinery are sequentially recruited to the endosomal membrane to perform cargo sorting, membrane budding and scission[8,22]. In the latter, ceramide accumulation, affinity interactions with tetraspanins and ESCRT-III fill the same roles[8,22]. Reused from [8], Copyright 2018, with permission from Springer Nature.

membrane curvature can lead to MV budding on its own, the disruption of PM-cytoskeleton interactions is generally believed to participate in the process[18,22]. PM-cytoskeleton disruptions occur through actomyosin contraction, which is tied to activation cascades initiated by factors such as GTP-binding protein ADP-ribosylation factor 6 (ARF6)[8,18,22], and to the activity of regulators like the RHO family of small GTPases and RHO-associated protein kinase (ROCK)[8]. Beyond membrane and cytoskeleton changes, proteins related to the endosomal sorting complex required for transport (ESCRT), mainly associated with exosome biogenesis, have been shown to be linked to

MV biogenesis in certain cases[8,22]. For instance, TSG101 (an ESCRT-I subunit generally considered an exosome marker) is thought to be able to recruit ESCRT-III (the machinery complex responsible for budding and fission) to the PM, resulting in the involvement of the ATPase VPS4 and membrane scission at the cell periphery[8,22,37].

MVs are involved in important functions in both health and disease, and their release is highly sensitive to cell signalling pathways[8]. A first important process in which MVs play a central role is coagulation. In that context, collagen-activated platelets shed PM-derived vesicles bearing tissue factor (TF) capable of acting as a catalyst for the assembly of pro-coagulant enzyme complexes, leading to rapid thrombin generation[22,23]. Furthermore, these TF-containing vesicles are thought to be able to interact with specific immune cells[9]. In malignancy, MVs released by tumour cells can facilitate tumour progression in several manners: by enabling extracellular matrix digestion through the metalloproteinases they carry[9,13]; by transporting cancer drugs out of cancer cells, increasing drug resistance[9]; by modulating immunosurveillance[9,24]; and through the transfer of oncogenic material[9,13,22]. It is important to note, however, that these functions might be shared with exosomes due to the empirical difficulties in obtaining pure preparations of a single EV subtype[38].

2.1.3 Exosomes

Exosomes are the smallest subtype of EVs. They have a diameter comprised between 30 and 100 nm, and a density between 1.13 and 1.19 g/mL[25,26]. In practice, subsets of apoptotic bodies and microvesicles (table 1) have similar sizes and densities, making it challenging to isolate exosomes experimentally and single out their specific functions and contributions[13,38]. However, exosomes are known to originate from a distinct subcellular compartment, the endosome. In general terms, exosomes are released in the extracellular space when multivesicular bodies (MVBs), originating from early endosomes and

containing small intraluminal vesicles (ILVs), fuse with the plasma membrane[13] (figure 1B).

First, the ILVs enclosed in the MVBs are formed by inward budding of the endosomal limiting membrane, a process which often involves—but not always—the ESCRT machinery[8,22] (figure 2). ESCRT, which is a large complex of about 30 proteins, can be divided in 4 subcomplexes (ESCRT-0 to -III)[13,39]. In the case of ESCRT-dependent ILV formation, these subcomplexes intervene sequentially to allow the sequestration of specific cargoes and the physical budding and fission of the newly formed vesicles[8,22]. More specifically, ESCRT-0 and -I are tasked with forming distinct microdomains on the MVB membrane, which contain specially tagged (i.e. ubiquitylated) transmembrane cargoes[13,39]. Beyond its sorting role, ESCRT-I also helps to recruit the ESCRT-II subunit[39], with which it is thought to initiate membrane deformation[13]. ESCRT-II also acts as a bridge to recruit ESCRT-III soluble components and connect them to ESCRT-I, leading to their polymerization and activation[13,39]. ESCRT-III then induces vesicle neck constriction and fission from the MVB membrane[13,22]. Although ESCRT-dependent mechanisms of ILV formation are the best-defined ones[13], ILVs can also arise following alternate pathways. These are generally categorized as ESCRT-independent, despite the fact that ESCRT-III remains necessary for vesicle budding and detachment[8]. One important such process is the conversion of sphingomyelin, preferentially found in cholesterol-rich lipid rafts, into ceramide by neutral type II sphingomyelinase[8,22]. The accumulation of ceramide is then believed to induce a negative curvature and put ILV formation into motion[8,22]. Cargo sorting also occurs differently in that case, and is partially operated by tetraspanins, a family of transmembrane proteins[8,22]. Tetraspanins include CD63, CD81 and CD9, which are generally considered to be enriched in exosomes[8].

Once formed, ILV-laden MVBs need to fuse with the PM, so that ILVs can reach the extracellular space and become exosomes. Whether PM fusion occurs depends on specific mechanisms, probably regulated by sorting machineries, which prevent the endocytic pathway from ending with degradation in lysosomes[8]. Moreover, MVBs targeted for secretion need to be transported to the PM before they can fuse with it. Small molecular switches acting in concert with molecular motors and the cytoskeleton support the transport to the PM[8]. For instance, RAB-GTPases RAB27A, RAB27B and RAB11 are known to participate in MVB transport (RAB27B), docking and fusion (RAB27A and RAB11) at the PM, as well as in the required cytoskeleton rearrangements[8,22]. Finally, fusion at the PM is believed to depend on membrane trafficking proteins such as SNARE and members of the synaptotagmin family[8].

Exosomes carry biomolecular cargo composed of a mixture of proteins, lipids and nucleic acids, selectively sorted in their membrane and lumen during biogenesis[13]. The different cargo components are delivered to potential receptor cells through affinity-based surface interaction, followed by endocytosis (phagocytosis, micropinocytosis, clathrin-mediated endocytosis) or by direct fusion[35,40]. Alternatively, vesicles can undergo "fading", in which case their membrane is compromised, leading to the dispersion of their contents into the extracellular space[35]. In all cases, the transferred biomolecules can lead to considerable downstream effects. Accordingly, the recent literature highlights the involvement of exosomes in homoeostasis and pathological conditions. However, due to the previously mentioned experimental difficulties in separating EVs, most exosome analyses are confounded by the presence of undesired EV subtypes[38]. Some authors have consequently chosen to refer to these sample mixtures as small extracellular vesicles (sEVs) in reference to size-based purification, or sometimes as exosome-like extracellular vesicles (ELEVs). In what follows, we will use the term *exosomes*, as more and more protocols and analysis platforms include steps that attempt to integrate what is known

of the specific biomolecular makeup of exosomes, despite some limitations and uncertainties[38].

2.1.3.1 Exosomal Nucleic Acids

Exosomes can influence cell behaviour in several manners. One way is by transferring the various nucleic acids enclosed in their lumen to target cells. Following the discovery in 2007 by Valadi and colleagues that exosomes contain mRNA and miRNA that can be delivered to and used by recipient cells[11], exosomal RNA has been linked to many relevant physiological phenomena. The interaction of T-cells and antigen-presenting cells (APCs) at the immune synapse is one such event. It was shown to involve extensive reorganization of the cytoskeleton and exocytic pathway, resulting in enhanced transfer of exosomes from the T-cell to the APC and consequent gene regulation by the exosomal miRNAs[27]. In cancer, exosomal RNAs contribute to disease progression via metastasis formation and drug resistance[17]. They modulate the tumour environment, for example by promoting inflammatory responses that strengthen malignant invasion[29,30]. In particular, it was discovered that miR-21 and miR-29a shuttled by exosomes can bind to Toll-like receptors in a paracrine manner, leading to a pro-inflammatory cascade that favors tumour growth[29]. Likewise, exosome-derived miR-1247-3p from high-metastatic hepatocellular carcinoma tumour cells have the ability to induce the transformation of fibroblasts into cancer-associated fibroblasts in lung metastasis, exacerbating disease progression through the secretion of pro-inflammatory cytokines[30]. Exosomal nucleic acids were also found to drive drug resistance[17]. Adriamycin and docetaxel-resistant breast cancer MCF-7 cells use exosomes to spread specific miRNAs implicated in cell cycle regulation and apoptosis to carry their resistant trait to susceptible neighbouring cells[28].

The presence of genomic DNA (gDNA) in exosomes in the form of DNA fragments has also been reported. Double-stranded DNA originating from all chromosomes[41,42] was

shown to be transferred and efficiently transcribed in recipient cells, leading to protein expression and thus, function[43]. Furthermore, the gDNA fragments shuttled by exosomes can contain mutations that are characteristic of the cell of origin[42]. Kahlert and colleagues showed that it was the case of *KRAS* and *p53* in pancreatic cancer exosomes from both cancer cell lines and patient serum samples, with potential clinical implications[41].

2.1.3.2 Exosomal Lipids

The lipids forming the vesicles' bilayer form a less explored, but nonetheless important cargo category. Indeed, there is evidence that some lipids—namely cholesterol, sphingomyelin, glycosphingolipids and PS—are selectively enriched in exosomes compared to the cells of origin, and that lipids and their associated processes are involved in the biogenesis and physiological function of exosomes[44]. Besides the involvement of neutral sphingomyelinase and sphingomyelin in the ESCRT-independent release of exosomes[8], another lipid metabolizing enzyme, phospholipase D2, was also reported to be important for exosome generation by contributing to the formation of ILVs via the reduction of phosphatidylcolines to phosphatidic acids in a subset of MVBs[44,45]. Other lipid-related processes have been linked to the fusion of MVBs with both the PM and lysosomes[44,46,47]. Exosomal lipids have also been explored for disease diagnosis and monitoring in a few studies, mainly in the context of cancer. In SOJ-6 pancreatic tumour cells, internalization of tumoral exosomes can interfere with Notch signalling, leading to apoptosis[48]. Further experiments using exosome-inspired all-lipid nanoparticles showed this to be due to the impact of exosomal lipids—lipid-forming raft microdomains—on the plasma and endosomal membranes of recipient cells, thus involving them in tumour progression[49]. An additional study used a mass spectrometry platform to test the potential of exosome lipids as biomarkers for renal cell carcinoma (RCC) detection[50]. The results brought out differences in the lipidome of RCC exosomes, hinting at the possibility of using exosomes lipidomics in biomarker discovery[44,50].

2.1.3.3 Exosomal Proteins

Lastly, proteins constitute a highly relevant cargo component in terms of downstream impact and have been the subject of many reports in recent years. Importantly, proteins embedded in the membrane of exosomes are involved in the interaction with recipient cells through affinity-based binding and subsequent signalling. For example, Wnt proteins, morphogens involved in development and disease, have been located on exosomes and are thought to represent one of their secretion routes[51]. The Wnt-bearing vesicles have been shown to induce Wnt signalling in target cells[51]. In cancer, the integrin content of exosomes influences the location of metastasis occurrence by binding specifically to certain tissues and contributing to pre-metastatic niche formation[1]. Moreover, certain proteins are overexpressed in exosomes from tumorous cells, with implications in disease progression and possibly in diagnosis. In a 2015 study, Costa-Silva and colleagues uncovered that the important presence of macrophage migration inhibitory factor (MIF), an immunostimulatory cytokine, in pancreatic ductal adenocarcinoma exosomes was implicated in the early stages of the formation of liver metastases, making exosomal MIF an attractive therapeutic target and potential biomarker[31]. Additionally, glypican-1, a proteoglycan, allows the distinction of cancer patients from healthy subjects when detected in exosomes from patient samples[2]. In neurodegenerative diseases, exosomes have been implicated in the trafficking of prion proteins, such as α-synucleic, prion protein, β-amyloid and tau[32,33]. For instance, the elevated phosphorylated tau levels in cerebrospinal fluid samples often noted in early Alzheimer disease were traced back to exosome-mediated secretion, hinting at active, not only passive (leaking from dying or dead cells) spreading of the lesions[33].

Given the wide-encompassing relevance of exosomal proteins, numerous techniques and platforms have been developed to look at the protein content of exosomes from a variety of cell lines and biological fluids. However, before protein targets can be

detected and the resulting data analyzed, the vesicles need to be isolated, be it from cell culture supernatant, blood or another biological fluid. Once the vesicles are purified, the specific proteins they contain can be identified and sometimes even quantified following two main strategies: high-throughput mass spectrometry and affinity-based approaches.

2.2 Exosome Purification and Sample Preparation

Before exosome analyses can be carried out, the vesicles need to be isolated, be it from cell culture supernatant, blood or another biological fluid. Commonly used methods to purify exosomes from their carrying fluid are (i) centrifugation, (ii) filtration, (iii) polymer-isolation precipitation, (iv) immunoaffinity purification, (v) size-exclusion chromatography (SEC), and (vi) asymmetric flow field-flow fractionation (AF4). In all cases, the separation principle is based on distinctive exosome characteristics, including their size, density and biomolecular composition[52]. In recent years, the gold standard and most commonly used method of separation has been centrifugation, and in particular differential centrifugation[52,53].

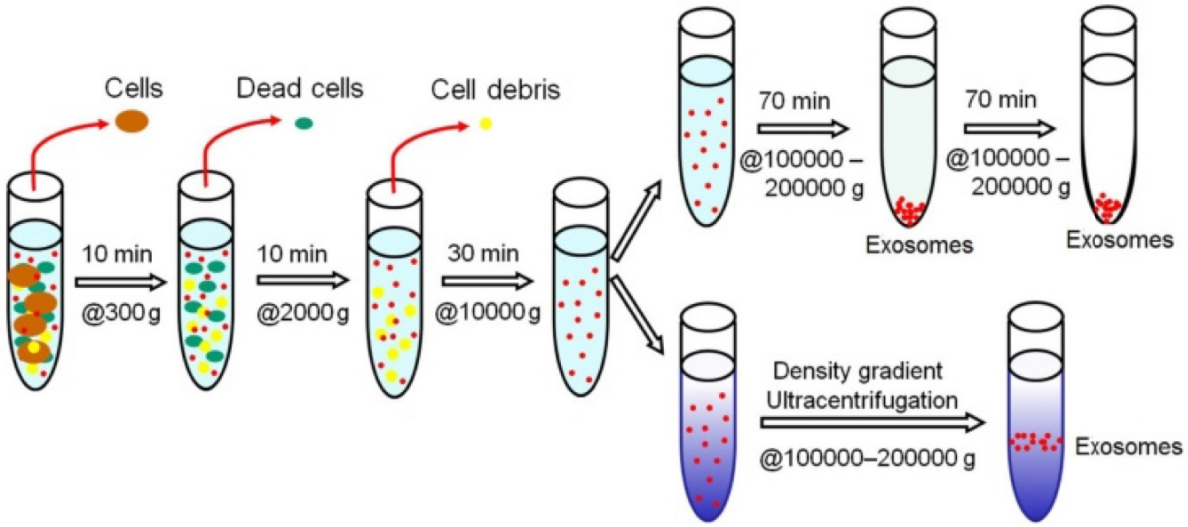

Figure 3 Principle of exosome isolation through differential ultracentrifugation[52]. The sample is first subjected to sequential centrifugation steps of increasing speed to remove contaminants, after what centrifugation steps of higher velocity or a density gradient ultracentrifugation step are used to pellet or isolate exosomes, respectively[52-54]. Reused from [52], licensed under CC BY-NC 4.0 (https://creativecommons.org/licenses/by-nc/4.0/).

2.2.1 Ultracentrifugation-Based Purification

Several variants of ultracentrifugation, with slightly different working principles, are used for exosome purification. Three common ones are (i) differential, (ii) density and (iii) moving-zone ultracentrifugation. Differential (ultra)centrifugation is an isolation method based on density, size and shape[26]. It consists of sequential centrifugation steps performed at increasing speeds, each aiming to pellet and eliminate a specific subset of particle contaminants (figure 3)[52-54]. The last step, generally performed at 100,000-200,000 g, pellets exosomes; an optional additional wash can then be carried out, followed by a final high-speed spin to recover the washed vesicles[52-54]. After most contaminants and debris have been eliminated by conventional ultracentrifugation steps, the vesicle suspension can be subjected to a density gradient centrifugation step for improved purity[52,54]. This uses a centrifuge tube containing a pre-constructed density gradient (most often composed of sucrose or iodixanol[55]), on top of which the sample, or a homogenous mixture of sample and density gradient medium, is loaded. During the centrifugation, particles settle at specific positions corresponding to their density along the gradient[52,54,56]. The various segregated fractions can then be recovered through simple elution[52]. In that case, the sharpness of each band, and thus the purity, is dependent on centrifugation time[56]. Alternatively, moving-zone ultracentrifugation can be used to separate similarly dense particles of different sizes. It relies on a medium of lower density than any of the sample constituents, such that different particle populations never reach an equilibrium position (but can pellet if spun for too long)[52]. Ultracentrifugation-based isolation protocols have many advantages which explain their popularity: they are relatively easy to use and implement[52], require some upfront investment but little to no regular expenses[52], and are very common and consequently well understood and described[56]. However, obtaining high purity vesicles is a lengthy and complicated process, and relying only on physical characteristics does not rule out contamination by similar

particles (e.g. viruses, which have very similar density and size)[53]. Furthermore, viscosity is an important limiting factor: biological matrices with higher viscosities generally lead to a lower EV yield[53,56], which is modest to start with[53].

2.2.2 Filtration-Based Purification

Multiple filtration methods have been developed to isolate exosomes, from a simple 0.22 μm syringe filter[56] to sequential ultrafiltration using filters with different cut-offs for separation and enrichment[52]. Membrane-based filtration is versatile and can readily be adapted to specific needs and workflows. For instance, membranes can be fit into compact devices, allowing for considerable miniaturization of the purification process[57], or even seamless microfluidic integration with downstream analysis steps[58]. Moreover, this technique is relatively fast and generally does not require highly specialized equipment[52]. That being said, filtration-based methods also have important drawbacks: the use of pressure to push the sample through the membrane can deform or damage the vesicles[52,59], and a non-negligible fraction of the purified vesicles can be lost due to adherence to or clogging of the membrane[59].

2.2.3 Polymer Isolation Precipitation

Polymer-isolation precipitation relies on polymer networks that trap vesicles within a defined size range (usually 60-150 nm)[60]. The chosen polymers have a high water retention capability, such as high molecular weight (~8 kDa) polyethylene glycol (PEG), to preferentially force exosomes out of solution compared to more soluble matrix components[52,59,61]. After overnight incubation, a filtration or centrifugation step is required to retrieve the precipitate[54,56,61]. This purification method is increasingly popular, mainly owing to its simplicity and rapidity[62,63]. Precipitation-based isolation is often performed using commercial kits that use proprietary reagents, which include ExoQuick (System Bioscience), and the Total Exosome Isolation Reagent (Life Technologies)[56,61,63]. Besides the ease of use, this technique has the advantage of being gentle on the vesicles,

mainly thanks to the separation being performed at neutral pH and high ionic concentrations[56,59]. Furthermore, it was shown to achieve yields 80 to 300 times higher than ultracentrifugation[63], but likely at the expense of non-exosome contaminants, while the precipitating polymer in the pellet may limit downstream applications[52,56,59,62].

2.2.4 Immunoaffinity Purification

Immunoaffinity relies on biochemical, rather than physical, properties to isolate exosomes, thus differing from the aforementioned techniques. It is based on the antibody recognition of specific antigens—most often tetraspanins, such as CD63 and CD9—at the surface of the vesicles[56,59]. The nature of the EVs isolated by immunoaffinity capture therefore highly depends on the targeted protein(s). While more specific isolation can thus be achieved, co-isolation of non-exosome vesicles cannot be ruled out, as there is no real consensus on the best targets to use[61], and that conventional exosome markers are also detectable on other EVs[64]. The preferential enrichment of vesicles bearing the targeted proteins may also introduce a bias in the isolated population[65]. However, if specific populations are under study, singling them out at the purification step can be the desired outcome[66]. The isolation workflow itself can take several forms—e.g. ELISA-based plates and antibody-coated magnetic beads[52,56]—depending on the support on which the antibodies are immobilized[59,61].

2.2.5 Size-Exclusion Chromatography

Size-exclusion chromatography (SEC) has become popular in the last few years[62], owing to the ability to obtain high purity (i.e. devoid of plasma proteins and high-density lipoproteins) vesicles from clinical samples[67]. SEC uses a porous gel filtration column to separate EV mixtures[62]. Bigger vesicles, which cannot pass through most pores, elute first, while smaller particles take longer paths and elute later[59,62]. EVs of various sizes are thus recovered in different fractions based on their elution times[62]. The short sample processing time (~20 min) compared to lengthier techniques like ultracentrifugation[67] and

the low shearing forces involved[56] make SEC both convenient and gentle on vesicles, contributing to the growing popularity of the method. However, pre-processing of the sample can include time-consuming steps such as enrichment of the mixture and removal of bigger components, like cell debris[67]. Moreover, SEC comes with a trade-off between the size range and the purity of the isolated exosomes, which both depend on the pore size of the column material. For instance, when CL-2B Sepharose columns (~70 nm pores) are used, EVs smaller than 70 nm cannot be efficiently purified, but the contamination of EV-rich fractions by lipoproteins remains low[67]. Matrices with smaller pores will help retrieve exosomes of less than 70 nm, albeit with higher levels of lipoproteins—especially very low density lipoproteins (30–80 nm)—in the purified sample[67,68]. Despite those drawbacks, SEC offers a well-defined particle distribution, and isolates small EVs enriched with proteins generally considered to be exosome markers (CD81, TSG101, synthenin-1)[67].

2.2.6 Acoustofluidic Separation

There exist many microfluidic designs that are geared towards on-chip separation of sample mixtures[69], many of which can be repurposed for on-chip exosome (or EV) separation. Acoustofluidics, which combines acoustics and microfluidics, was harnessed by Wu *et al.* to achieve on-chip separation of exosomes from cells and other EVs from whole blood without prior purification steps[70]. The device in question comprises two modules, one for cell removal and one for exosome isolation from the remaining complex EV mixture, both relying on specially adjusted tilted surface acoustic wave fields[70]. When acoustics are activated, the interplay between the acoustic radiation force and the opposing Stokes drag force, which depend on particle size, determines the position of the vesicles in the channel and thus separates them laterally[70]. Alternatively, viscoelastic flows can be leveraged to separate exosomes from other EVs. By adding a small amount of poly-(oxyethylene) to an EV mixture in order to increase its viscosity, Liu and

colleagues were able to achieve in-channel lateral separation of EV subtypes using differences in size-dependent elastic lift forces[71].

2.2.7 Asymmetric Flow Field-Flow Fractionation

Asymmetric flow field-flow fractionation (AF4)[75] is a chromatography-centrifugation hybrid[73] that was used for exosome separation in a number recent publications[74,76,77]. The technique uses a thin, ribbon-like channel, along which the sample and its carrier fluid flow laminarly, establishing a parabolic Newtonian flow profile[73] (figure 4). While the upper wall of the channel is impermeable to the solvent, the lower wall is composed of an ultrafiltration membrane and a frit, allowing the carrier fluid to exit the channel either through the channel wall or at the output[73]. The two-exit configuration introduces gradients in both the axial and transverse flows, creating a "cross-flow" perpendicular to the main axial flow[73,75]. Given that the cross-flow leads to the formation of concentration gradients, a diffusive flow forms in the opposite direction. Hence, the diffusive coefficient of the separated particles governs their position across the channel section, which in turn determines their axial velocity[73]. During the separation, smaller sample components accumulate further from the channel wall, travelling at a higher axial velocity and eluting earlier than bigger components[73,74]. AF4 has important advantages: it is very gentle[74], does not require affinity binders (but can be combined with them for improved specificity)[74],

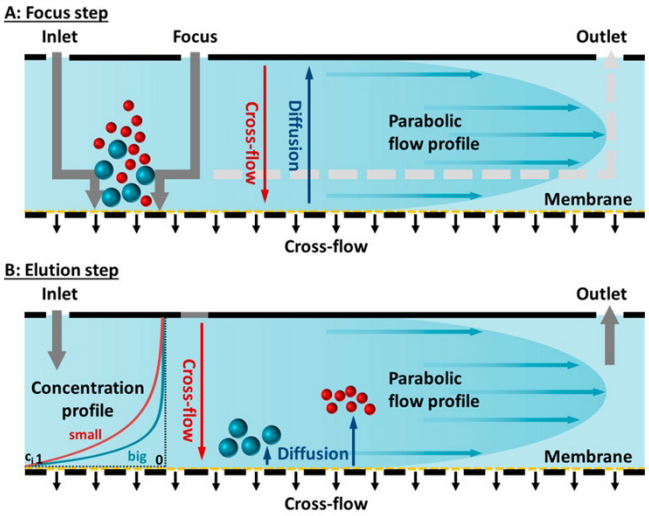

Figure 4 Principle of AF4-based separation[72]. The position of sample particles along the parabolic flow profile, and thus their axial speed, depends on their specific diffusion coefficient. Since smaller particles diffuse faster than bigger ones, they stabilize further from the channel wall and elute faster[73-75]. Reused with permission from [72]. Copyright 2014 American Chemical Society.

and is able to separate materials over a very wide size range (low nanometer range up to tens of micrometers)[73]. However, it is technically complex and requires careful optimization[74].

2.3 Characterization of Exosome Samples

Purified exosome samples need to be characterized before downstream analysis. The exosome size distribution, morphology, particle count, zeta potential, and protein concentration are common parameters of interest[78,79]. Characterization methods include (i) dynamic light scattering (DLS), (ii) nanoparticle tracking analysis (NTA), (iii) tunable resistive pulse sensing (TRPS), (iv) spectrophotometry measurements, (v), electron microscopy (EM), and (vi) atomic force microscopy (AFM).

2.3.1 Dynamic Light Scattering

In DLS, a monochromatic and coherent laser light source is used to illuminate the particulate sample[80]. The scattered light is analyzed to look for time-dependent intensity variations, which can then be used to derive information about the sample size distribution[81]. More specifically, interaction of the illuminating light beam and the scattered light leads to patterns of constructive and destructive interference, which change over time due to the Brownian motion of the suspended particles[80,81]. How quickly the resulting intensity changes occur is dependent on the particle size: the smaller the particles, the faster they move and the faster the intensity varies[81]. This is captured mathematically by a time autocorrelation function, the relaxation of which is used to obtain the diffusion coefficient[82]. Size information is then derived using the Stokes-Einstein equation, which relates the hydrodynamic radius to the diffusion coefficient[82].

DLS is routinely used to obtain size information about exosome (or EV) suspensions[79]. As it can detect and analyse particles as small as a few nanometers, it is theoretically well suited to the characterization of exosomes and EVs[78,80]. In practice

however, DLS only provides reliable data for nearly monodispersed samples[79,80]. When a sample contains both large and small particles, big particles scatter light more efficiently and are more readily detected than small ones, leading to a size distribution that is skewed in favor of the larger subpopulations[78,83]. As vesicle samples, particularly those obtained from biological fluids, are often heterogeneous, the results obtained using DLS should be reviewed with care[79,84]. Furthermore, as DLS does not look at the biomolecular content of the analyzed particles[80], contaminants and aggregates can be confused with vesicles in the sample[84]. Coupling DLS to additional size-based purification steps, such as SEC or field flow fractionation, can help improve the reliability of the technique[78].

2.3.2 Nanoparticle Tracking Analysis

NTA, like DLS, relies on the detection of scattered light, but tracks individual particles instead of using ensemble-averaged information[78]. The path of each detected particle, which is mainly governed by Brownian motion, is monitored as a function of time using a camera[79,80]. The particle size can then be computed from the time-dependent displacement using the Stokes-Einstein equation[79,80]. By simultaneously tracking the trajectories of hundreds to thousands of particles in a field of view of known volume, NTA can provide, in addition to the size distribution, a concentration value (or particle count) for the sample analyzed[78,84]. Furthermore, NTA can be used to obtain zeta potential information through the application of an electric field and measurement of the electrophoresis-induced vesicle velocity[84]. Fluorescence detection can also be integrated to NTA, allowing preliminary phenotyping through the detection of fluorescent antibody staining on individual vesicles[79,83,85]. As of yet, this is restricted to abundantly expressed markers, given that studies using NTA and fluorescent monoclonal antibodies for phenotyping have so far known very limited success[80].

NTA fares better with polydisperse samples than DLS, which makes it well suited to characterize heterogenous EV samples[78]. However, the sensitivity of NTA is limited to

vesicles bigger than 50-70 nm, as small vesicles have weak scattering properties[78,80]. Since exosomes can be as small as 30 nm, NTA tends to mostly detect subpopulations of larger sizes and to underestimate the number of smaller exosomes[78,80] Moreover, NTA can produce confusing results for measurements performed in complex biological samples, as exosomes and similarly sized impurities and aggregates cannot be readily distinguished with NTA[78].

2.3.3 Tunable Resistive Pulse Sensing

In TRPS, a voltage is applied between two fluid cells separated by membrane with a single tunable nanopore[86]. One cell contains the sample, while the other is filled with a filtered electrolyte, allowing current to flow between the two cells[87,88]. At the moment when a particle in the suspension passes through the pore, the electrical resistance momentarily increases, and the resulting discrete "blockade" events can be monitored as current dips proportional to the particle volume[78,80,88]. As the nanopore is tunable, its size can be modified to tailor the size dynamic range to the sample under study[88].

TRPS, like NTA, assesses particles individually, and is well suited to the analysis of polydisperse EV samples[80]. Furthermore, it requires small sample volumes, relies minimally on instrument settings and is a very versatile technique, as it can simultaneously measure the size, concentration and zeta potential of the particulate sample[88]. However, just like DLS and NTA, TRPS cannot distinguish between exosomes and protein aggregates of the same size range[88]. Another important issue is clogging, which is exacerbated when using a small nanopore in order to increase the sensitivity to small EVs, and which can hamper the measurements[89].

2.3.4 Spectrophotometry measurements

Spectrophotometry in the UV and visible range of the electromagnetic spectrum has been used for decades to quantify the concentration of biological macromolecules[90].

Spectrophotometers work by illuminating the sample, contained in a glass cuvette, with a light beam and measuring the amount of transmitted light[90]. To obtain this information as a function of wavelength (i.e., a spectrum), some spectrometers change the wavelength of the incident light and perform many punctual measurements, while others image all the wavelengths simultaneously by using a broad-spectrum lamp and a prism to decompose the transmitted light[90]. To obtain the concentration of a sample component that absorbs light at a specific wavelength, the absorbance of the sample at that wavelength is computed, then related linearly to the concentration using the Lambert-Beer law[90].

Exosomes are rich in proteins, which are known for their strong absorption at 280 nm[91,92]. Measuring the absorbance of a purified exosome sample at 280 nm provides a protein concentration value, which in turn gives an idea of the number of exosomes in the sample[93,94]. Spectrophotometry is a fast, simple and convenient way of assessing exosome content, as spectrophotometers are standard laboratory equipment[90,92]. However, this method is sensitive to the presence of contaminants that absorb at or around the same wavelength, such as protein and free nucleic acids[92]. Thus, if the chosen purification method does not remove such impurities in the sample, an overestimation of the exosome content can result. Along the same line, if the protein concentration within exosomes changes, different readings will be obtained even though the total number of exosomes is constant.

2.3.5 Electron Microscopy

In EM, samples are imaged using an electron beam instead of light as in fluorescence microscopy[78,80]. As electrons are characterized by a much shorter wavelength than the conventional fluorescence photons, structures which normally could not be resolved with visible light can be probed with nanometer resolution[80,85].

EVs and exosomes have been imaged with both scanning electron microscopy (SEM) and transmission electron microscopy (TEM), which are the two main types of EM[78]. In SEM, as the name suggests, the electron beam is scanned over the sample, and ejected or secondary electrons are detected[78,84]. This method requires preparation steps to make the sample conductive, commonly the addition of a thin layer of gold at the surface[78]. TEM, on the other hand, is more similar to conventional light microscopes and works by focusing the electrons that pass through the sample into an image[85]. The deposition of a metallic layer is not necessary with TEM, however substantial sample preparation, including fixation, dehydration, and negative staining, is still required and can affect vesicle morphology[78,84]. While TEM is most often used to image EVs and has a higher resolution, SEM yields 3D images, which can provide additional insight[85]. TEM nevertheless has the advantage of being compatible with immunolabeling (using antibodies conjugated with gold), making it possible to visualize the distribution of a given target at the structural level[78].

2.3.6 Atomic Force Microscopy

AFM works by scanning a sample deposited on a flat surface using a mechanical cantilever equipped with a sharp tip, whose position is continuously monitored using a combination of a laser and a photodiode[78-80,95]. The tip of the cantilever oscillates around a resonance frequency and gets deflected as it interacts with 3D structures on the planar surface[78,95,96]. The spatially-dependent deflections are measured as changes in oscillation amplitude, phase, or frequency, and are used to build a map of the sample topography[78,95,96]. AFM can be operated in several different modes and paired with functionalized tips to tailor it to the nature of the sample and allow the assessment of additional properties, such as viscoelasticity and biomolecular interactions[78].

In EV and exosome studies, AFM is primarily used to characterize vesicle morphology due to its high lateral and vertical resolutions[78]. Unlike EM, it is compatible

with aqueous samples, minimizing the required preparation and maintaining the vesicles in a state close to their native one[78,80]. Nevertheless, as vesicles are soft, they can readily deform, or depending on the strength of the attachment, move around, which can lead to confounding results[78]. Thus, care has to be taken when interpreting the resulting images, and deriving quantitative information about the vesicle size may not be possible[78].

2.4 Exosome Proteomics

2.4.1 Mass Spectrometry Proteomics

In mass spectrometry (MS) proteomics, sample proteins are digested, and the mass-to-charge ratio (m/z)[97] of the resulting ionized peptides or peptide fragments[7] is measured. As MS encompasses several technologies and methods, the workflow depends on the approach chosen and the instrument used. In this section, the principles and technologies involved at each experimental step are first presented, followed by a description of the two main strategies used in MS protein analysis—discovery and targeted proteomics—and their application to the study of exosomes.

2.4.1.1 MS Workflow

MS protein analysis comprises three main experimental steps: separation/fractionation, ionization, and spectra acquisition. During separation/fractionation, the analyzed sample is fractionated into its components using gel electrophoresis-based or chromatography-based methods, or a combination of both[98]. The gel electrophoresis family of techniques includes SDS-PAGE, a one-dimensional gel separation approach that segregates peptides according to their molecular weight prior to tryptic digestion, and 2D gel electrophoresis, in which the second dimension of separation is the isoelectric point of the species to be separated[98,99]. After separation, sections of the gel containing the peptides of interest are extracted and their content digested and fed to the instrument[99]. High-performance liquid chromatography (HPLC) methods work according to different separation principles and

can be combined to offer multidimensional separation of pre-digested peptides[100]. For instance, reverse phase HPLC—a mode with a polar mobile phase and a non-polar/hydrophobic stationary phase[101]—is often combined with strong cation exchange chromatography (SCX), a form of ion exchange HPLC[100]. SCX uses a charged polymeric stationary phase whose association with charges in the sample depends on the pH and/or ionic strength of the mobile phase[101].

After separation and digestion, the sample has to be ionized before it can enter the mass analyzer. Since proteins and peptides are non-volatile and unstable at high temperatures, electrospray ionization (ESI) or matrix-assisted laser desorption/ionization (MALDI) are most commonly used[97]. In ESI, small charged droplets are generated when a solution containing the sample flows in a small capillary held at a specific voltage compared to a counter electrode[97]. In MALDI, the sample is crystalized together with a solid matrix and pulsed with a laser in a vacuum. The resulting gas ions are then collected and transferred to the mass analyzer[97]. Both ESI and MALDI detect peptides containing basic amino acids with limited efficiency, particularly cysteine, methionine and tryptophan, due to their tendency to form disulfide bonds[102]. However, while MALDI mostly produces singly charged ions, ESI outputs higher charged ions[102]. The high charge obtained with ESI makes it difficult to detect light peptides (small m/z)[102], but brings heavier peptides back into the detectable m/z range[103]. ESI also allows for more effective quantitation than can be achieved with MALDI, which is limited by the heterogeneity of its matrix[103]. MALDI, however, mitigates the impact of sample impurities, as they tend to remain trapped in the matrix during ionization[103]. Overall, the low degree of identification overlap (39%) obtained after a comparative study of the two setups led investigators to conclude that ESI and MALDI should be considered complimentary[102].

Peptide ions are detected by the mass analyzer, which outputs the mass spectra, a plot of the number of detection events as a function of the mass-to-charge ratio[97]. There

exist several types of analyzers, which use different strategies for acquisition. Time-of-flight (TOF), sector and quadrupole analyzers leverage the effect of a potential difference on the ions' velocity, the focusing capabilities of electric and magnetic fields, and the impact of carefully tuned radio frequency magnitude and direct current voltages on ion path stability, respectively[97]. TOF detectors have a very wide *m*/*z* detection range, but there is a trade-off between the resolution of the acquired spectra and the length and/or complexity of the ion tube, which in turn impact compactness and cost[103]. By contrast, quadrupole analyzers are usually compact, affordable and robust, but have a limited detection range[103]. Sector instruments integrating magnetic and electric sectors combine high resolution, accuracy, *m*/*z* range and speed, but are large, costly and require high voltages that restrict integration to other instruments[104].

2.4.1.2 Discovery MS Proteomics

The goal of discovery proteomics is exploratory: researchers aim to "catalog" the proteins within a sample, as opposed to tracking specific protein species. Discovery studies can be quantitative, with quantitation achieved using a label-free or label-based approach[7,99,100].

One popular workflow for discovery experiments is multidimensional HPLC on-line with MS/MS[99,100,105]. In MS/MS, digested (parent) peptides undergo mass analysis, followed by dissociation and a second round of mass spectra acquisition for the product ions[97]. There are two main modes of MS/MS: data dependent acquisition (DDA) and data-independent acquisition (DIA). In DDA, the most common mode[105,106], abundant peptides are preferentially selected for further analysis after the first MS stage, with the number of selected peptides depending on the scanning speed[107]. In the increasingly popular DIA, all the parent peptides belonging to a specific mass "window" are sent for dissociation and secondary MS acquisition[107]. Bioinformatics tools are then used to deconvolve the multiplexed spectra and extract identifications and quantitative information[107]. The window is moved, and the process repeated until the entire mass range of interest has

been analyzed[107]. While DIA, unlike DDA, is not restricted to a limited number of preselected peptides, it presents data analysis challenges, as the output data needs to be deconvolved[108].

In quantitative label-free experiments, no external label is incorporated in the sample before analysis. To extract quantitative information from the mass spectra, it is assumed that the signal intensity varies linearly with the analyte concentration[99]. Spectral counting (SC) and spectral peak intensity (Total Ion Chromatogram, TIC) are two approaches that use the linear assumption to derive abundance values from the mass spectra[7,99,100]. SC requires several MS/MS datasets[99] and is based on the fact that high abundance peptides are more likely to be selected for the second MS run than less common ones[7,99,100]. Hence, the number of mass spectra that can be tied back to a particular peptide gives an idea of the concentration of its protein of origin in the sample[7,99,100]. By contrast, TIC can be used for non-tandem MS datasets (like HPLC-MS) or for DIA HPLC-MS/MS[99], and uses the correlation between the area under chromatographic peaks (elution times just before the first MS stage) and the analyte concentration in the sample mixture[7]. Alternatively, if 2D gel electrophoresis is used for fractionation, optical density measurements of the peptide spots in the gel can be used for quantification[99]. The following MS analysis then serves solely for identification purposes[99].

Label-based strategies generally incorporate stable isotopes as labels to facilitate quantification[99]. There exist several labeling methods, each with features that make it preferable for certain applications. In stable isotope-labeling with amino acids in cell culture (SILAC), heavy isotope-containing amino acids are incorporated in the cell media during culture[100]. Therefore, this method is especially suited to studies involving cell media-derived exosomes[99]. Isotope tags for relative and absolute quantitation (iTRAQ) and tandem mass tags (TMT) instead rely on a post-digestion chemical reaction to attach

the isotope tags[100]. As such, they work well for experiments where exosomes have to be purified from biological fluids[99]. When using tags, each sample can be specifically labeled (using a specific isotope, e.g. light or heavy), allowing the mixing and simultaneous analysis of several samples[100]. The multiplexing capability can reach 8-10 samples, depending on the method used[100].

The main advantage of label-free methods is their flexibility, both in terms of experimental design (number of samples analyzed) and execution (simplicity)[99]. However, this comes at the price of a greater variability, as each sample is processed individually; a form of normalization thus has to be introduced[7,99,100]. By contrast, label-based methods are more complicated to implement, but generally result in better linearity and accuracy[99].

2.4.1.3 Targeted MS Proteomics

Targeted proteomics experiments look at specific, pre-defined peptide or protein targets using MS/MS and include quantitative analysis of associated transitions[7,100]. In selected reaction monitoring (SRM) or multiple-reaction monitoring (MRM), a triple quadrupole mass spectrometer is used, where the three quadrupoles serve to select the parent ion, fragment it into smaller parts and analyze the resulting fragments, respectively[100]. It then becomes possible to track a specific parent-product pair, several product ions (sequentially) for a given parent ion to achieve greater specificity, or several parent-product pairs by cycling between them[97]. Quantitation can be relative or absolute, depending on whether it relies only on the comparison of transition intensities or also on the addition of isotope-labeled standard peptides[7,100]. Parallel-reaction monitoring (PRM), a variant, is performed on quadrupole-Orbitrap hybrid instruments, where the Orbitrap replaces the third quadrupole of the triple quadrupole machine in the workflow[7]. This allows full scans to be acquired for each parent ion analyzed (as opposed to specific transitions that have to be monitored chronologically), from which the transitions of

interest are obtained[7]. It also solves the issue posed by the limited resolution of precursor ion measurements when using a triple quadrupole machine[7].

In 2012, sequential window acquisition of all theoretical spectra (SWATH)[109] was introduced as a DIA technique. SWATH-MS combines fast, high resolution DIA acquisition over a wide *m/z* range with targeted data extraction and alignment using a DDA-derived spectral library[110]. The generated complex fragment ion maps can be interrogated for peptides of interest using information contained in the DDA library[109]. The fast cycling time of the instrument allows the reconstitution of time-resolved chromatographic peaks, or extracted ion chromatograms (XICs), which can be used for quantitation[110]. SWATH-MS thus brings together high accuracy and reproducibility and breadth of coverage, bridging the gap between SRM/MRM and discovery approaches[111].

Overall, targeted MS analyses benefit from high sensitivity, reproducibility and precision when looking at select proteins, but require *a priori* knowledge of peptides or proteins of interest[7]. These can be provided by previous discovery studies, making the two families of approaches complementary.

2.4.1.4 MS Analysis of Exosome Proteins

Exosome proteins have been identified and analyzed using both label-free and label-based quantitative strategies. Notably, Multidimensional Protein Identification Technology, or MudPIT[113], a popular MS workflow (figure 5), has been used with both.

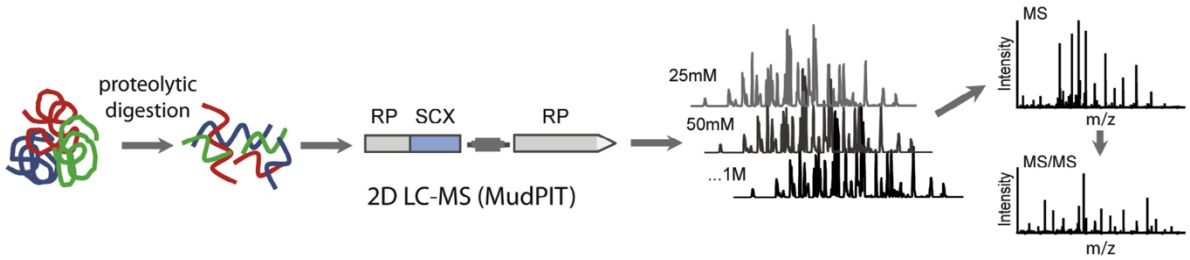

Figure 5 MudPIT workflow[100]. Following proteolytic digestion, protein samples are separated using 2D liquid chromatography before being analyzed and identified by MS/MS and SEQUEST analysis, respectively[100,112]. Reused from [100], Copyright 2015, with permission from Elsevier.

In MudPIT, digested protein samples are separated by 2D chromatography—a mix of SCX and reversed-phase HPLC—before being subjected to MS/MS in DDA mode[100,112]. Protein identification is then achieved through database searching using the SEQUEST algorithm[112]. In a 2012 study, Wang and colleagues used this strategy in combination with in-solution digestion and SC to look at the protein content of urine exosomes[114]. The authors were able to identify close to 3280 proteins across 9 human urine samples, including all the members of the ESCRT machinery, and carried out gene ontology (GO) analysis to gain insight on the functionality of the detected proteins[114]. In another 2012 study looking into urinary exosomes, Raj *et al.* harnessed four-plex iTRAQ to quantify 114 exosomal proteins in human urine samples from two distinct age groups[115]. The quantitative data revealed that six proteins had significantly different expression in the two groups, and that there were 9 upregulated and 12 downregulated proteins in a single compared to pooled samples[115]. A more recent study by Kowal *et al.*, this time using a nanoHPLC-MS/MS workflow and a TIC-based label-free quantitative analysis, aimed to compare the protein content of EV fractions obtained at different ultracentrifugation steps[64]. Their analysis revealed that specific protein markers were expressed in differentially isolated EV subpopulations, while others—including some common "exosome markers", such as MHC class I or II—were shared across all[64].

Targeted approaches are especially useful in exosome studies looking at condition-specific changes in protein expression[100]. For instance, while looking into the protein content of exosomes derived from mutant KRAS colon cancer cells, Demory Beckler and colleagues used LC-MRM to distinguish between the wildtype and mutant forms of the protein in cell and vesicle samples, something standard LC-MS/MS could not achieve[116]. This was done by targeting transitions involving peptides specific to each form of the protein[116]. Furthermore, in a 2017 study, Dozio & Sanchez looked at protein cargo modulations in brain endothelial EVs (exosomes and microvesicles) after stimulation

with tumour necrosis factor (TNF) using label-free discovery (shotgun) proteomics[117]. Once expression variations were found for specific proteins, they used PRM analysis as a validation step[117].

2.4.2 Affinity-Based Analysis of Exosome Proteins

Affinity-based exosome proteomics include a variety of approaches relying on affinity binders to recognize specific targets in the studied samples. Due to their sensitive, high-throughput, tunable and flexible nature[99,118], these techniques nicely complement MS-based strategies. However, they are limited to already known proteins for which affinity binders exist and are well-characterized, and analogously to targeted MS proteomics, the set of proteins under study needs to be chosen prior to the experiment[118]. Given the versatility of affinity reagents, methods used to identify and quantify proteins can take many forms, ranging from flow cytometry and lab-on-a-chip devices to bead-based immunoassays and arrays.

2.4.2.1 Flow Cytometry-Based Platforms

In flow cytometry (FCM), a suspension of particles (most often cells or beads) in carrier fluid is flowed past multiple laser sources[119]. The laser beams can either be scattered or induce fluorescence when they reach the particles, and the resulting light is picked up by detectors that are specific for either directionality (for scattering) or wavelength (for fluorescence)[119]. FCM has been used with cells for decades. It can be combined with various types of staining and labels to achieve effective analysis and sorting of cell suspension samples[119], and allows multiparameter characterization and high-throughput quantitative analysis[120]. Nevertheless, conventional flow cytometers are ill-equipped to deal with nanometer-sized particles like EVs. Indeed, difficulties in distinguishing subtle (<200 nm) size differences and in detecting vesicles smaller than 500 nm hinder their use with EV samples[120,121]. Although vesicles sized under the expected detection limit have

been shown to be detectable when several of them are illuminated by the laser beam simultaneously—a phenomenon termed *swarm detection*[121]—, such measurements come with some caveats attached. Namely, the signal from the smaller vesicles can easily be drowned out by that of the bigger particles in the sample if the latter are concentrated enough, the concentration is considerably underestimated, and no subpopulation information can be extracted from such measurements[121]. Fortunately, several recent studies present ways of working around those limitations, which can range from direct modification of the flow cytometer to additional signal amplification.

Van der Vlist and colleagues combine bright fluorescent labeling of the vesicle samples and optimization of a commercial flow cytometer to achieve single vesicle detection[120]. More specifically, a jet-in-air flow cytometer with a high-power laser is supplemented with a small particle detector characterized by its high numerical aperture and magnification power, allowing better wide-angle forward scatter detection and thus improved detection of particles in the nanometer range[120,122]. Moreover, fluorescence thresholding is integrated to help distinguish signal from noise[120,122], and the particle dwell time is increased by lowering the sheath pressure, giving more time to the particles to interact with the laser light[120]. Prior to analysis, the vesicles are stained with PKH67, a bright membrane intercalating dye, and can additionally be stained with fluorescent antibodies[120,122]. To rule out swarm detection, dilution curves were made and shown to be linear[120], as expected for single particle detection[121]. Using this method, the authors were able to differentiate LPS-activated and nonactivated dendritic cells-derived EVs labeled with PKH67 and fluorescent MHC class II-specific antibodies[122]. Of note, this approach is limited to fairly abundant targets and is highly dependent on the specific antibody used, namely its affinity and the number and brightness of its associated fluorophores[120].

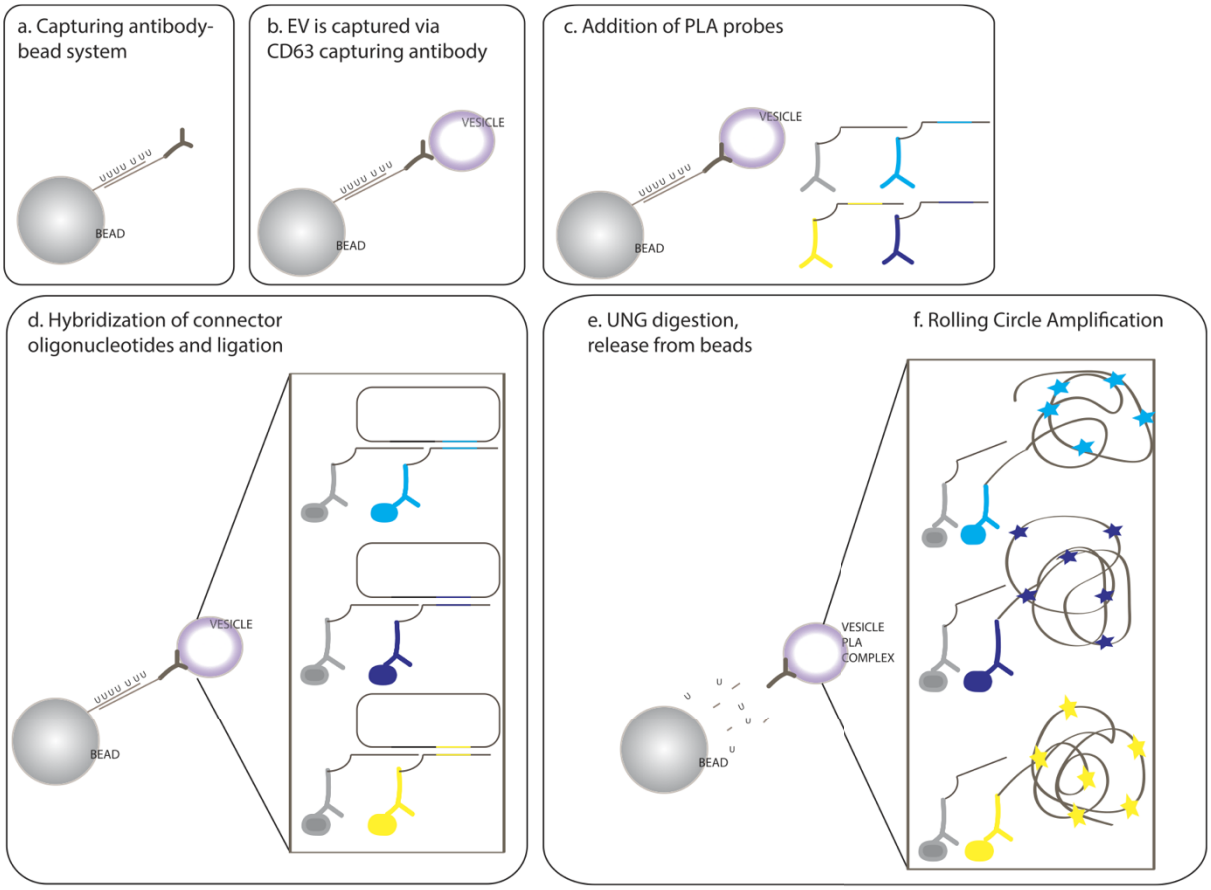

Figure 6 ExoPLA principle and workflow[123]: a) antibodies conjugated to oligonucleotides are attached to the beads through hybridization, b) EVs are incubated with the beads and captured by the tethered antibodies, c) the 4 different PLA probes, each attached to an antibody targeting a specific marker, are added to the mix, d) the connector oligonucleotides hybridize with their complementary PLA probes and are circularized through ligation, e) the tagged vesicles are released from the capturing antibody-bead system through UNG digestion, and f) subjected to RCA before detection using flow cytometry. Reused from [123], licensed under CC BY 4.0 (https://creativecommons.org/licenses/by/4.0/).

An alternative to improving the sensitivity of the setup is to adjust the signal to fit the detection range of the instrument. This can be done by altering the size of the sample particles, or by amplifying the emitted signal. One possible approach involves fixing exosomes to micrometer-size beads before probing them using fluorescent antibodies, thus making the vesicles detectable by the cytometer[54,79,123]; while convenient, this approach sacrifices an important advantage of the technology, which is its ability to sort individual particles into subpopulations with similar attributes[123]. To address this concern, Löf *et al.* developed ExoPLA, a bead-based method using the principle of the *in*

situ proximity ligation assay[123] (figure 6). In this strategy, streptavidin-modified beads are used as a capture system: biotinylated oligonucleotides bind to them, which then allows hybridization with complementary oligonucleotides conjugated to anti-CD63 capture antibodies. Exosomes can then be captured on the beads, and the resulting complex incubated with a set of 4 different antibodies, each conjugated to a unique PLA probe. One of these probes acts as a wildcard and can be combined to any of the other three to allow the circularization of connector oligonucleotides; these serve as templates for rolling circle amplification (RCA) once individual vesicles are freed from the beads through UNG digestion. Given that all but the wildcard probe lead to the generation of a specific RCA product that can be labeled with a distinct fluorophore, this technique allows multiplexed detection of protein targets at the surface of the vesicles under study[123]. As a proof of concept, the authors showed that they could distinguish prostasomes spiked in a complex biological matrix, female plasma, as a distinct vesicle population using a probe selective for the marker Thy-1[123].

2.4.2.2 Lab-on-a-Chip Devices

Microfluidic devices, which handle fluids in micrometer-sized channels and features, can be made into integrated platforms, or lab-on-a-chips (LOCs), which combine several experimental steps in a single miniature chip. LOCs have been frequently used for exosome isolation and analysis, applications for which their high-throughput nature, sensitivity, precise sample handling and ease of integration[124,125] have made them especially useful. Various features of microfluidic chips, like channel walls, geometric structures and beads can be functionalized with affinity binders for capture and detection of specific targets in the samples. Additionally, these miniaturized devices can easily be integrated with external elements, such as magnets and electrodes, allowing for considerable flexibility in terms of isolation and detection methods.

Complete exosome analysis can be performed in lab-on-a-chip devices incorporating bead-based assays. For instance, in a 2014 publication, He and colleagues presented an integrated microfluidic platform capable of performing isolation, enrichment, chemical lysis, and protein capture and analysis of circulating non-small-cell lung cancer (NSCLC) exosomes[124]. The different assay steps, from immunomagnetic capture to lysis and protein detection, are implemented in the form of distinct inlets, in which the sample, buffers, antibodies and labels are flowed (figure 7). The technology was used to perform quantitative analysis of a promising NSCLC biomarker present on exosomes, type 1 insulin growth factor receptor (IGF-1R). Both extravesicular (α subunits) and intravesicular (phosphorylatable β subunits) epitopes were targeted, highlighting the potential of the technique for the detection of both external and internal proteins in exosomes[124]. In a 2016 follow-up paper, Zhao *et al.* added multi-marker probing capabilities to an adapted, single-chamber device, named ExoSearch[126]. This time, intact exosomes captured on magnetic beads are probed in a multiplexed manner for surface proteins using detection antibodies labeled with various fluorophores[126].

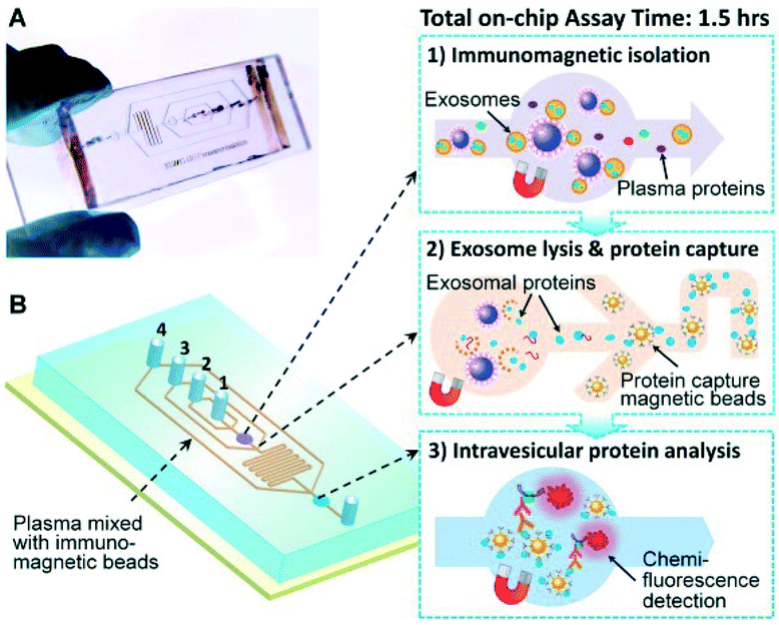

Figure 7 Integrated microfluidic platform for detection of exosomal proteins[124]: *1)* the sample and the antibody-coated magnetic beads are flowed together through the inlet, and the exosome-coated beads are washed while being pulled down with a magnet; *2)* captured exosomes are lysed, freeing exosomal proteins which are captured by a second set of targeted magnetic beads; and *3)* detection antibodies and chemifluorescent labels are flowed in. Reused from [124], published by The Royal Society of Chemistry and licensed under CC BY-NC 3.0 (https://creativecommons.org/licenses/by-nc/3.0/).

Bead-based assays owe their high capture and detection efficiency in part to the increased surface area provided by the use of beads. However, there are other ways to improve the surface area available for exosome capture and analysis in microfluidic chips. For example, Zhang and colleagues used a combination of surface functionalization, nanopatterning and coating to improve exosome capture efficiency while limiting non-specific interactions[127]. The chip design is characterized by an array of Y-shaped PDMS microposts, which improve the surface area and mixing capabilities of the device, and by a 3D nanostructured graphene oxide/polydopamine (GO/PDA) coating covalently coupled to Protein G. A high density of oriented capture antibodies can then be achieved inside the device's channels through Protein G-IgG interaction[127]. Proof-of-concept experiments were performed on both exosome standards and plasma samples from ovarian cancer patients, demonstrating the capabilities of the device for exosome surface marker profiling (CD63, CD81, CD9 and EpCAM) and quantitative detection for clinical applications, respectively[127].

2.4.2.3 Microarrays

Microarrays are periodic arrangements of affinity binders or proteins patterned on a flat substrate. Each microarray spot can have a distinct target, such that multiplexed analyses can be performed in a high-throughput and sensitive manner[4]. Arrays are also flexible, as they can be made using different types of biomolecules and integrated with various technologies for signal detection and amplification. In a 2013 study, Jørgensen *et al.* presented an antibody microarray platform, the EV array, for phenotyping and quantification of EV proteins (figure 8)[4]. The analysis uses two distinct microarrays, one composed of identical spots containing a mix of exosome marker antibodies (anti-CD9, CD63 and CD81) and the other containing a panel of 21 distinct capture antibodies on individual spots. The first array allows the quantification of the EVs in the sample based on the fluorescent detection signal, as well as their enrichment for further characterization

by NTA. The second array yields multiplexed phenotyping of the sample EVs for 21 protein targets, including cancer antigens, cellular surface antigens, and controls. Testing on plasma samples revealed unique protein expression patterns in the EVs of the 7 healthy donors under study[4].

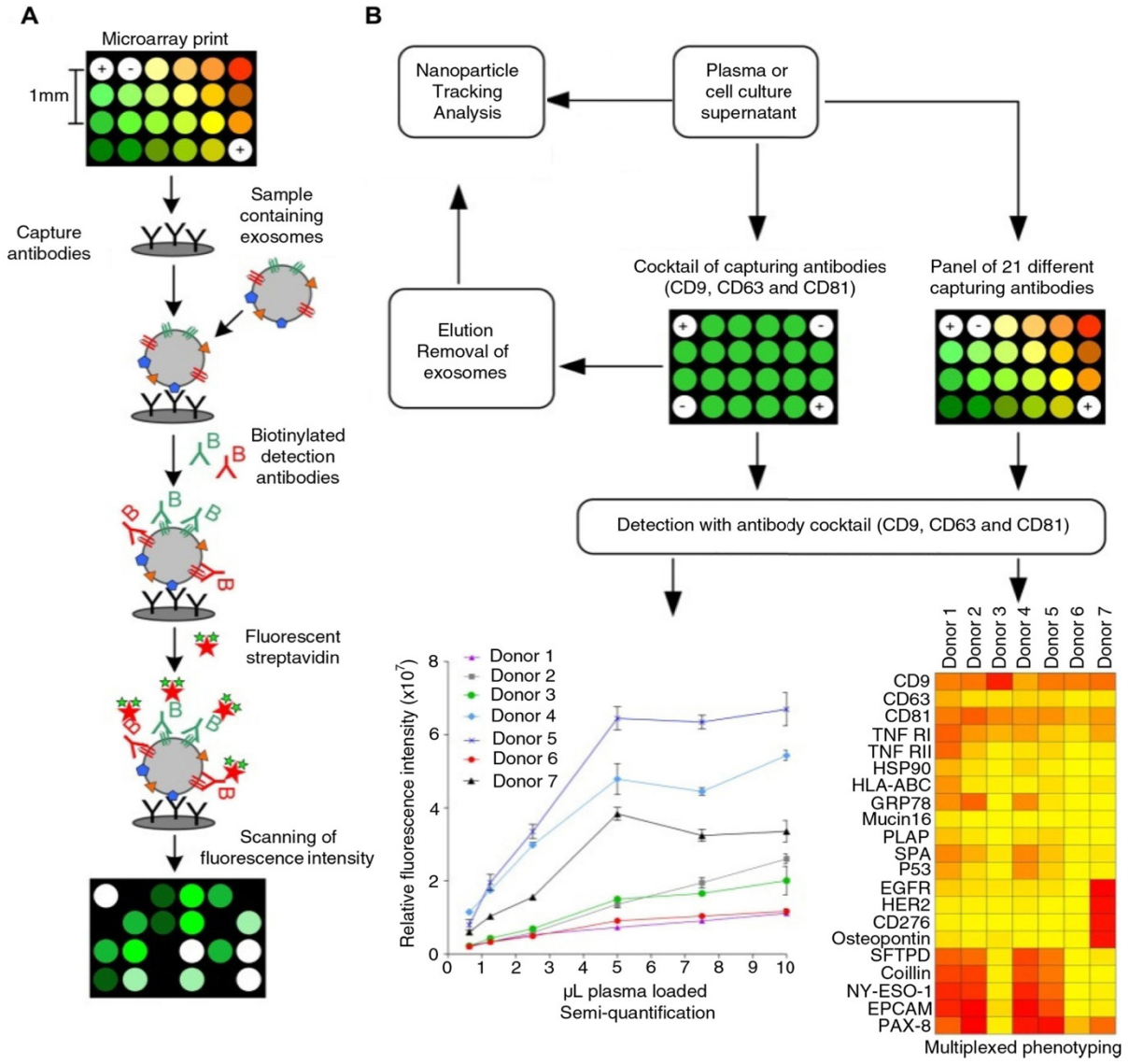

Figure 8 Profiling of EV proteins using the EV array[4]. (**A**) Multiplexed exosome protein analysis using the EV array. EVs are incubated with a microarray targeting 21 proteins and detected using a cocktail of biotinylated detection antibodies (anti-CD9, CD63 and CD81 antibodies) and fluorescent streptavidin[4]. (**B**) EV Array workflow. Two distinct microarrays are used, one for semi-quantification and one for protein analysis; exosomes capture for semi-quantification are eluted and characterized using NTA[4]. Reused from [4], licensed under CC BY-NC 3.0 (https://creativecommons.org/licenses/by-nc/3.0/).

Alternatively, aptamers can be used as affinity binders instead of antibodies. In particular, SOMAmers, or slow off-rate modified aptamers, are particularly well suited to large-scale proteomics analysis. They incorporate chemically modified nucleotides and are preferentially selected for their low dissociation rate, resulting in improved stability, specificity and target range[128,129]. Webber and colleagues used the array platform SOMAscan™—which includes 1129 distinct SOMAmers raised against protein targets — to look at the protein content of continuous sucrose gradient-purified prostate cancer exosomes and compare it to that of their parent cells[128]. Bioinformatic analysis was performed on the exosome-enriched proteins identified using SOMAscan™ to help interpret the proteomics results. The biological themes emphasized by the analysis were consistent with the presence of exosomes in the sample and included terms related to membrane trafficking, vesicle secretion and the extracellular environment[128].

Plasmonics can also be used for the detection of array-bound species. Notably, Im *et al.* developed an antibody-functionalized periodic nanohole array with transmission surface plasmon resonance (SPR)-based detection[130]. Upon vesicle binding to the array, the refractive index changes locally, causing wavelength shifts in the SPR transmission spectra (or variations in intensity at a given wavelength) that are proportional to the number of bound vesicles. Since vesicles are bound to the array through antibodies, the signal of each spot correlates with the level of its protein target in the sample[130]. The method brings several of the key advantages of SPR to exosome detection, including label-free analysis and real-time monitoring[130]. Further exploring the possibilities of SPR, the same group developed a complementary platform which can detect both intravesicular exosome proteins and transmembrane targets in exosome lysates[131]. Using immunolabeling with gold nanoparticles, stronger signal amplification is achieved than for EV binding alone[131].

2.4.3 Comparison of Current Exosome Proteomics Approaches

The approaches presented in the previous sections are a testament to the growth of the field of exosome proteomics, which is continuously supplemented with new strategies. Not all methods are equivalent however, as they each have specific advantages and disadvantages that determine how useful they are for a given application (table 2). For discovery-type studies mostly concerned with understanding the biogenesis and roles of exosomes, MS is especially advantageous: it can identify many proteins quickly, including modified/mutated ones[99,116] and ones for which no stable affinity binders have been obtained yet[118], and provides useful complementary capabilities, such as structural analysis[97].

Array platforms are increasingly popular for exosome proteomics. They support multiplexed analysis[99] and offer advantages like high sensitivity[4], low sample consumption[4,7] and the possibility of automation[4]. However, unlike MS, their reliance on affinity binders means they can suffer from limited target range and cross-reactivity problems[128]. Nevertheless, the development of improved affinity binders, such as SOMAmers[128], has the potential to bridge the gap between the breadth of analysis of both techniques.

For targeted analyses where specific markers need to be detected or quantified, or when specific subsets of exosomes need to be investigated, approaches like flow cytometry and LOCs have attractive features. Flow cytometry, not unlike MS and arrays, is a high-throughput technique, but its multiparametric nature and sorting capabilities make it particularly well suited to the study of exosome subpopulations, or even of single vesicles[120,123]. As for LOCs, they are especially attractive for clinical applications, in particular when limited amounts of biological samples are available: they generally require small sample volumes (usually in the μL range) and offer tight control over how reagents and samples are handled[125]. If the fabrication process can sometimes be

complicated[126], the flexibility it offers makes intricate chip designs possible, and several assay steps can thus be seamlessly integrated[124].

APPROACH	STRENGTHS	WEAKNESSES
MASS SPECTROMETRY	No affinity binders[118] Speed of analysis[97] Sensitivity[97] Structural analysis[97]	Relative abundance in complex samples[128] Reproducibility[128] Time-consuming workflow[124,128]
FLOW CYTOMETRY	High-throughput[120] Multiparameter[120] Subpopulations[120] Individual EVs/exosomes[123]	Affinity binders[120,123] Limited sorting[120]
MICROFLUIDIC LAB-ON-A-CHIPS	High-throughput[124] Small volume requirements[125] Precise liquid handling[125] Functional integration[124]	Affinity binders[7] Complicated/costly fabrication (in some cases)[126] Need for off-chip steps[125]
MICROARRAYS	Sensitivity, multiplexed analysis[4,7,99] High-throughput, fast, automated[4] Small sample requirement[4,7]	Affinity binders[7] Cross-reactivity (antibodies)[128]

Table 2 Strengths and weaknesses of exosome proteomic approaches

Overall, different approaches to exosome analysis offer specific combinations of attributes, like detection sensitivity and multiplexity[132], speed, and throughput. For a given EV study, the choice of protein analysis method will ultimately depend on the scope and objectives of the research, which will in turn determine the features to prioritize.

Each of the exosome proteomics approaches presented above can also be implemented several ways, and the choices made in the design of the platform can affect assay outcome. For instance, antibody microarrays have been described which use various printing technologies[133], printing additives[134], surface chemistries[135,136], blocking agents[137] and assay formats[137]. Since careful optimization of the methods to the specific application and sample under examination is important[138], tailoring antibody microarrays for exosome analysis is a necessary step towards the use of this technology for vesicle research. However, despite notable interest in the downstream impact of exosome

isolation and sample processing techniques[59,63,139], there are few reports on the optimization of microarray platforms for exosome proteins analysis.

The overall performance of an exosome surface-based affinity assay depends on both the efficient (i) capture of exosomes and (ii) detection of the exosome and its cargo. To achieve adequate capture, the small size and delicate nature of exosomes must be considered. Most importantly, however, suitable exosome surface proteins need to be targeted for capture—which is problematic[18,140]. Following capture, careful selection of protein targets and associated antibodies is also needed for the detection of the captured exosomes. In this work, we used two microarray-based assay formats to characterize and optimize the capture and detection of exosomes from CD63-GFP-expressing A431 cells individually, and also optimize the complete assay towards obtaining a high signal intensity and reproducibility. Using the optimized exosome microarray protocol, exosomes from 4 cancer cell lines were phenotyped using a panel of 15 capture antibodies.

3. Materials and Methods

3.1 Cell Culture

CD63-green fluorescent protein (GFP)-transfected A431 cells (provided transfected from ATCC® CRL-1555™ by Dr. Janusz Rak, McGill University, Montreal, Canada), MDA-MB-231 cells (ATCC® HTB-26™) and SK-BR-3 cells (ATCC® HTB-30™) were cultured in Dulbecco's Modified Eagle Medium containing 4.5 g/L D-glucose, L-glutamine and 110 mg/L sodium pyruvate (Gibco, Thermo Fisher Scientific) and supplemented with 10% fetal bovine serum (FBS, Gibco, Thermo Fisher Scientific) and 1% penicillin-streptomycin (PS, Thermo Fisher Scientific). BT-474 cells (ATCC® HTB-20™) were cultured in Roswell Park Memorial Institute medium (Gibco, Thermo Fisher Scientific) supplemented with 10% FBS and 1% PS. All cells were kept at 37°C in a 5% CO_2 environment with constant humidity.

3.2 Exosome Purification from Cell Culture

On the day after passaging, the cell media in the flasks designated for exosome purification was replaced by media supplemented with 5% exosome-depleted FBS (Gibco, Thermo Fisher Scientific) and 1% PS. After two to three more days in culture, depending on the cell line, the cell media was removed from the flasks, filtered with a syringe filter (pore size 0.22 μm, diameter 33 mm, MilliporeSigma) and concentrated down to 500 μL per 30 mL of media using ultracentrifugation filters (Amicon® Ultra-15 10k, MilliporeSigma) centrifuged at 4000 rpm in iterative 25-min spins. For SEC separation, qEV columns (Izon Science), stored with PBS containing 20% ethanol, were first pre-equilibrated by flushing 10 mL of phosphate buffer saline (PBS, diluted to 1X from a 10X solution, Thermo Fisher Scientific) through each column, after what 500 μL of concentrated sample was added to each column and gradually allowed to go through the

column using PBS as a buffer. Eleven 500 μL eluate fractions were collected for each column; a NanoDrop™ 1000 spectrophotometer (Thermo Fisher Scientific) and a NanoDrop™ 3300 fluorospectrometer (Thermo Fisher Scientific) were then used to measure the protein content (absorbance at 280 nm) and GFP fluorescence intensity (emission at 510 nm) of collected fractions, respectively, in order to estimate their exosome content. For each fraction set, the fractions corresponding to a peak in terms of protein content and intensity values (generally 8, 9 and 10) were pooled, concentrated as required to reach a protein concentration of 0.05 to 0.1 mg/mL using centrifuge filters (Amicon® Ultra-2 10k, MilliporeSigma), and used for assay experiments.

3.3 Microarray Production

The microarrays used in all experiments were patterned using the sciFLEXARRAYER SX inkjet bioprinter (Scienion). Unless otherwise indicated, all slides were incubated at 70% humidity overnight after patterning, washed in a bath of 0.1% Tween®20 (Thermo Fisher Scientific) in a high-throughput washing station (ArrayIt®), blocked for 3 h in a solution of 3% bovine serum albumin (BSA, Jackson ImmunoResearch) and 0.1% Tween®20, dried using a slide centrifuge (Microarray High-Speed Centrifuge, ArrayIt®), and inserted into 16-well gaskets (ProPlate® Multi-Well Chambers, Grace Bio-Labs) before being used for assays.

For the detection of printed exosomes, poly-L-lysine (PLL)-coated slides were prepared by sonicating glass microscope slides twice, once in acetone and once in ethanol, plasma treating the dried clean slides for 1 min (PE-50 Compact Benchtop Plasma Cleaning System, Plasma Etch), and incubating each pre-treated slide in 5 mL of 0.1 mg/mL PLL solution (Sigma Aldrich) with gentle agitation (150 rpm) for 30 min. The coated slides were then washed gently with deionized (DI) water and dried with nitrogen gas prior to patterning. Three printing solutions were made (purified exosomes in PBS with 20% glycerol [Thermo Fisher Scientific]; purified exosomes in PBS; and PBS) and

filtered using a syringe filter (pore size 0.22 μm, diameter 13 mm, Millipore Sigma). The different suspensions were patterned onto slides in 6 lines of 10 100 μm-wide spots with 1000 μm spacing, with 2 lines per printing solution.

In prevision of multi-buffer experiments, solutions of 7 hygroscopic additives (PEG 1000, Sigma-Aldrich; glycerol; DMSO, Sigma Aldrich; ethylene glycol, Sigma-Aldrich; 1,3-butanediol, Sigma-Aldrich; 2,3-butanediol, Sigma-Aldrich; and betaine, Sigma-Aldrich) were first prepared at 30% (or 2.4 M for betaine) concentration in PBS, forming the 7 first printing buffers. The 21 mixed printing buffers, each containing 15% of two additives, were then made by mixing these 7 intermediate solutions at a 1:1 ratio in a pairwise manner. All 28 resulting solutions, as well as an aliquot of PBS, were then filtered with a syringe filter (pore size 0.22 μm, diameter 13 mm, Millipore Sigma) prior to antibody addition and patterning.

In the case of exosome capture in solution, three types of microarrays were printed on PolyAn 2D-Aldehyde slides (PolyAn): microarrays of biotinylated antibodies in 20% glycerol, microarrays of biotinylated antibodies in 29 printing buffers for testing purposes, and microarrays of biotinylated antibodies in the 4 best performing buffers. For all arrays, biotinylated goat anti-mouse secondary antibodies (Invitrogen) were diluted in the aforementioned printing buffers at a concentration of 100 μg/mL and patterned into 100 μm spots with a 500 μm pitch in a 9 x 10 (29 buffers with 3 replicates per well per buffer [6 for PBS]) or 10 x 10 (20% glycerol; 4 buffers with 25 replicates per well per buffer) randomized array format. The randomization of array patterns was done using a custom MATLAB (MathWorks®) script.

For experiments involving testing of surface-based capture and detection of exosomes, mouse anti-CD9 (Biolegend), anti-CD63 (Biolegend), anti-CD81 (Biolegend) and polyclonal goat anti-EGFR (R&D Systems) antibodies were diluted at a concentration of 100 μg/mL in all 29 printing buffers and spotted in randomized 9 x 10 arrays (29

buffers, 3 replicates per well per buffer [6 for PBS]) on PolyAn 2D-Aldehyde slides. For experiments concerning the effect of the printing antibody concentration, anti-CD63 antibodies were diluted in the 4 best performing buffers at concentrations of 50 μg/mL, 100 μg/mL, 150 μg/mL and 200 μg/mL and spotted in randomized 10 x 10 arrays (25 replicates per well per buffer). For exosome phenotyping experiments, antibodies were diluted at 100 μg/mL in a solution of 15% 2,3-butanediol and 1 M betaine in PBS and printed on a PolyAn 2D-Aldehyde slides in 16 x 16 randomized arrays (16 replicates per antibody per well). The chosen antibodies are mouse monoclonal antibodies from R&D Systems unless noted otherwise and include: anti-ADAM10, anti-CD44, anti-CD82, anti-CD133, anti-integrin αVβ5, anti-integrin α2, anti-integrin α6, anti-integrin β1, anti-integrin β4, anti-PD-1, anti-PD-L1, anti-CD63 (Biolegend), polyclonal goat anti-EGFR, anti-EpCAM, goat anti-rabbit Alexa Fluor® 546 (Invitrogen), and anti-CCR5.

3.4 Detection of Printed Exosomes

Primary antibodies (anti-CD63, biotinylated mouse anti-CD63 [Biolegend], anti-CD81, anti-CD9, anti-EGFR and goat biotinylated anti-EGFR [R&D Systems]) were diluted at a concentration of 1 μg/mL in PBS before being applied to the different wells of the exosome microarray slide and incubated for 2 h at room temperature under mild agitation (350 rpm). After that, the antibodies were removed, and the wells washed 3 times in PBS under mild agitation (350 rpm). Fluorescent secondary antibodies (goat anti-mouse Alexa Fluor® 647, Life Technologies) or fluorescent streptavidin Alexa Fluor® 647 (Invitrogen) were diluted to 1 μg/mL in PBS or PBS with 1% BSA, respectively, added to the wells, and incubated for 1 h (30 min for streptavidin). The wells were then washed once in PBS, after what the gaskets were removed and the slide washed in a PBS bath under mild agitation (350 rpm) for 10 min, followed by a manual wash with DI water. Lastly, the slides were dried with nitrogen gas and imaged using a confocal microarray

scanner (InnoScan 1100 AL, Innopsys) or an inverted fluorescent microscope (TE2000-E, Nikon).

3.5 Exosome Capture from Solution

Purified exosome samples, biotinylated antibodies (anti-CD63 or anti-EGFR at 5 μg/mL), and blocking agents (0.03% Tween®20 or 1% BSA) were combined in 1.5 mL tubes and incubated under mild agitation (450 rpm) first at room temperature for 2 h, then overnight at 4°C. The next day, exosome-antibody complexes were separated from unbound antibodies and exosomes using the qEV columns, as described in section 3.2. Fluorescence and protein content spectrophotometer (NanoDrop) measurements were performed on the obtained fractions to validate which ones contained the purified complexes. The relevant fractions were pooled, concentrated to a protein concentration between 0.1 and 0.15 mg/mL using centrifuge filters (Amicon® Ultra-2 10k, MilliporeSigma), and supplemented with 1% BSA. In parallel, before the addition of the gasket to the slide, streptavidin was added to the microarray spots by incubating them with a 0.1 μg/mL solution of streptavidin Alexa Fluor® 647 for 25 min under mild agitation (450 rpm) at room temperature, followed by a 15 min bath wash in PBS with 0.1% Tween®20. Once both the slide and the exosome-antibody complexes were ready, the complexes were incubated on the microarray for 30 min under mild agitation (450 rpm) at room temperature. An exosome suspension without bound antibodies and PBS was added in two of the wells as controls. After that, the gasket was removed, the slide was washed in a bath of PBS with 0.03% Tween®20 followed by a manual wash with MilliQ water, and the array was dried in a slide centrifuge. The resulting array was imaged with a confocal microarray scanner.

3.6 Exosome Microarray-Based Capture and Detection

Exosome samples were supplemented with 1% BSA or 0.03% Tween®20 and incubated over the antibody spots with mild agitation (450 rpm) first 2 h at room temperature, then overnight at 4°C. Controls were implemented by incubating PBS (for the entire incubation time) and a 10 μg/mL solution of goat anti-mouse Alexa Fluor® 647 antibodies in PBS with 0.1% Tween®20 (for 1 h) in specific wells. The next day, individual wells were washed in PBS with 0.03% Tween®20. If the experiment design comprised a detection step, the arrays were next incubated with a 2.5 μg/mL solution of biotinylated anti-CD63 or anti-EGFR antibodies with 1% BSA for 2 h under mild agitation (450 rpm) at room temperature, followed by a 25 min incubation in the same conditions with a 5 ug/mL solution of streptavidin Alexa Fluor® 647 with 1% BSA. Slides were then washed in a bath of PBS with 0.03% Tween®20, followed by a manual wash with DI water, and dried using a slide centrifuge before being imaged with a confocal microarray scanner.

3.7 Phenotyping of Exosomes from 4 Cancer Cell Lines

Staining of exosome samples was achieved using the ExoGlow™-Protein EV Labeling Kit (System Biosciences). Exosome samples were supplemented with 1% BSA or 0.03% Tween®20 and incubated over the antibody spots with mild agitation (450 rpm) first 2 h at room temperature, then overnight at 4°C. Samples were then removed from the wells, and each well was washed three times with PBS supplemented with 0.03% Tween®20 under mild agitation (450 rpm). The arrays were next incubated with a 1 μg/mL solution of biotinylated anti-CD63 antibody for 2 h, the wells washed three times with PBS supplemented with 0.03% Tween®20, and the spots detected through a 30-min incubation with a 2 μg/mL solution of streptavidin Alexa Fluor® 647, all under mild agitation (450 rpm) at room temperature. Slides were then washed in a bath of PBS with

0.03% Tween®20, followed by a manual wash with DI water, and dried using a slide centrifuge before being imaged with a confocal microarray scanner.

3.8 Data Analysis

For quantitative analysis, the array data was extracted from the slide images using the Array-Pro® Analyzer software (MediaCybernetics®), and the intensity values de-randomized and analyzed using a custom MATLAB® script. For each studied condition, corrected intensity values were first computed for each replicate by subtracting the median of the background (four local corners of each spot) from the average intensity value of the spot. The obtained corrected values of all replicates of a given condition were next used to compute the averaged intensity value and standard deviation for that condition. The coefficient of variation (CV) was then obtained by taking the ratio of the standard deviation (σ) to the mean (μ) for each individual condition:

$$\mathrm{CV} = \frac{\sigma}{\mu} \times\ 100\%$$

In the case of printing buffer optimization experiments involving different markers or combinations of markers, corrected intensity values were normalized (S_{norm}) on a marker-by-marker basis by dividing them by the highest signal obtained among all buffers tested ($S_{\max marker}$) for the marker combination under consideration:

$$S_{norm} = \frac{\overline{\left(x_{signal} - \tilde{x}_{background}\right)}}{S_{\max marker}} \times 100\% = \frac{\mu}{S_{\max marker}} \times 100\%$$

S_{norm} provides a quantitative metric for qualifying the printing buffers for each studied combination, i.e. without bias from the varying capture/detection efficiency of the antibodies used.

4. Results and Discussion

4.1 Development of the Assay Format for Improved Exosome Capture and Detection

Our antibody microarray platform for exosome capture, termed **Ex**osome **A**ntibody **M**icroarray (ExAM), was realized in three phases: the separate development of exosome (i) capture and (ii) detection followed by (iii) the optimization of the full assay protocol. Exosomes from CD63-GFP-expressing A431 cells (epidermoid carcinoma) were used as they were readily available via a collaborator, had intrinsic CD63-GFP expression that could be used for calibration and control, and were previously characterized in terms of protein content[141]. Exosome samples were purified by SEC from cell culture supernatant and their protein content characterized by spectrophotometry before experiments. Purified exosomes were concentrated where required to reach a protein concentration of 0.05 to 0.1 mg/mL.

In this section, we present two methods for the development of exosome capture and detection, respectively, along with their strengths and weaknesses. Standalone detection was performed by using an inkjet spotter to directly array an exosome suspension on a functionalized glass surface, which was incubated overnight at 70% humidity to ensure bonding. The immobilized exosomes were then detected using antibodies against selected membrane proteins. For capture optimization, the exosomes were incubated with biotinylated antibodies in solution, and the resulting exosome-antibody complexes were anchored to the surface using biotin-streptavidin interactions. In parallel, we compared and contrasted the performance of antibodies targeting different commonly accepted exosome markers (CD63, CD81 and CD9) and epidermal growth factor receptor (EGFR), a transmembrane protein overexpressed in A431 cells[142].

4.1.1 Detection of a Directly Printed Exosome Suspension

To optimize the detection of protein markers at the surface of exosomes, exosomes were spiked into different buffers (PBS and 20% glycerol in PBS) and arrayed using the inkjet spotter on a poly-L-lysine (PLL)-coated glass slide. Since the surface of exosomes is negatively charged at neutral pH, they bind electrostatically to the positively-charged PLL, and were found to remain bound following long incubation and washing steps. The immobilized exosomes were then detected with antibodies targeting membrane proteins known to be expressed in exosomes (figure 9). The printed vesicles were detected with combinations of antibodies and labels targeting EGFR, CD63, and CD9, but not CD81 (figure 10). However, despite a dedicated blocking step, high levels of unspecific binding were detected for both secondary antibody and streptavidin-based fluorescent detection. Interaction between the charged surface and detection antibodies could account for the high background signal, especially on the edges of the wells, where mixing tends to be less efficient.

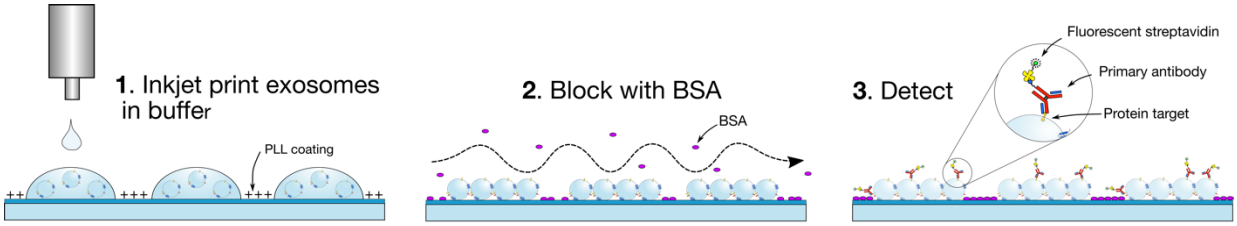

Figure 9 Direct spotting of exosome microarrays using inkjet spotting: *1)* the exosome suspension is inkjet-printed on a PLL-functionalized slide in a microarray format leading to electrostatic adsorption of negatively charged exosomes on the positively charged PLL surfaces, *2)* the printed slide is washed and the non-patterned surface is blocked, and *3)* the immobilized vesicles are detected with combinations of marker-targeting antibodies and fluorescently-labeled detection antibodies or streptavidin.

The combination of a biotinylated anti-CD63 primary antibody and fluorescent streptavidin yielded the strongest and clearest signal, while detection using a biotinylated anti-EGFR antibody and fluorescent streptavidin or an anti-CD9 antibody and a fluorescent secondary antibody led to weaker signals (figure 10). Interestingly, for CD63 detection, the background was more uniform and of lower intensity when fluores-

cent streptavidin was used for labeling, compared to a fluorescently labeled secondary antibody. Due to the strength of the biotin-streptavidin interaction, fluorescent streptavidin was incubated for a shorter time than secondary antibodies, which may have helped mitigate unspecific interactions. Alternatively, the small size and near-neutrality of streptavidin at neutral pH may have played a role[143]. Overall, it was determined that CD63, EGFR and CD9 could be detected above background on arrayed exosomes immobilized through simple electrostatic interactions. However, the filtration and inkjet spotting of the exosome sample are additional steps that can lead to exosome loss, resulting in a reduced number of vesicles at the surface. In addition, unspecific electrostatic interactions can lead to high backgrounds and co-immobilization of negatively charged impurities, including small microvesicles, apoptotic bodies, and lipoproteins co-purified during sample processing, which could also carry proteins and

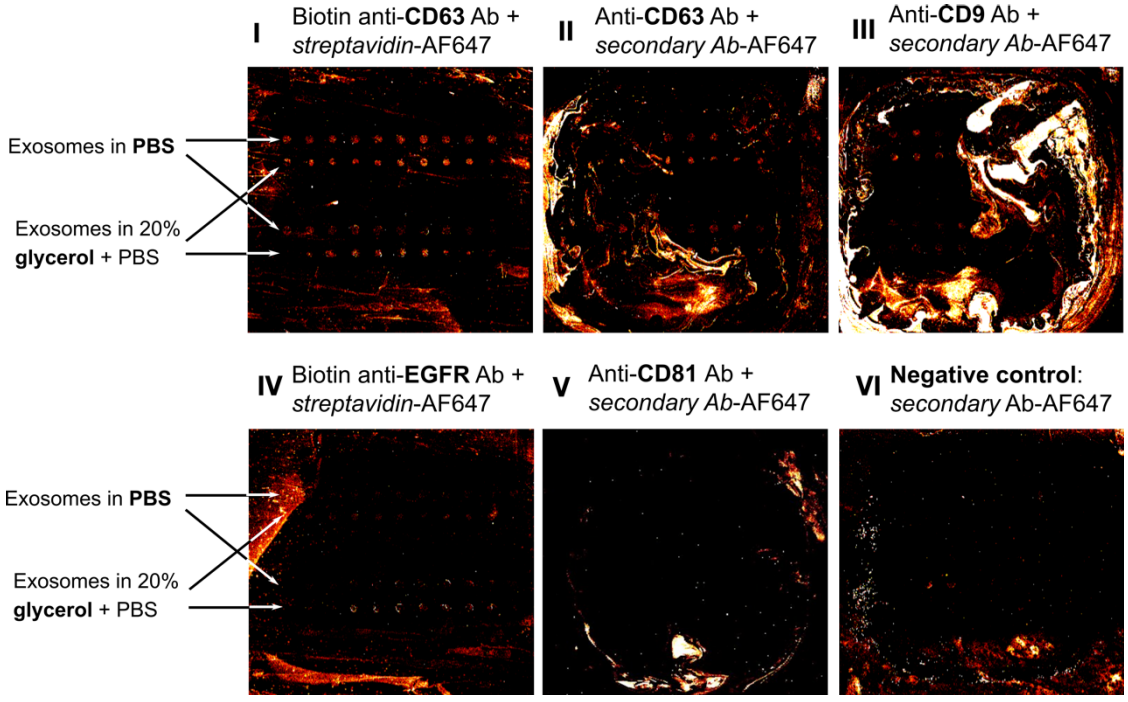

Figure 10 Fluorescent micrographs of the immunolabeled surface-bound exosomes. Each row of spots represents a series of duplicates of the same condition, with each condition repeated twice. Detection with antibodies against CD63 (*I, II*), CD9 (*III*), and EGFR (*IV*), but not CD81 (*V*), resulted in detectable fluorescent binding signal. The negative control condition (*VI*) did not yield any specific signal. Binding was detected using either a fluorescent secondary dAb or streptavidin, which bound unspecifically to the charged surface, resulting in high background signal. Streptavidin was less susceptible to non-specific binding. AF-647: Alexa Fluor® 647; Ab: antibody; dAb: detection antibody.

skew the protein expression results. Also, the difficulty in effectively blocking the positively charged PLL surface limits the detection sensitivity. Nevertheless, the results confirmed that pre-immobilized exosomes can be detected by incubating them with surface receptor-specific detection antibodies, and highlighted expression patterns of the model exosomes.

4.1.2 Exosome Capture from Solution Followed by Surface Anchorage and Detection

Towards optimization of exosome capture, we started by incubating exosomes with antibodies in solution prior to their immobilization on the surface through biotin-streptavidin interactions (figure 11). Proceeding this way has two key advantages: 1) efficient mixing of antibodies and exosomes and thus potentially greater contact and binding between the two species, and 2) efficient surface anchorage of the exosome-

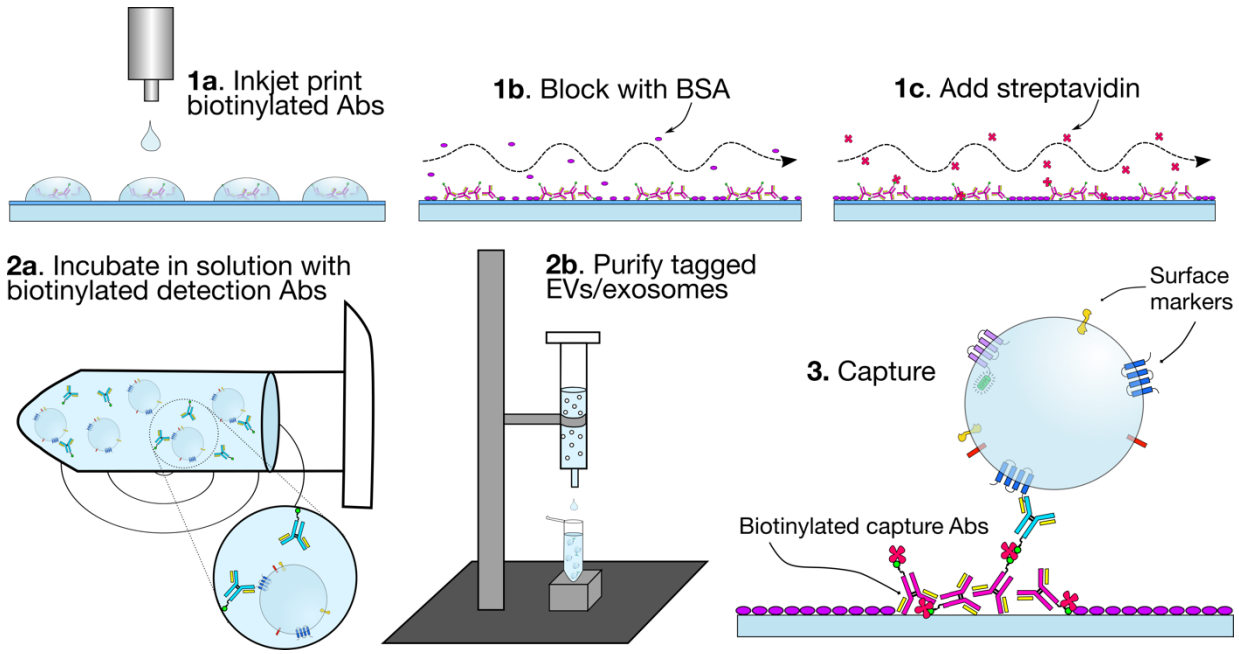

Figure 11 Workflow for capture of exosomes from solution: *1a)* biotinylated antibodies are inkjet-printed on an aldehyde-functionalized slide (PolyAn 2D-Aldehyde), *1b)* the slide is washed and unoccupied sites are blocked, and *1c)* the resulting microarray is incubated with a streptavidin solution and washed; in parallel, *2a)* the exosome suspension is incubated in solution with biotinylated anti-CD63 or anti-EGFR antibodies before undergoing *2b)* chromatographic separation to separate the exosome-antibody complexes from the mixture, and *3)* the retrieved complexes are incubated over the streptavidin spots for surface anchorage and detection. The washing steps that occur after printing, streptavidin addition and exosome incubation are not shown.

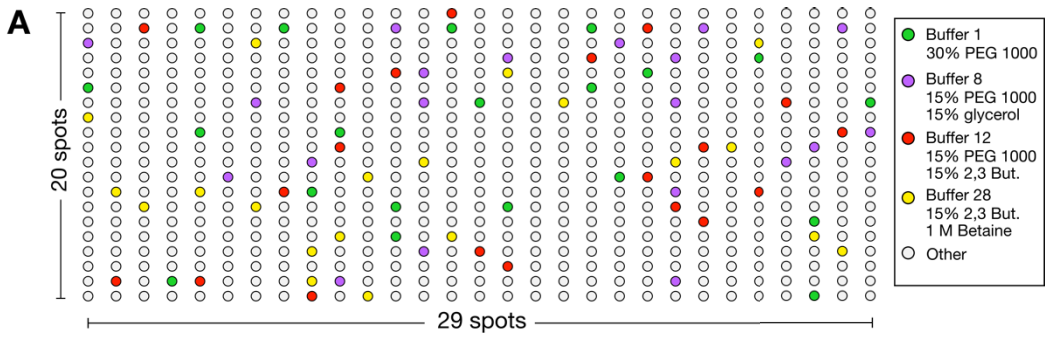

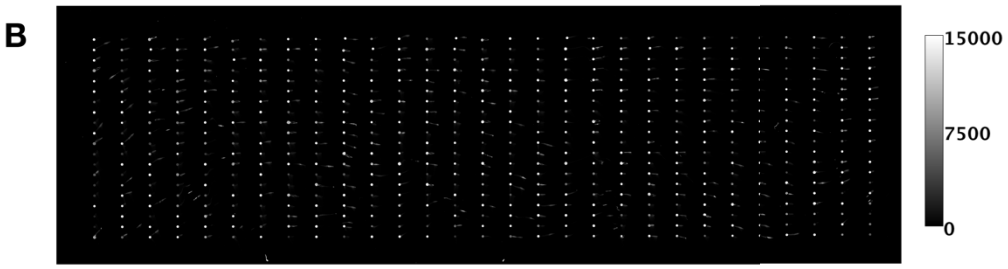

C

	BIOTINYLATED AB BUFFER	STREPTAVIDIN FLUO. SIGNAL INTENSITY	CV
1	30% PEG 1000	80%	8%
2	30% Glycerol	17%	27%
3	30% DMSO	19%	24%
4	30% Ethylene Glycol	24%	17%
5	30% 1,3-butanediol	32%	25%
6	30% 2,3-butanediol	39%	16%
7	2 M Betaine	100%	15%
8	15% PEG 1000, 15% Glycerol	73%	7%
9	15% PEG 1000, 15% DMSO	82%	11%
10	15% PEG 1000, 15% EtGly	83%	12%
11	15% PEG 1000, 15% 1,3 But.	90%	13%
12	15% PEG 1000, 15% 2,3 But.	81%	9%
13	15% PEG 1000, 1 M Betaine	35%	22%
14	15% Glycerol, 15% DMSO	12%	27%
15	15% Glycerol, 15% EtGly	12%	22%
16	15% Glycerol, 15% 1,3 But.	16%	24%
17	15% Glycerol, 15% 2,3 But	18%	25%
18	15% Glycerol, 1 M Betaine	59%	13%
19	15% DMSO, 15% EtGly	21%	21%
20	15% DMSO, 15% 1,3 But.	27%	25%
21	15% DMSO, 15% 2,3 But.	28%	18%
22	15% DMSO, 1 M Betaine	73%	13%
23	15% EtGly, 15% 1,3 But.	36%	25%
24	15% EtGly, 15% 2,3 But.	36%	24%
25	15% EtGly, 1 M Betaine	82%	14%
26	15% 1,3 But., 15% 2,3 But.	43%	19%
27	15% 1,3 But., 1 M Betaine	89%	13%
28	15% 2,3 But., 1 M Betaine	93%	11%
29	PBS	22%	23%

COLOR SALE INTENSITY	CV
100%	30%
75%	25%
50%	20%
25%	15%
0%	10%

Figure 12 Optimization of biotinylated antibody spotting. (**A**) Microarray design used for the optimization. Each of the 29 buffers tested was used to print 20 spots at random positions on the slide surface, for a total of 580 spots. The randomized positions of the 4 best performing printing buffers are highlighted. (**B**) Fluorescence microarray scan obtained after the incubation of fluorescent streptavidin with biotinylated antibody spots printed using 29 different buffers. The spot positions are as illustrated in A. The fluorescence intensities are expressed in arbitrary units. (**C**) Normalized corrected signal intensities and CVs for the data shown in B (n=20).

antibody complexes through the strong biotin-streptavidin interaction. At first, a microarray of biotinylated IgGs printed in 20% glycerol—a common printing additive used to limit buffer evaporation[134]—was used and incubated with biotinylated anti-CD63 and anti-EGFR antibodies as the capture mix. This protocol yielded very low exosome binding signal and poor spot morphology (data not shown). Since the substrate-printing buffer combination had previously been shown to greatly impact antibody binding, with glycerol offering limited performance when paired with an aldehyde slide[134], we sought to identify the optimal combination of antibody printing buffer and slide. Consequently, we tested 29 printing buffers made using binary combinations of 7 additives in PBS to find which ones result in strong, reproducible binding between fluorescently-labeled streptavidin and printed biotinylated antibodies. Each buffer was spotted at 20 different randomized positions in an array of 20 by 29 spots in order to limit the impact of spatial bias on the results (figure 12A and B). For each buffer tested, a normalized corrected fluorescent signal was computed. To do so, the fluorescent signal was first averaged over the spot area. The median of the four-corner background was then subtracted from the average signal to yield the corrected fluorescent signal, which was averaged across all replicate spots. Finally, all averaged and corrected values were normalized by the highest fluorescent signal obtained among all buffers tested. Buffer performance was measured based on (i) the normalized corrected fluorescent signal intensity and (ii) the reproducibility assessed by calculating the coefficient of variation (CV) (figure 12C). The weak signal and high variation obtained when printing with glycerol confirmed that the choice of printing buffer contributed to the poor results obtained in the initial experiment. The best additives and combinations of additives for inkjet spotting were: PEG-1000, betaine, 1.3-butanediol, 2.3-butanediol and several of their pairwise combinations.

The four best printing buffers—1, 8, 12 and 28 in figure 12C, highlighted in figure 12A—were selected and used to test the capture of exosomes from solution using

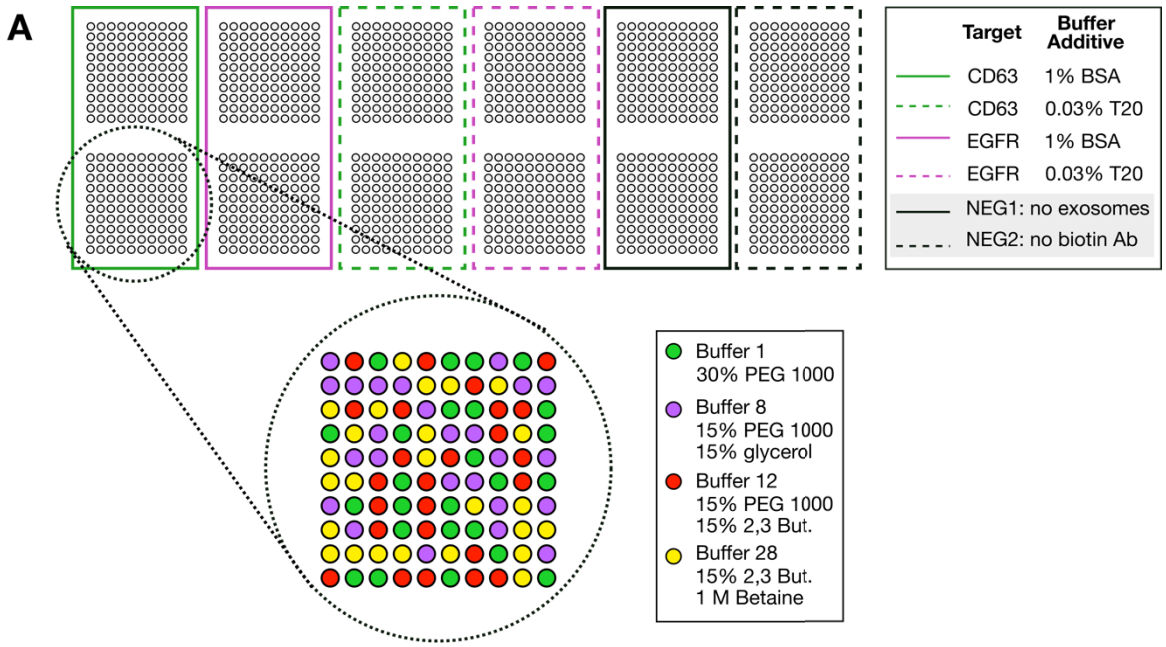

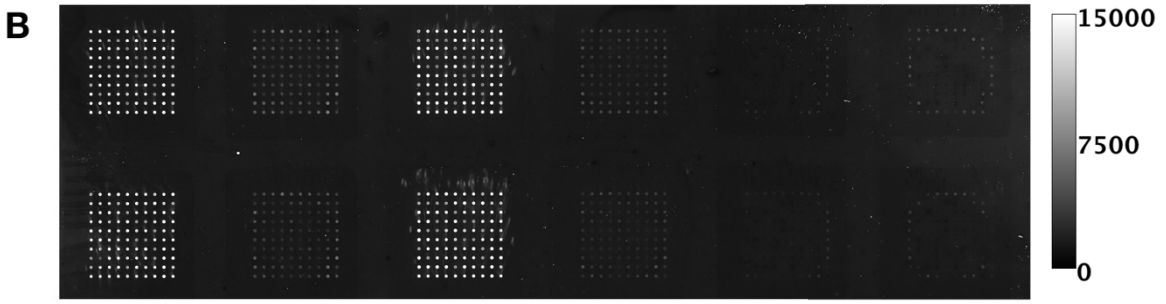

C

BUFFER	ANTI-CD63 SOLUTION CAPTURE				ANTI-EGFR SOLUTION CAPTURE				COLOR SCALE	
	0.03% TWEEN-20		1% BSA		0.03% TWEEN-20		1% BSA			
	INTENSITY	CV	INTENSITY	CV	INTENSITY	CV	INTENSITY	CV	INTENSITY	CV
1	8 389	31%	6 925	24%	1 331	55%	717	67%	17 000	30%
8	16 531	26%	18 128	18%	2 599	46%	1 352	52%	12 500	25%
12	13 686	31%	12 785	12%	1 902	43%	1 056	50%	8 000	20%
28	17 244	23%	20 926	14%	3 279	35%	1 862	34%	3 500	15%

Figure 13 Exosome capture from solution using biotinylated anti-CD63 and anti-EGFR antibodies. (**A**) Slide layout and microarray design used for the experiment. Each condition was tested on two replicate microarrays. Each 10x10 microarray comprised 25 randomized replicate spots for each printing buffer tested, as illustrated (*inset*). (**B**) Scanner image showing the raw fluorescence microarray data for the experiment illustrated in A. Fluorescence intensities are expressed in arbitrary units. (**C**) Corrected exosome GFP fluorescence intensities and CVs computed from B for all tested buffers and incubation conditions. CD63 capture led to significantly higher signal than EGFR, with printing buffers 8 and 28 yielding the highest intensities and lowest CVs. Addition of 1% BSA during the incubation of exosome-antibody complexes gave higher intensities and lower CVs than 0.03% T20. NEG1, NEG2: negative controls 1 and 2; Ab: antibody. Buffer numbers refer to the compositions presented in figure 12.

biotinylated anti-CD63 and anti-EGFR antibodies, with either 1% BSA or 0.03% Tween®20 (T20) as additives during incubation (figure 13A). The former, being a blocking agent, is mainly geared at limiting unspecific binding on the array—a considerable issue for long incubation times—, while the latter helps prevent the aggregation of exosomes in solution. In the case of T20, a 0.03% concentration was chosen in order to benefit from the dispersive action of the detergent while avoiding perturbation of exosomal membranes, which can start occurring at a concentration of 0.05%[88,144]. Buffers 8 and 28 resulted in comparably stronger GFP exosome signals than buffers 1 and 12, with CD63 capture leading to significantly more surface binding of exosomes than EGFR (figure 13C). Interestingly, while incubation with 0.03% T20 or 1% BSA did not result in significantly different signal intensities, CVs tended to be slightly lower when incubation was performed in the presence of BSA than when T20 was used for CD63-based capture. However, the high CVs and low signals obtained for EGFR-based capture did not allow any significant trends to be identified.

In summary, using this assay format, exosomes could successfully be anchored to the microarray surface and directly detected through GFP fluorescence. Nevertheless, despite the good performance of certain additives, this specific exosome capture workflow suffers from a number of flaws. Particularly, as it requires an additional chromatographic separation step—to separate the exosome-antibody complexes from unbound vesicles and antibodies—and subsequent concentration of the eluted complexes, non-negligible sample losses occur throughout the experiment. These losses can lead to weak signals and limited sensitivity, underlined by the high imaging gains (75 to 100%) that were required for data acquisition and the low signals obtained for EGFR despite its high expression in our model cell line. Moreover, biotinylated capture antibodies are required, which are not always commercially available. The requirement

for in-house or outsourced conjugation can then contribute to add even more steps and delays to an already time-consuming workflow.

Notwithstanding their shortcomings, both of these capture or detection-focused approaches highlighted promising markers and helped identify parameters that can be tuned towards the optimization of the full protocol. Consequently, we next combined the best of the two protocols to optimize an antibody microarray platform integrating both the capture of exosomes and the immunological detection of surface protein markers.

4.2 Optimization of the Exosome Capture and Detection Protocol

A full antibody microarray protocol for exosome capture and detection, presented in figure 14, comprises 6 main steps: 1) the patterning and immobilization of monoclonal primary antibodies targeting surface markers onto a functionalized glass slide, 2) the washing and blocking of the patterned surface, 3) the incubation with and surface-based affinity capture of sample exosomes, 4) the washing and incubation with primary detection antibodies against proteins of interest, 5) the washing and incubation with fluorescently-labeled secondary antibodies or streptavidin, and 6) the detection of the bound and immunolabeled exosomes. For capture and detection, the markers considered included 3 exosome markers—CD63, CD9 and CD81—and the A431-overexpressed EGFR.

Each step of the assay comprises several parameters which can be optimized to improve the assay output. For inkjet printing, the printing buffers, the antibody concentration, and the surface chemistry of the functionalized slide can be varied. For the washing and blocking steps, the choice of washing method and the contents of the washing buffers have to be considered, while the nature of the incubation buffer and antibody concentration are important for both the capture and detection steps. Out of those parameters, we chose to focus on the printing buffer and antibody concentration

for inkjet printing, and on the additives in the sample incubation buffer for the capture and detection steps. Indeed, the printing buffer and capture antibody concentration were previously shown to strongly influence the binding capabilities of an antibody microarray[134], while the optimization of the sample incubation buffer is essential to minimize unspecific binding and preserve sample integrity during incubation with the array.

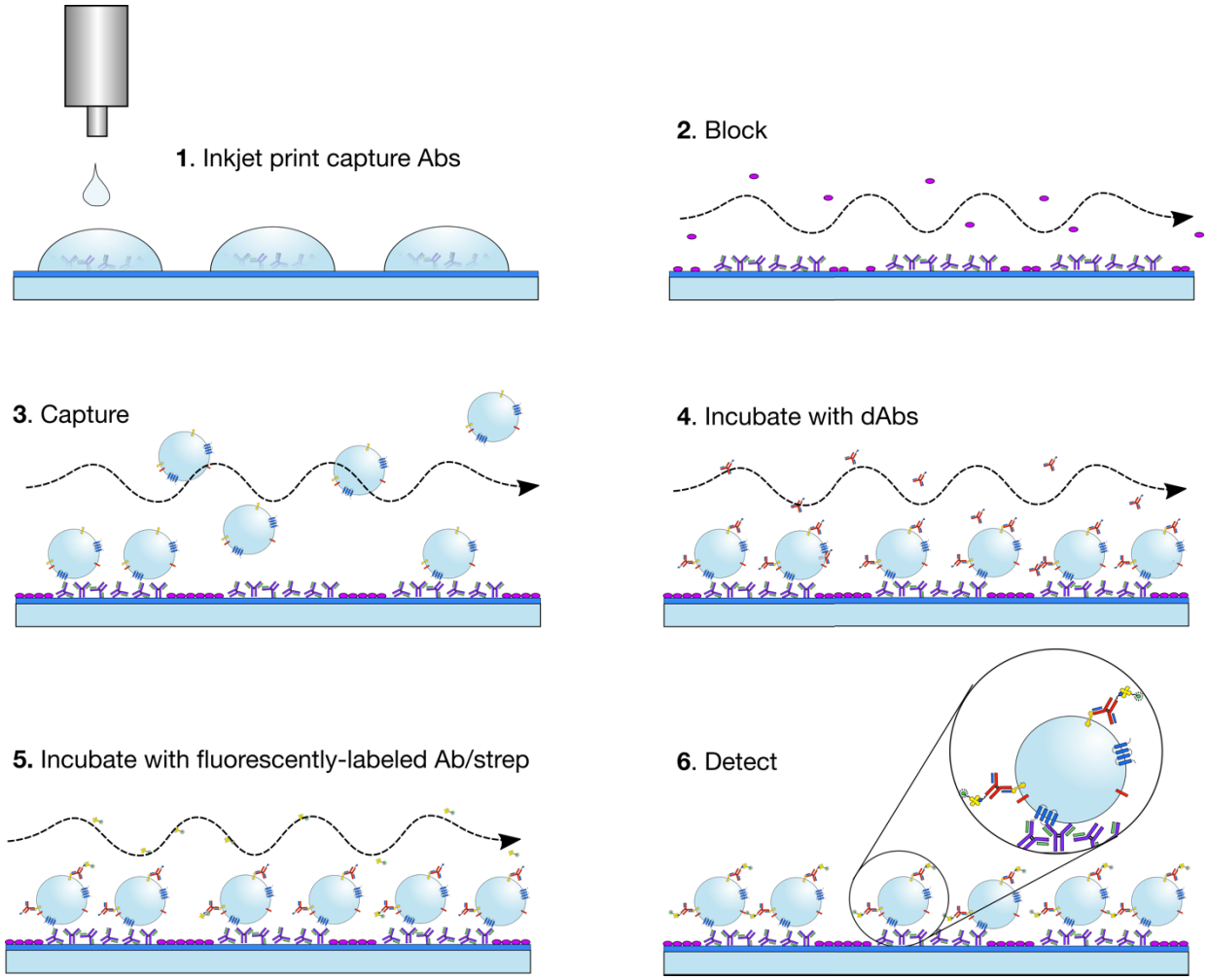

Figure 14 Workflow of the exosome capture and detection assay: *1*) capture antibodies are inkjet-printed on an aldehyde-functionalized slide (PolyAn 2D-Aldehyde), *2*) the slide is washed and unoccupied sites are blocked, *3)* the sample is incubated on the antibody spots and the exosomes captured based on their surface protein markers, *4*) the slide is washed and incubated with unconjugated or biotinylated (as illustrated) primary dAbs, *5*) the slide is washed and incubated with fluorescently-labeled secondary antibodies or streptavidin (as illustrated), and *6*) immobilized immunolabeled exosomes are detected using a confocal microarray scanner.

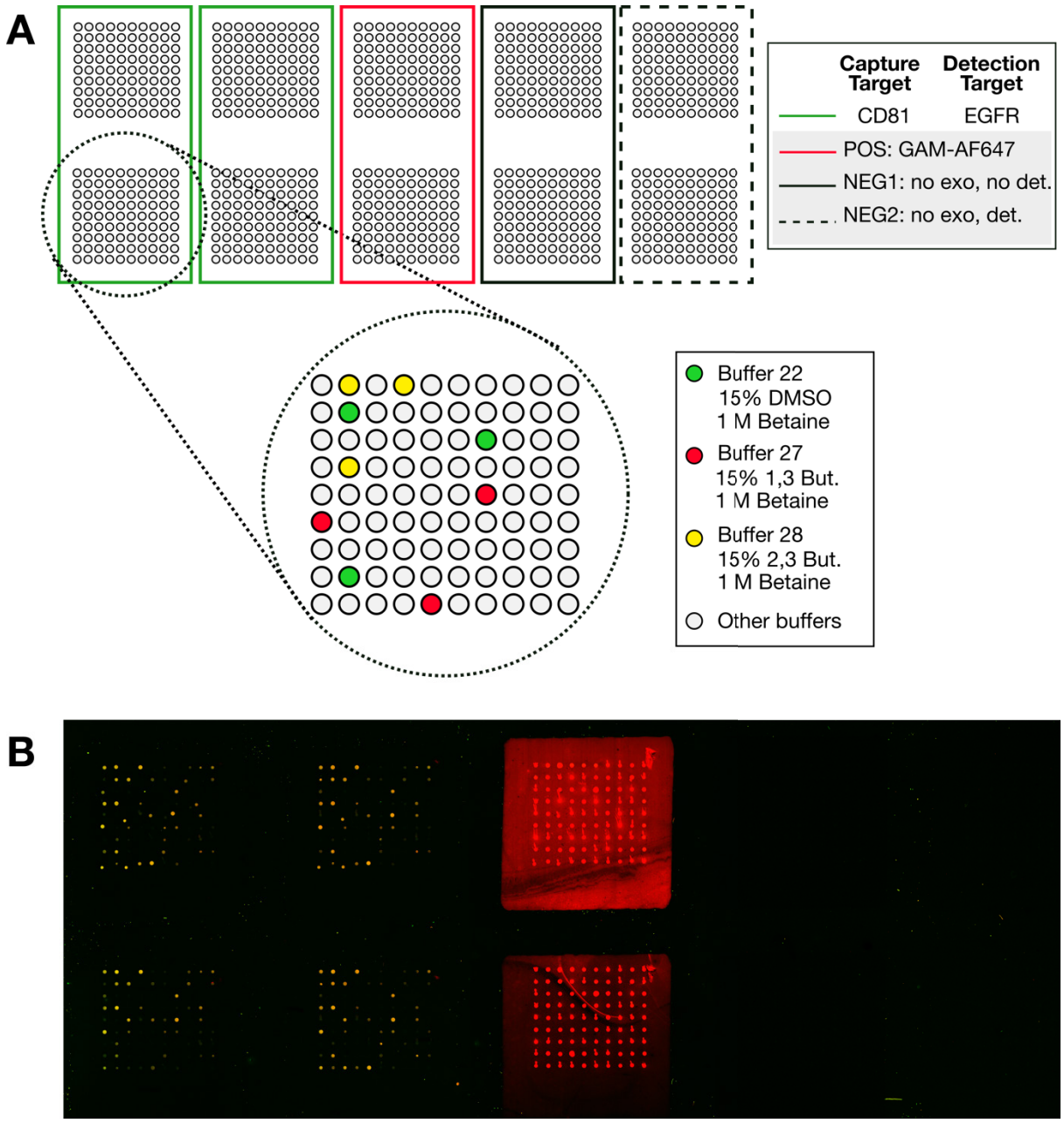

Figure 15 Example microarray layout and microarray scanner image for the printing buffer optimization experiments. (**A**) Experimental layout of the anti-CD81 Ab printing buffer testing experiment with EGFR detection. There were 12 technical replicates, or spots, per printing buffer tested, and 3 controls: *i)* a secondary goat anti-mouse (GAM) antibody which detects the spotted mouse anti-CD81 antibody (positive control); *ii)* incubation with buffer (PBS) instead of the exosome and detection antibody incubation steps (negative control); and *iii)* incubation with PBS at the exosome incubation step, but not at the detection step (negative control). The randomized positions of the 3 overall best printing buffers within an individual microarray well are shown. (**B**) Microarray scanner image of the microarray wells, disposed as presented in A. The exosome GFP signal is colored green, while the anti-EGFR and GAM signals are colored red. Colocalization results in a yellow signal. The image highlights significant but low CD81-driven exosome capture that colocalizes with EGFR detection, with negligible signal in the negative controls. AF647: Alexa Fluor® 647; POS: positive control; NEG: negative control; exo: exosome.

To guide the optimization of the printing buffer, corrected signals and CVs were again used to assess the intensity and reproducibility of each combination of capture and detection antibodies, or "condition", which was tested on 6 to 18 distinct randomized microarray spots (3 per individual microarray) depending on exosome sample availability. For direct capture experiments, the intrinsic exosome GFP fluorescence signal was measured for each capture antibody spotted on the array. For full assay experiments, three distinct capture-detection pairs—CD9/CD63, EGFR/CD63, and CD81/EGFR—were evaluated through the fluorescent signal from fluorescently-labeled secondary antibodies or streptavidin. The experimental layout and scanner image of the CD81/EGFR experiment are presented in figure 15 as an example.

To compare all printing buffers for each individual targeted surface protein (or protein combination), the corrected signals were normalized on a condition-by-condition basis through division by the maximum corrected fluorescence value obtained for each capture antibody or combination of capture and detection antibodies. Since some antibodies yielded very low intrinsic GFP and/or immunolabeling signals, proceeding this way helped emphasize the best buffers for each individual condition, independently of the abundance of the targeted proteins in the sample. There were also a few reasons for computing the corrected intensity instead of the signal-to-noise ratio (SNR) in this case. The SNR quantifies the precision of a system and its computation considers both the intensity and the variance of the signal[145]. It helps characterize the performance of a system, but is generally not the chosen metric when comparing the fluorescent signal associated with different biologically-relevant targets, where the fluorescent signal to which the background has been subtracted is usually preferred[145]. When looking at the

A

	PRINTING BUFFER	NORMALIZED CORRECTED EXOSOME GFP SIGNAL				NORMALIZED DETECTION SIGNAL			AVERAGE	RANK
		CD63	EGFR	CD9	CD81	CD9/CD63	EGFR/CD63	CD81/EGFR		
1	30% PEG 1000	41%	76%	17%	3%	23%	70%	0%	33%	21
2	30% Glycerol	52%	27%	36%	37%	48%	25%	36%	38%	19
3	30% DMSO	96%	58%	44%	6%	61%	60%	6%	47%	17
4	30% Ethylene Glycol	94%	69%	59%	34%	70%	75%	40%	63%	9
5	30% 1,3-butanediol	88%	77%	76%	1%	86%	83%	0%	58%	13
6	30% 2,3-butanediol	86%	54%	72%	1%	89%	53%	0%	50%	16
7	2 M Betaine	75%	89%	93%	48%	92%	91%	51%	77%	5
8	15% PEG 1000, 15% Glycerol	18%	25%	12%	14%	16%	22%	11%	17%	25
9	15% PEG 1000, 15% DMSO	10%	48%	4%	1%	6%	45%	0%	16%	26
10	15% PEG 1000, 15% EtGly	4%	43%	3%	1%	4%	40%	0%	14%	28
11	15% PEG 1000, 15% 1,3 But.	5%	60%	3%	1%	4%	58%	0%	19%	24
12	15% PEG 1000, 15% 2,3 But.	4%	41%	4%	2%	5%	38%	0%	13%	29
13	15% PEG 1000, 1 M Betaine	59%	48%	35%	4%	49%	48%	1%	35%	20
14	15% Glycerol, 15% DMSO	51%	19%	54%	50%	64%	18%	53%	44%	18
15	15% Glycerol, 15% EtGly	48%	11%	42%	29%	49%	8%	27%	30%	22
16	15% Glycerol, 15% 1,3 But.	38%	7%	20%	10%	27%	4%	9%	16%	27
17	15% Glycerol, 15% 2,3 But	47%	8%	28%	21%	38%	5%	19%	23%	23
18	15% Glycerol, 1 M Betaine	62%	51%	87%	84%	92%	52%	78%	73%	6
19	15% DMSO, 15% EtGly	91%	94%	59%	4%	68%	94%	2%	58%	14
20	15% DMSO, 15% 1,3 But.	96%	97%	78%	1%	93%	98%	1%	66%	7
21	15% DMSO, 15% 2,3 But.	100%	79%	78%	3%	95%	81%	2%	62%	10
22	15% DMSO, 1 M Betaine	80%	81%	92%	81%	97%	86%	82%	86%	3
23	15% EtGly, 15% 1,3 But.	99%	80%	77%	2%	92%	83%	1%	61%	11
24	15% EtGly, 15% 2,3 But.	100%	74%	80%	10%	93%	81%	13%	64%	8
25	15% EtGly, 1 M Betaine	75%	81%	95%	84%	97%	86%	80%	86%	4
26	15% 1,3 But., 15% 2,3 But.	94%	81%	72%	1%	89%	87%	0%	60%	12
27	15% 1,3 But., 1 M Betaine	82%	100%	92%	95%	99%	100%	97%	95%	1
28	15% 2,3 But., 1 M Betaine	80%	87%	100%	100%	100%	90%	100%	94%	2
29	PBS	59%	64%	N/A	31%	N/A	67%	36%	51%	15
	AVERAGE	63%	60%	54%	26%	62%	60%	26%		

SCALE
100%
80%
60%
40%
20%
0%

B

	PRINTING BUFFER	CORRECTED EXOSOME GFP CV				DETECTION CV			AVERAGE	RANK
		CD63	EGFR	CD9	CD81	CD9/CD63	EGFR/CD63	CD81/EGFR		
1	30% PEG 1000	15%	9%	24%	24%	25%	20%	58%	26%	12
2	30% Glycerol	20%	26%	85%	46%	59%	26%	36%	42%	25
3	30% DMSO	21%	15%	15%	27%	24%	13%	33%	21%	7
4	30% Ethylene Glycol	23%	28%	40%	55%	35%	30%	62%	39%	24
5	30% 1,3-butanediol	25%	11%	22%	22%	21%	13%	39%	22%	9
6	30% 2,3-butanediol	21%	15%	18%	28%	23%	14%	68%	28%	15
7	2 M Betaine	12%	13%	29%	21%	22%	17%	17%	19%	6
8	15% PEG 1000, 15% Glycerol	40%	12%	43%	20%	39%	19%	18%	27%	14
9	15% PEG 1000, 15% DMSO	104%	15%	17%	14%	30%	20%	126%	48%	27
10	15% PEG 1000, 15% EtGly	30%	12%	48%	24%	42%	18%	88%	39%	23
11	15% PEG 1000, 15% 1,3 But.	39%	8%	56%	14%	47%	16%	53%	34%	20
12	15% PEG 1000, 15% 2,3 But.	26%	13%	49%	73%	40%	22%	92%	46%	26
13	15% PEG 1000, 1 M Betaine	17%	30%	46%	24%	37%	31%	53%	35%	21
14	15% Glycerol, 15% DMSO	29%	23%	34%	38%	25%	30%	36%	31%	17
15	15% Glycerol, 15% EtGly	14%	24%	69%	42%	41%	31%	36%	37%	22
16	15% Glycerol, 15% 1,3 But.	22%	19%	60%	65%	50%	47%	75%	49%	28
17	15% Glycerol, 15% 2,3 But	25%	43%	67%	63%	52%	60%	57%	53%	29
18	15% Glycerol, 1 M Betaine	12%	12%	27%	30%	26%	14%	31%	22%	8
19	15% DMSO, 15% EtGly	24%	13%	32%	29%	32%	13%	28%	24%	11
20	15% DMSO, 15% 1,3 But.	20%	11%	17%	50%	17%	18%	65%	29%	16
21	15% DMSO, 15% 2,3 But.	16%	15%	24%	63%	15%	16%	64%	31%	18
22	15% DMSO, 1 M Betaine	4%	9%	23%	11%	15%	12%	15%	13%	1
23	15% EtGly, 15% 1,3 But.	18%	11%	20%	48%	20%	16%	48%	26%	13
24	15% EtGly, 15% 2,3 But.	21%	16%	14%	28%	18%	19%	42%	23%	10
25	15% EtGly, 1 M Betaine	27%	9%	29%	15%	18%	15%	8%	17%	4
26	15% 1,3 But., 15% 2,3 But.	18%	14%	20%	86%	24%	18%	49%	32%	19
27	15% 1,3 But., 1 M Betaine	6%	11%	22%	23%	18%	14%	22%	17%	3
28	15% 2,3 But., 1 M Betaine	11%	13%	22%	16%	19%	12%	5%	14%	2
29	PBS	14%	16%	N/A	22%	N/A	18%	19%	18%	5
	AVERAGE	23%	16%	35%	35%	30%	21%	46%		

SCALE
30%
25%
20%
15%
10%
5%

Figure 16 Normalized corrected signal intensities (**A**) and CVs (**B**) obtained for exosome capture (left portion of the tables) and detection (right portion of the tables) when probing selected markers or combinations of markers, respectively, using antibody microarrays printed with the 29 buffers under study. Each printing buffer is assigned a rank in terms of both intensity and CV based on its average performance across all examined conditions. Capture and detection conditions were weighted equally to obtain the average. There are several good buffer options for CD63, EGFR and CD9 antibodies, with the highest signals and lowest CVs obtained with buffers that contain betaine, 1,3-butanediol and 2,3-butanediol. CD81-driven capture yielded notably low signal intensities (see also figure 15) and high CVs with most buffers, which may be due to its low expression in the exosome samples analyzed.

fluorescent signal obtained when labeling different exosome proteins, the corrected signal provides a straightforward way to draw conclusions about protein expression. Furthermore, the variance of the signal for each studied combination is already considered through the computation and comparison of CVs.

4.2.1 The Choice of Printing Buffer Impacts Exosome and Detection Signal Intensity and Reproducibility

Figure 16 presents the normalized intensity and CV values for all examined capture and detection conditions. With regards to both signal intensity and reproducibility, some buffers perform much better than others in general, but there are also important differences between how individual buffers fare depending on the proteins(s) under study. For instance, while buffers incorporating 1,3 and 1,2-butanediol, individually or combined, provide reasonably high normalized signals for capture and detection combinations involving CD63, EGFR and CD9, they perform badly when CD81 is part of the combination. Contrastingly, buffers containing glycerol are associated to better performances when CD63 and CD81 are targeted than when EGFR and CD9 are probed. Interestingly, there is considerable overlap between the patterns observed for CVs and those associated with intensity values. A possible explanation is that stronger signals are relatively less sensitive to variations due to extrinsic factors, such as patterns in the slide coating or local changes in the amount of unspecific binding. However, signal intensity and reproducibility can also diverge, as evidenced by the differences between the two tables of figure 16; for instance, while buffers containing PEG-1000 as an additive (8, 9, 10, 11, 12, and 13) offer good reproducibility compared to other options for EGFR targeting, the signal intensity remains fairly low on the comparative scale. This can be explained by the fact that consistently low signals can still produce good CVs.

For normalized intensities and CVs, there is a strong correlation between capture and detection performances. For example, targeting CD81 for capture generally leads to

poor results—overall high CVs and low normalized intensities for buffers that otherwise perform well—, while EGFR offers more consistency. Accordingly, CD81-targeted capture followed by EGFR detection gives suboptimal results, but EGFR-targeted capture followed by CD63-detection offers better performance. Such patterns tend to confirm our earlier assumption that efficient exosome capture is paramount to the detection of additional markers with high sensitivity. Of note, the limited robustness achieved with CD81, and possibly CD9, might be related to the abundance of such markers in the analyzed samples. Indeed, given that conventional exosome markers, including CD81 and CD9, have been shown to be more abundant in specific exosome subsets (large or small exosomes) in a cell type-dependent manner[77], and considering that our chosen exosome purification method limits the number of smaller exosomes that can be retrieved, our analyzed samples simply could have had a low CD81/CD9 content.

Overall, it is preferable to opt for buffers that offer consistent performance for intensity and CVs across all studied conditions. To compare all the options, buffers were first ranked independently for their performance in terms of intensity and reproducibility, yielding two buffer lists. For each buffer and list, the ranks were derived from the average performance for each criterion, expressed in percentage (see figure 16). Comparison of the two lists identifies buffers 22, 27 and 28 as yielding the highest intensity and best reproducibility. Interestingly, all of those buffers contain betaine, which hence seems to be an important additive for signal strength and robustness. Moreover, the good performance obtained with buffer 28, which also contains 2,3-butanediol, is consistent with previous work involving antibody microarrays[134]. Between the three best-ranking buffers, the difference in performance is minimal, and all are likely to perform well for experiments integrating numerous antibodies and antibody combinations. Buffer 28 was chosen to print the antibody microarrays used in the paneling experiment, presented in a later section.

A

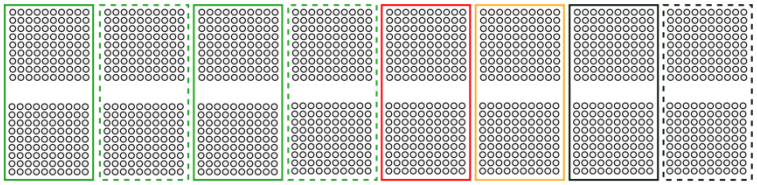

Capture Target	Sample Buffer Particularity
CD63	1% BSA
CD63	0.03% T20
CD63	GAM-AF647
CD63	PBS, no exo
R (GAR)	1% BSA
R (GAR)	0.03% T20

B

C

	PRINTING BUFFER (ANTI-CD63 AB)	CORRECTED EXOSOME GFP SIGNAL			
		PBS + 0.03% TWEEN-20		PBS + 1% BSA	
		INTENSITY	CV	INTENSITY	CV
1	30% PEG 1000	3 204	52%	14 771	15%
2	30% Glycerol	2 713	39%	18 691	20%
3	30% DMSO	9 287	18%	34 444	21%
4	30% Ethylene Glycol	11 915	45%	33 563	23%
5	30% 1,3-butanediol	8 640	14%	31 362	25%
6	30% 2,3-butanediol	9 840	28%	30 808	21%
7	2 M Betaine	4 456	14%	26 918	12%
8	15% PEG 1000, 15% Glycerol	904	20%	6 372	40%
9	15% PEG 1000, 15% DMSO	1 198	34%	3 622	104%
10	15% PEG 1000, 15% EtGly	776	19%	1 524	30%
11	15% PEG 1000, 15% 1,3 But.	1 080	72%	1 771	39%
12	15% PEG 1000, 15% 2,3 But.	778	31%	1 440	26%
13	15% PEG 1000, 1 M Betaine	3 652	17%	21 168	17%
14	15% Glycerol, 15% DMSO	2 629	24%	18 229	29%
15	15% Glycerol, 15% EtGly	3 095	54%	17 132	14%
16	15% Glycerol, 15% 1,3 But.	1 806	30%	13 679	22%
17	15% Glycerol, 15% 2,3 But	3 338	64%	16 719	25%
18	15% Glycerol, 1 M Betaine	3 499	20%	22 029	12%
19	15% DMSO, 15% EtGly	9 557	25%	32 515	24%
20	15% DMSO, 15% 1,3 But.	10 665	22%	34 269	20%
21	15% DMSO, 15% 2,3 But.	11 270	27%	35 640	16%
22	15% DMSO, 1 M Betaine	4 749	21%	28 489	4%
23	15% EtGly, 15% 1,3 But.	9 687	11%	35 219	18%
24	15% EtGly, 15% 2,3 But.	11 031	23%	35 697	21%
25	15% EtGly, 1 M Betaine	4 912	18%	26 860	27%
26	15% 1,3 But., 15% 2,3 But.	8 297	17%	33 398	18%
27	15% 1,3 But., 1 M Betaine	5 627	27%	29 427	6%
28	15% 2,3 But., 1 M Betaine	5 968	43%	28 589	11%
29	PBS	7 122	29%	30 650	13%
	AVERAGE	5619	30%	22931	23%

COLOR SCALE	
INTENSITY	CV
40 000	30%
30 000	25%
20 000	20%
10 000	15%
0	10%

Figure 17 Incubation of exosomes on a microarray of anti-CD63 antibodies with two different buffer additives. (**A**) Layout of the experiment. Each buffer additive was tested in 4 replicate wells containing 3 replicate spots per printing buffer (6 for PBS). The incubation of exosomes on a microarray of unspecific goat anti-rabbit antibodies and the incubation of exosome-free PBS were implemented as negative controls. Successful microarray spotting was validated through incubation with fluorescent goat anti-mouse (GAM) antibodies which bind to the patterned mouse antibodies. (**B**) Scanner image of the microarray results. The exosome GFP signal is colored green, while the printing test appears in red. (**C**) Absolute corrected fluorescent intensities and CVs obtained when sample exosome suspensions are incubated overnight in incubation buffers containing two different additives, T20 at a concentration of 0.03% (*left*) and BSA at a concentration of 1% (*right*). Incubation with T20 results in generally lower intensities and higher CVs, probably due to the interaction of T20 with the exosomal membranes. Exo: exosome, AF: Alexa Fluor®.

4.2.2 *The Sample Incubation Conditions and Printing Buffer Concentration Also Impact Signal Intensity and Reproducibility*

Because targeting CD63 consistently gave strong absolute intensity values in buffer optimization experiments, we chose to use microarrays composed of anti-CD63 antibody spots for further optimization experiments. To look at the impact of the exosome incubation buffer on the direct GFP exosome signal, BSA and T20 were again investigated as additions to the incubation buffer, following the experimental layout in figure 17A. Spots patterned using the different printing buffers were again randomized within each microarray well.

A micrograph of the results is shown in figure 17B, while figure 17C presents the exosome GFP fluorescent intensities and associated CVs obtained when A431 exosome suspensions are incubated on anti-CD63 antibody spots in buffers containing 1% BSA or 0.03% T20. The fluorescent intensities were averaged and corrected as described previously. The average intensity for the two studied conditions was significantly different, and the effect was independent of the printing buffer used. Indeed, corrected intensity values obtained for exosomes incubated with 1% BSA mostly range between 20,000 and 35,000 RFU, with an average of around 23,000 RFU, while values for 0.03% T20 rarely exceed 10,000 RFU with an average of around 5,500 RFU (figure 17C). Given that the GFP signal used for quantification comes from a transmembrane fusion protein, these discrepancies point at some effect of the T20 on membrane integrity, despite the low concentration used. More specifically, it is possible that the recommended 0.03% concentration, which was originally chosen to address aggregation concerns in TRPS measurements[88], gradually damages membranes when used for long incubation times. Such effects would be more likely to go unnoticed when performing shorter measurements or experiments. Interestingly, this effect was not observed previously when the two buffer additives were tested for exosome capture from solution (section

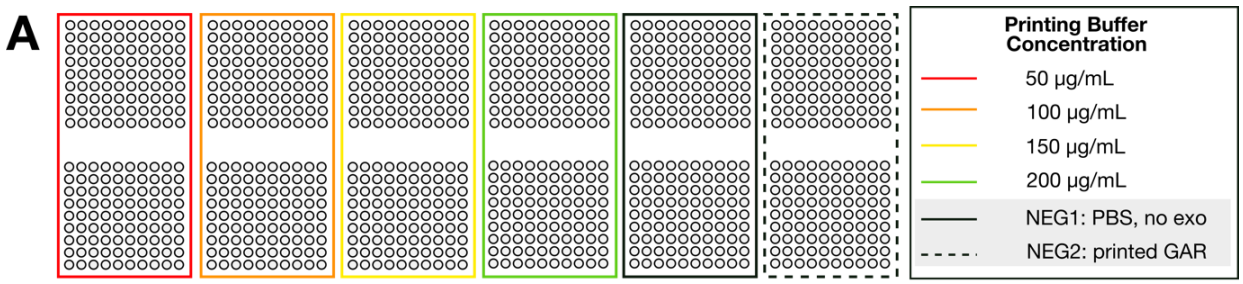

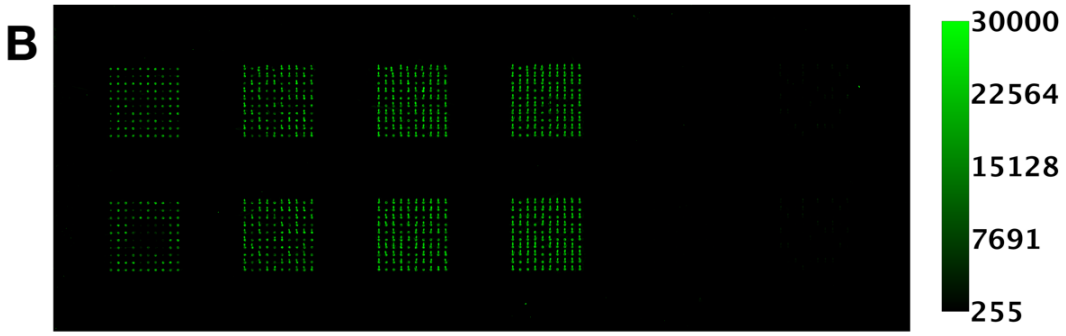

C

	PRINTING BUFFER	CAPTURE ANTIBODY CONCENTRATION (µg/mL) 50 INTENSITY	50 CV	100 INTENSITY	100 CV	150 INTENSITY	150 CV	200 INTENSITY	200 CV
22	15% DMSO, 1 M Betaine	16 003	39%	19 391	30%	21 118	17%	21 140	12%
27	15% 1,3 But., 1 M Betaine	17 341	25%	18 198	32%	21 594	21%	21 042	12%
28	15% 2,3 But., 1 M Betaine	16 825	36%	18 500	31%	21 289	21%	21 248	16%
29	PBS	6 810	39%	20 838	25%	21 240	19%	20 932	14%
AVERAGE		14 245	34%	19 232	29%	21 310	20%	21 090	14%

COLOR SCALE							
INTENSITY	25 000	20 000	15 000	10 000	5 000	0
CV	30%	25%	20%	15%	10%	5%

Figure 18 Incubation of exosomes on microarrays of anti-CD63 antibodies spotted at different concentrations. (**A**) Layout of the experiment. There were 2 replicate wells per concentration tested, each with 25 replicate spots per buffer. Incubation on microarrays of unspecific goat anti-rabbit (GAR) antibodies and with exosome-free PBS were implemented as negative controls. **(B)** Fluorescence scanner image obtained when exosome suspensions are incubated over anti-CD63 antibody spots printed at 4 different concentrations . The exosome GFP signal is shown in green. The wells follow the layout in A. **(C)** Corrected fluorescent intensities and CVs for the data shown in B. The corrected intensity increases and the CV decreases when the antibody concentration increases.

4.1.2). It may be that the more efficient mixing achievable in solution, and the ensuing saturation of the free antibodies, helped counteract the effects of membrane damage. As for CVs, no drastic differences are observed between the average values obtained for the two buffers, although the addition of T20 seems to increase variability.

We evaluated the effects of the printing antibody concentration on exosome binding by printing anti-CD63 at concentrations of 50 to 200 µg/mL as antibody microarrays and incubating them with exosome suspensions (figure 18A). A considerable increase in intensity was observed by increasing the concentration from 50 µg/mL to

100 μg/mL, with only modest increases for 100, 150 and 200 μg/mL (figure 18C). Higher printing concentrations were associated with lower CVs, even for the highest concentrations tested. Indeed, a 6% difference on average can be observed between antibody concentrations of 150 and 200 μg/mL (figure 18C). It may be that intensities plateau due to steric hindrance (i.e. a limited number of exosomes can bind to any given spot), while higher printing buffer concentrations help saturate the active sites on the functionalized glass surface, lowering interspot variability and thus CVs. Overall, a concentration of 100 to 150 μg/mL offers a good compromise in terms of performance and reagent cost.

4.3 Assay Validation: Phenotyping of Exosomes from 4 Cell Lines Using a Panel of 15 Antibodies

A phenotyping experiment involving exosomes from 4 cell lines—MDA-MB-231 (metastatic adenocarcinoma), A431 (epidermoid carcinoma), SK-BR-3 (metastatic adenocarcinoma), and BT-474 (ductal carcinoma)—was carried out to validate the optimized platform. A selection of 15 markers including integrins (αVβ5, α2, α6, β1, β4), cancer-related markers (CD44, PD-1, PDL-1, ADAM10, CD133, CCR5, EGFR, EpCAM), and common exosome proteins (CD82, CD63) was targeted through printed capture antibody spots, which were randomized as previously described (figure 19A). Surface-bound exosomes were detected using biotinylated anti-CD63 antibodies and Alexa Fluor® 647-labeled streptavidin, as CD63 gave higher and more robust capture and detection signals than CD9 and CD81 in previous experiments.

4.3.1 Chosen Protein Targets Carry Out Important Roles in Cancer Pathogenesis

The protein targets were chosen in part due to their expression or upregulation in MDA-MB-231 and/or epithelial (or mesenchymal) A431 cells, as reported by a collaborator and in the literature[1,141], but also because of their implication in cancer progression and

metastasis, or their known expression in exosomes and EVs.

Firstly, CD44, CD133 and EpCAM are known cancer-initiating cell markers[146-148]. CD44 is a member of the cell adhesion molecule (CAM) family[149] and is involved in the regulation of cellular processes such as growth, survival, differentiation and motility[150]. In cancer, its mode of action can either be favorable or unfavorable to malignancy depending on extracellular cues[150]. CD133 is a transmembrane glycoprotein of the prominin family[151] expressed by hematopoietic stem cells and progenitor cells of the bone marrow[152]. While its function is still unclear, it is known to participate in the formation of membrane protrusions, and its expression has been found to correlate to a stem cell phenotype in several cancers[151]. Epithelial cell adhesion molecule (EpCAM) is an atypical cell adhesion protein which, through interaction with E-cadherin, negatively regulates adhesion[153]. In normal epithelial tissue, it is essential to epithelial development, function, and integrity, but in malignancy, high expression levels can favour enhanced plasticity, resulting in increased cell proliferation and motility[153].

Secondly, integrins are cell adhesion receptors with affinities for extracellular matrix (ECM) building blocks (e.g. laminin, collagen, fibronectin) that mediate how cells bind and respond to the ECM[154-156]. Their implication in cancer is multifaceted. For instance, changes to the composition and mechanical properties of the ECM, mediated by and sensed through integrins, have been linked to increased cell proliferation[154]. Furthermore, integrins were found to contribute to pre-metastatic niche formation and to determine to which organs metastases spread[1].

Thirdly, members of the a disintegrin and metalloproteinase (ADAM) family—membrane-associated metalloproteinases, some of which have proteolytic potential[157]—including ADAM10, are overexpressed in several cancers and are thought to contribute to cell growth and invasion[158]. ADAMs cleave transmembrane proteins, solubilizing the ectodomain of various proteins (cytokines, growth factors, receptors, adhesion molecules)[157,159]. They are thus potentially involved in several aspects of the tumour

microenvironment (inflammation, immunity, angiogenesis, etc.)[157] ADAM10, more specifically, truncates HER2, making it constitutively active, and sheds HER2 ligands that participate in HER receptor activation[160]. This phenomenon is believed to mediate resistance in cancer cells during breast cancer treatment with anti-HER2 antibodies[160].

Fourthly, programmed cell death protein 1 (PD-1) and programmed death-ligand 1 (PD-L1) form an immunoreceptor-ligand pair that regulates T-cell activation, tolerance and immune-mediated tissue damage[161]. The costimulatory pathway it is involved in can result in inhibitory signals that make anti-tumour defenses ineffective[161-163].

Fifthly, CC chemokine receptor 5 (CCR5) is a G protein-coupled receptor that is mainly known for being the principal HIV coreceptor[164]. However, it also plays important roles in the trafficking and function of various immune cells, including memory and effector T-lymphocytes, macrophages, and immature dendritic cells[165]. In cancer, these functions make the receptor instrumental in the establishment of an immunosuppressive environment[166]. CCR5 is also a pro-tumour chemokine receptor[164] and was shown to have pro-invasive effects on migration and invasion in human cancers[166,167], and to promote proliferation in basal breast cancer subtypes[166].

Sixthly, epidermal growth factor receptor (EGFR), a common target in cancer therapy[168], is a transmembrane glycoprotein belonging to the erbB family of tyrosine kinase receptors[169]. Following ligand binding, it recruits, through autophosphorylation, important transducers and activator molecules that trigger signal transduction pathways involved in proliferation, differentiation and survival[169]. Its overexpression in cancer results in enhanced signal generation, fostering growth and invasiveness in altered cells[169]. Finally, CD63 and CD82, commonly found in exosomes and EVs[8], are tetraspanins—proteins characterized by their four transmembrane domains and role in membrane protein trafficking and compartmentalization[170]. CD82, specifically, was also found to have a tempering effect on migration and cell invasion, thus contributing to metastasis suppression[171].

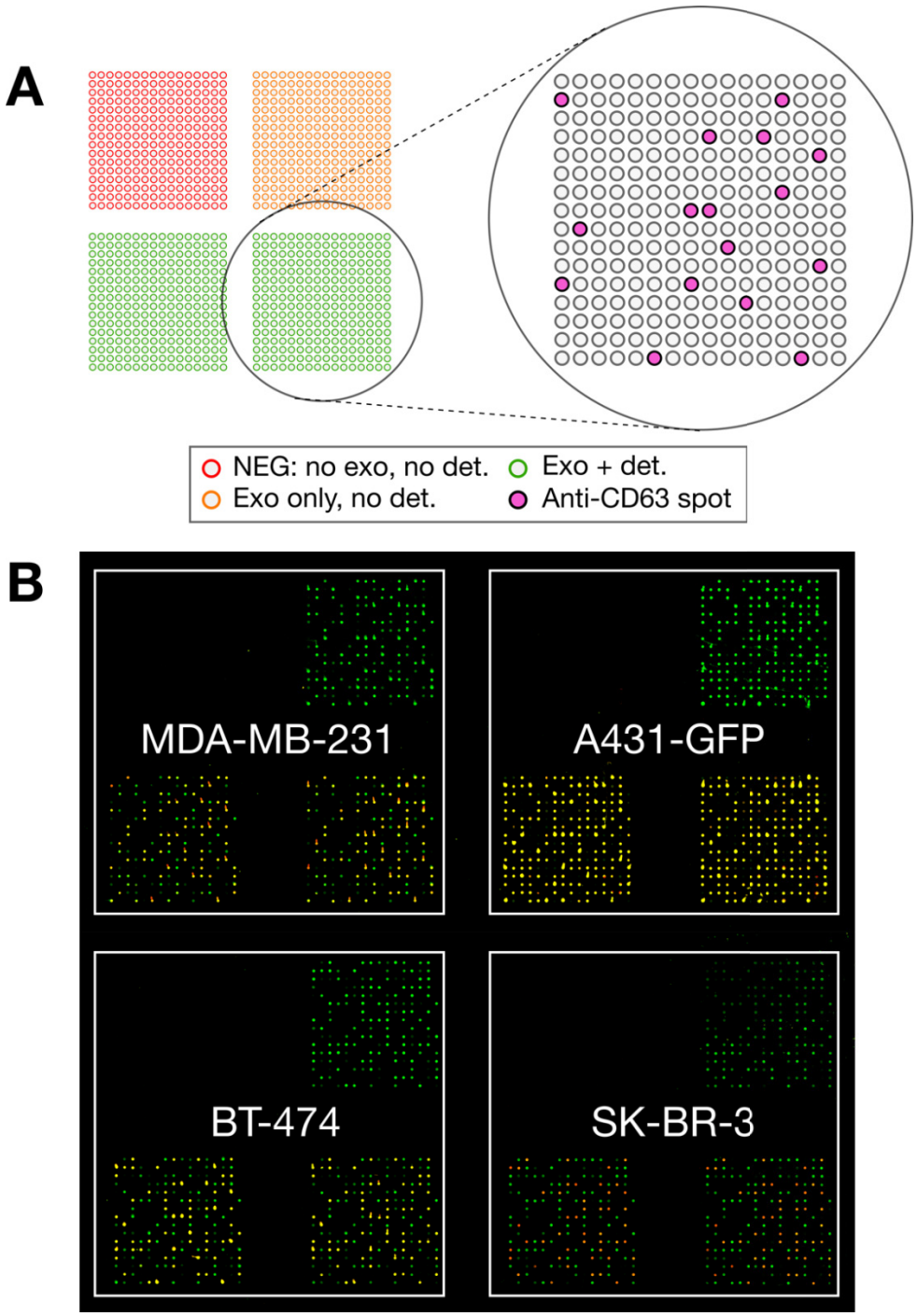

Figure 19 Experiment layout and fluorescence results of a phenotyping experiment (one biological replicate) involving exosomes from 4 different cancer cell lines. (**A**) Experimental layout used for each cell type analyzed. There were two replicate wells for the complete assay, one well for exosome capture only (without CD63 detection) and one well for a negative control (buffer only). 15 capture antibodies were spotted with 16 replicates each per microarray in random positions. The layout of the random anti-CD63 capture spots is shown for reference, and the positions of other antibodies are described in Supplementary Table I. (**B**) Microarray scanner images of anti-CD63 binding on exosomes bound by the different capture antibodies. Exosomes are stained with ExoGlow™ Green (except for A431 exosomes which also express a GFP fusion protein) and represented in green, while the detection signal (Alexa Fluor® 647) is colored red. Colocalization of the exosome and detection signal appears yellow.

4.3.2 *Phenotyping of Four Cancer Cell Lines Confirms Known Expression Patterns and Highlights New Ones*

Figure 19A presents the experimental layout, which includes two technical replicate wells for the complete sandwich assay, a well for exosome capture without CD63 detection, and a negative control without exosomes and detection antibodies. Figure 19B presents a fluorescence scanner image of the resulting microarray spots, while table 3 presents the CD63 detection fluorescence intensities (corrected as previously described) and CVs obtained for the 15 markers of interest, plus a negative control that also serves as a printing control (fluorescent goat anti-mouse antibodies, GAR-AF546). Figure 19B and table 3 illustrate that cell-line specific protein expression patterns can be successfully highlighted using ExAM. Notably, A431 exosomes show particularly strong expression of many of the probed surface proteins, including high levels of ADAM10, integrin β1, and integrin α2, which have all previously been found to be upregulated in mesenchymal A431 cells[141]. MDA-MB-231 exosomes were found to contain moderate-to-low levels of integrins β1 and α2, which have been reported to be upregulated in lung-tropic sub-lines of MDA-231 cells[1]. Interestingly, integrin β4, also upregulated in one lung metastatic cell line[1], integrin α6, previously found to be enriched in MDA-MB-231 exosomes compared to cell lysates[172], and CD44, also previously detected in MDA-231 cells[173], were not detected. It is possible that their expression was too low to yield significant signal. By contrast, exosomes from BT-474 and SK-BR-3 cells only revealed a few of the markers under study, with EGFR, CD82, ADAM10 and CD63 being detected in all the samples. Since EGFR is known to be expressed in all cell types analyzed[142,174], CD82 and CD63 are common in exosomes[8], and ADAM10 is ubiquitous in most tissues[175], their presence in the probed samples was to be expected. EpCAM, which was previously found in MDA-231, BT-474 and SK-BR-3 cells, was also detected in the exosomes samples prepared from those three cell lines[173]. To our knowledge, the other proteins in the panel have not yet

been identified or found to be upregulated in proteomic studies of BT-474 and SK-BR-3 cells and their secretome (including EVs)[176-178].

MDA-MB-231, BT-474 and SK-BR-3 breast cancer cells are regularly used in research and represent different subtypes of the disease, with MDA-231 belonging to the claudin-low or basal B subtype, BT-474 to luminal B, and SK-BR-3 to HER2[179,180]. Several of the protein targets included in the present panel have been studied in the context of breast cancer heterogeneity, and parallels can thus be drawn between our results and previous histological and immunological efforts. For instance, ADAM10, given its HER2 shedding activity, is important in HER2-expressing cancers[181], such as the luminal B and HER2 subtypes to which BT-474 and SK-BR-3 cells belong[179]. Its presence in MDA-MB-231 cells, which do not express high HER2 levels, is therefore expected to be less consistent, which is indeed what is observed in MDA-231 exosomes. CCR5 is also associated with subtype-specific expression, as it is known to be overexpressed in basal and HER2 subtypes[166,182]. However, FACS analysis highlighted that only a small subpopulation of MDA-MB-231 cells expressed CCR5, and the situation is likely to be similar in other breast cancer cell lines[182]. This low expression frequency might explain why the receptor was not detected in exosomes by ExAM. Probed integrins likewise show patterns consistent with molecular classification. For example, integrin αvβ5 plays a physiological and pathological role in angiogenesis and can be targeted by an inhibitor drug, cilengitide, in breast cancer treatment[183]. The approach is supported by β5 integrin subunit expression in luminal breast cancer cell lines[184], consistently with the hint of expression we found in BT-474-derived exosomes. Moreover, integrins β2 and β4 are known to mainly associate with basal-like breast tumours[179,185,186], in agreement with our findings. Finally, our obtained EGFR and EpCAM expression patterns also match previous studies. EpCAM was reported to have a higher frequency (around 50%) in BT-474 (luminal B) and SK-BR-3 (HER2) cells compared to MDA-MB-231 cells (claudin-

low/basal B), which displayed a very low expression of the marker (< 10%)[187]; and EGFR expression was previously found to be higher in SK-BR-3 cells than in MDA-231 or BT-474 cells[188].

The CVs obtained for this experiment varied from less than 20% for targets detected with moderate-to-high signal (corrected signal above 1,500 RFU) to more than 100% for low-to-nonexistent signal (below 50 RFU). In previous microarray work, values with a replicate-to-replicate variation higher than 50% have been removed before further analysis[189]. However, the closer an intensity value is to zero, the higher the CV is going to be as background and noise represent an increasingly important fraction of the signal. Hence, while very high CVs are normal for negative detection events, a CV threshold of around 50% should be kept in mind when considering statistical and quantitative significance of positive detection events.

Of note, despite the use of samples of comparable protein concentrations for this experiment, the detection intensities obtained when the exosome marker CD63 is

SURFACE MARKER	MDA-MB-231		A431-GFP		BT-474		SK-BR-3	
	INTENSITY	CV	INTENSITY	CV	INTENSITY	CV	INTENSITY	CV
ADAM10	1 314	44%	26 914	17%	3 223	15%	1 630	20%
CD44	0	NaN	60	97%	0	NaN	0	566%
CD82	2 585	45%	19 840	26%	2 278	31%	2 869	25%
CD133	0	566%	65	93%	1	566%	0	566%
Integrin αVβ5	0	NaN	330	66%	39	125%	1	160%
Integrin α2	1 128	37%	22 607	25%	1	393%	2	201%
Integrin α6	0	248%	15 371	24%	0	566%	0	NaN
Integrin β1	1 184	36%	26 455	12%	32	124%	0	513%
Integrin β4	3	127%	21 847	11%	0	NaN	0	NaN
PD-1	0	NaN	2 313	31%	0	NaN	0	NaN
PD-L1	0	NaN	53	102%	0	NaN	0	566%
CD63	3 928	17%	32 070	13%	2 576	15%	1 601	16%
EGFR	40	120%	7 957	29%	6	115%	139	59%
EPCAM	0	375%	12 508	16%	1 987	12%	69	82%
CCR5	0	566%	0	566%	0	NaN	0	566%
NEG: GAR-AF546	0	566%	1	398%	0	566%	0	NaN

COLOR SCALE	
INTENSITY	CV
35 000	40%
28 000	35%
21 000	30%
14 000	25%
7 000	20%
0	15%

Table 3 Corrected fluorescent intensities and CVs obtained when exosomes from 4 cancer cell lines are incubated with antibody microarrays targeting 15 surface markers of interest (and one unspecific negative control, goat anti-rabbit-AF546) and subsequently detected with biotinylated anti-CD63 antibodies and fluorescent streptavidin. CD82, ADAM10 and CD63 were detected in all samples, while high and low levels of integrins were detected in A431 and MDA-MB-231 cells, respectively. NaN indicates that the CV could not be computed (i.e. when there was no signal). AF: Alexa Fluor®

targeted for both capture and detection vary significantly. These differences may come in part from cell line-to-cell line variations in secretion behaviour, with some cells secreting more CD63-bearing vesicles than others. To minimize the possible impact due to variation in CD63 expression levels on the results, a detection antibody cocktail targeting multiple highly expressed exosomal proteins along with CD63 could be used. This cocktail would need to be tested, optimized and validated with exosomes from A431 along with other cell lines.

5. Conclusion

5.1 Summary

We have presented the optimization and phenotyping capabilities of ExAM, an antibody microarray platform which can detect extravesicular exosome proteins with high signal intensity and reproducibility. Capture and detection-focused assays were first tested separately, then combined into a full antibody microarray protocol for exosome capture and exosomal protein detection. The (i) antibody printing buffer, (ii) sample incubation buffer, and (iii) capture antibody concentration were individually optimized using the intensity and reproducibility of both the detection signal and intrinsic GFP exosome signal as optimization criteria. The combination of printing buffer 28 (composed of 15% 2,3-butanediol and 1 M betaine in PBS), 1% BSA in the sample incubation buffer, and a capture antibody concentration between 100 and 150 μg/mL resulted in strong and robust signals, did not overly damage exosome samples during long incubations, and stroke a good balance between microarray performance and reagent cost.

To validate and demonstrate the capabilities of ExAM, exosomes from 4 cancer cell lines were phenotyped using a panel of 15 antibodies against exosome marker CD63; integrins αVβ5, α2, α6, β1, and β4; receptors EGFR, CCR5, and PD-1; and transmembrane proteins ADAM10, EpCAM, PD-L1, CD44, CD82, and CD133. The results highlighted known and new expression patterns, and aligned for the most part with the molecular breast cancer subtypes corresponding to the analyzed cell lines. We have hence shown that ExAM can be used to simultaneously detect more than a dozen protein markers at the surface of exosomes produced by cancer cells in culture, rivalling with other approaches[4,190]. Where data was available, the semi-quantitative results obtained were for the most part consistent with exosome/EV proteomic reports in the literature. Furthermore, although preliminary, the collected data contributes to a more rounded

molecular and behavioural picture of the examined cancer exosomes. ExAM could thus be used to screen exosomes from additional, previously uncharacterized cell types. The assay format could readily be expanded by including additional antibodies targeting a broader selection of exosomal surface proteins, and help chart exosomal diversity.

5.2 Future Work

Important next steps are to (i) determine the limit of detection (LOD) of ExAM, (ii) develop a robust detection cocktail, and (iii) use ExAM for biological and patient samples. To determine the LOD, absolute vesicle numbers will first need to be obtained by using suspensions with known exosome content (established for example by TRPS) and then measuring them in a dilution series on the antibody microarray. Importantly, the LOD will depend on the cocktail of antibodies used for exosome capture and detection. For a given exosome-targeting antibody cocktail, a separate LOD could be obtained for each surface protein probed. Determining the LOD (in exosome number) associated to a well-characterized surface protein would help quantify the platform's sensitivity. In this work, anti-CD63 antibodies have been used for detection, but targeting a single protein marker may prove limiting as it makes the results dependent on the sample's CD63 content. Optimizing a detection IgG cocktail that produces robust results across cell types would thus also be a desirable next step. Lastly, the complex biological matrices of fluids such as blood and urine are expected to require additional optimization of the assay protocol, most probably at the purification, blocking and sample incubation steps. These adjustments will be essential to the use of the platform for the phenotyping of clinical samples.

A natural extension of the platform would be the combination of various capture and detection antibodies to look for co-expression of various proteins in the probed samples. By using fluorescent labels of different wavelengths for the detection antibodies, several proteins could be probed on a single spot. The integration of additional detection

antibodies and imaging wavelengths would however require additional optimization to address cross-reactivity issues and ensure accurate quantification. Of note, multiplexing without mixing—thus circumventing the cross-reactivity problem—was previously achieved on microarrays by spotting capture and detection antibodies at the same physical coordinates before and after sample incubation, respectively[189].

The analysis could also be extended to include not only extravesicular proteins, but also intravesicular proteins. As our current protocol does not lyse or otherwise alter the membrane of exosomes, additional steps would be required. Intravesicular proteins could be detected following two main strategies: (i) post-purification exosome lysis, or (ii) non-destructive membrane permeabilization. The first option is simpler and less likely to call for a lot of optimization, but information about the correlation between extra- and intravesicular proteins will inevitably be lost. The second option, on the other hand, will require the testing of several pre-treatments and membrane-disruptive agents at various concentrations in order to strike a balance between antigen availability and vesicle integrity.

Signal amplification could be added to the platform to improve sensitivity and take full advantage of the imaging dynamic range. Several amplification schemes, including fluorescent polymerization[191], gold nanoparticle-based plasmonics[192], and nucleic acid-based amplification are compatible with antibody microarrays. The latter, which includes techniques such as rolling circle amplification (RCA)[193], immuno-PCR[194] and hybridization chain reaction (HCR)[195], could be a good choice for our platform due to its flexibility and compatibility with multiplexing on a single antibody spot. Indeed, detection antibodies can be conjugated in-house to the oligonucleotide probes required for amplification, which can be customized to include unique sequences, or barcodes[196]. Those sequences can then be used to distinguish different targets. The chosen amplification strategy would first have to be tested with a small number of targets, but

barcoding could eventually allow single-spot multiplexing beyond the number of fluorescent channels available.

ExAM's phenotyping capabilities could be used in the context of various studies looking at the protein content of exosome samples. For instance, ExAM could be used to thoroughly characterize and compare the expression of a set of proteins of interest in exosomes from established cell lines, similarly to what has previously been done for cell lysates[197]. Moreover, once the platform has been optimized for use with biological samples, it could be used to phenotype exosomes extracted from biological fluids, and to look for specific disease-relevant proteins. With the addition of multiplexing in the form of combinatorial analysis, including the simultaneous analysis of intravesicular and surface exosome proteins, ExAM will help enable extensive characterization of protein expression in exosomes and the discovery of new markers, which may ultimately guide patient diagnosis and prognosis.

6. Abbreviations

AB	Apoptotic body
Ab	Antibody
ADAM10	A disintegrin and metalloproteinase domain-containing protein 10
AF	Alexa Fluor®
AF4	Asymmetric flow field-flow fractionation
AFM	Atomic force microscopy
BSA	Bovine serum albumin
But.	Butanediol
cAb	Capture antibody
CCR5	C-C chemokine receptor type 5
CDx	Cluster of differentiation x
dAb	Detection antibody
DDA	Data dependent acquisition
DI	Deionized water
DIA	Data independent acquisition
DLS	Dynamic light scattering
DMSO	Dimethyl sulfoxide
EGFR	Epidermal growth factor receptor
ELISA	Enzyme-linked immunosorbent assay
EM	Electron microscopy
EpCAM	Epithelial cell adhesion molecule
ESCRT	Endosomal sorting complex required for transport
ESI	Electrospray ionization
EtGly	Ethylene glycol
EV	Extracellular vesicle
ExAM	Exosome Antibody Microarray
FBS	Fetal bovine serum
FCM	Flow cytometry
GAM	Goat anti-mouse
GAR	Goat anti-rabbit
GFP	Green fluorescent protein
HPLC	High-performance liquid chromatography

IgG	Immunoglobulin G
iTRAQ	Isotope tags for relative and absolute quantitation
LOC	Lab-on-a-chip
LOD	Limit of detection
MALDI	Matrix-assisted laser desorption/ionization
MHC	Major histocompatibility complex
MRM	Multiple reaction monitoring
MudPIT	Multidimensional Protein Identification Technology
MV	Microvesicle
MVB	Multivesicular body
MS	Mass spectrometry
NTA	Nanoparticle tracking analysis
PBS	Phosphate buffer saline
PD-1	Programmed cell death protein 1
PDL-1	Programmed death-ligand 1
PEG	Polyethylene glycol
PLL	Poly-L-lysine
PM	Plasma membrane
PRM	Parallel-reaction monitoring
PS	Penicillin-streptomycin
SC	Spectral counting
SCX	Strong cation exchange chromatography
SNR	Signal-to-noise ratio
SOMAmer	Slow off-rate modified aptamer
SPR	Surface plasmon resonance
SRM	Selected reaction monitoring
SWATH	Sequential window acquisition of all theoretical spectra
T20	Tween®20
TIC	Total ion chromatogram
TMT	Tandem mass tags
TNF	Tumour necrosis factor
TOF	Time-of-flight
TRPS	Tunable resistive pulse sensing

7. Appendix

ANTIBODY PROTEIN TARGET	MICROARRAY SPOT POSITIONS (ROW/COLUMN)
ADAM10	1/3, 4/8, 5/5, 5/13, 7/10, 7/12, 7/15, 11/5, 11/10, 11/12, 12/12, 13/1, 13/13, 14/8, 15/11, 15/16
CD44	1/13, 2/5, 2/7, 2/8, 3/16, 4/3, 6/2, 6/8, 8/2, 8/15, 9/5, 9/7, 9/9, 13/6, 13/10, 16/7
CD82	1/8, 1/15, 2/2, 4/14, 5/7, 6/10, 9/15, 10/7, 10/12, 11/3, 11/14, 13/7, 13/16, 14/4, 15/2, 15/12
CD133	1/5, 3/9, 4/16, 5/4, 5/12, 6/6, 8/4, 8/5, 9/14, 10/6, 10/11, 11/2, 13/9, 14/2, 14/12, 16/9
INTEGRIN ALPHA V BETA 5	1/2, 1/10, 2/14, 3/3, 3/5, 3/12, 4/6, 5/6, 5/8, 5/10, 6/12, 11/13, 12/5, 13/15, 16/2, 16/16
INTEGRIN ALPHA 2	1/9, 1/12, 3/2, 3/11, 5/1, 6/5, 6/13, 7/3, 9/8, 10/2, 13/2, 13/12, 14/3, 14/9, 15/9, 16/4
INTEGRIN ALPHA 6	2/9, 4/5, 6/1, 6/11, 6/14, 7/11, 10/3, 10/13, 10/15, 11/9, 13/5, 14/10, 14/15, 15/4, 15/7, 15/15
INTEGRIN BETA 1	1/14, 2/4, 2/10, 2/12, 3/7, 4/15, 8/3, 8/7, 8/12, 10/5, 12/6, 13/3, 14/7, 14/16, 16/1, 16/8
INTEGRIN BETA 4	1/7, 3/4, 3/8, 3/10, 4/13, 5/2, 5/11, 6/9, 6/16, 8/14, 9/10, 10/8, 11/6, 12/9, 14/13, 15/13,
PD-1	1/6, 2/11, 4/11, 5/14, 7/2, 7/8, 8/6, 8/16, 11/16, 12/10, 12/13, 13/4, 13/14, 15/5, 15/14, 16/10
PD-L1	1/1, 1/4, 5/3, 7/4, 7/6, 7/16, 8/11, 8/13, 10/4, 11/7, 11/11, 12/6, 12/7, 15/1, 15/8, 15/10,
CD63	2/1, 2/13, 4/9, 4/12, 5/15, 7/13, 8/8, 8/9, 9/2, 10/10, 11/15, 12/1, 12/8, 13/11, 16/6, 16/14
EGFR	2/15, 4/1, 4/7, 6/4, 9/1, 9/6, 9/13, 11/4, 12/2, 12/11, 12/14, 13/8, 14/1, 14/6, 15/3, 16/11
EPCAM	1/11, 2/3, 2/6, 3/1, 3/14, 3/15, 6/3, 6/7, 7/7, 8/1, 8/10, 10/16, 11/1, 12/3, 12/4, 16/5
GAR-AF546	1/16, 2/16, 4/2, 4/4, 4/10, 5/16, 7/1, 7/5, 7/14, 9/4, 9/11, 10/1, 10/9, 14/5, 15/6, 16/12
CCR5	3/6, 3/13, 5/9, 6/15, 7/9, 9/3, 9/12, 9/16, 10/14, 11/8, 12/15, 14/11, 14/14, 16/3, 16/13, 16/15

Supplementary Table I Randomly generated positions of the capture antibody spots from the antibody microarray used in the validation phenotyping experiment presented in section 4.3.

8. Bibliography

1 Hoshino, A. *et al.* Tumour exosome integrins determine organotropic metastasis. *Nature* **527**, 329-335, doi:10.1038/nature15756 (2015).

2 Melo, S. A. *et al.* Glypican-1 identifies cancer exosomes and detects early pancreatic cancer. *Nature* **523**, 177-182, doi:10.1038/nature14581 (2015).

3 Sandfeld-Paulsen, B. *et al.* Exosomal Proteins as Diagnostic Biomarkers in Lung Cancer. *Journal of Thoracic Oncology* **11**, 1701-1710, doi:https://doi.org/10.1016/j.jtho.2016.05.034 (2016).

4 Jorgensen, M. *et al.* Extracellular Vesicle (EV) Array: microarray capturing of exosomes and other extracellular vesicles for multiplexed phenotyping. *J Extracell Vesicles* **2**, doi:10.3402/jev.v2i0.20920 (2013).

5 Pugholm, L. H. *et al.* Phenotyping of Leukocytes and Leukocyte-Derived Extracellular Vesicles. *Journal of immunology research* **2016**, 6391264, doi:10.1155/2016/6391264 (2016).

6 Bæk, R., Varming, K. & Jørgensen, M. M. Does smoking, age or gender affect the protein phenotype of extracellular vesicles in plasma? *Transfusion and Apheresis Science* **55**, 44-52, doi:https://doi.org/10.1016/j.transci.2016.07.012 (2016).

7 Greening, D. W., Xu, R., Gopal, S. K., Rai, A. & Simpson, R. J. Proteomic insights into extracellular vesicle biology - defining exosomes and shed microvesicles. *Expert Rev Proteomics*, 1-27, doi:10.1080/14789450.2017.1260450 (2016).

8 van Niel, G., D'Angelo, G. & Raposo, G. Shedding light on the cell biology of extracellular vesicles. *Nat Rev Mol Cell Biol*, doi:10.1038/nrm.2017.125 (2018).

9 Cocucci, E., Racchetti, G. & Meldolesi, J. Shedding microvesicles: artefacts no more. *Trends Cell Biol* **19**, 43-51, doi:10.1016/j.tcb.2008.11.003 (2009).

10 Johnstone, R. M., Adam, M., Hammond, J. R., Orr, L. & Turbide, C. Vesicle formation during reticulocyte maturation. Association of plasma membrane activities with released vesicles (exosomes). *J Biol Chem* **262**, 9412-9420 (1987).

11 Valadi, H. *et al.* Exosome-mediated transfer of mRNAs and microRNAs is a novel mechanism of genetic exchange between cells. *Nat Cell Biol* **9**, 654-659, doi:10.1038/ncb1596 (2007).

12 Al-Nedawi, K. *et al.* Intercellular transfer of the oncogenic receptor EGFRvIII by microvesicles derived from tumour cells. *Nat Cell Biol* **10**, 619-624, doi:10.1038/ncb1725 (2008).

13 Colombo, M., Raposo, G. & Thery, C. Biogenesis, secretion, and intercellular interactions of exosomes and other extracellular vesicles. *Annu Rev Cell Dev Biol* **30**, 255-289, doi:10.1146/annurev-cellbio-101512-122326 (2014).

14 Garnier, D., Jabado, N. & Rak, J. Extracellular vesicles as prospective carriers of oncogenic protein signatures in adult and paediatric brain tumours. *PROTEOMICS* **13**, 1595-1607, doi:10.1002/pmic.201200360 (2013).
15 Raposo, G. & Stoorvogel, W. Extracellular vesicles: exosomes, microvesicles, and friends. *J Cell Biol* **200**, 373-383, doi:10.1083/jcb.201211138 (2013).
16 Atkin-Smith, G. K. & Poon, I. K. H. Disassembly of the Dying: Mechanisms and Functions. *Trends Cell Biol* **27**, 151-162, doi:10.1016/j.tcb.2016.08.011 (2017).
17 Samanta, S. *et al.* Exosomes: new molecular targets of diseases. *Acta Pharmacol Sin*, doi:10.1038/aps.2017.162 (2017).
18 Akers, J. C., Gonda, D., Kim, R., Carter, B. S. & Chen, C. C. Biogenesis of extracellular vesicles (EV): exosomes, microvesicles, retrovirus-like vesicles, and apoptotic bodies. *J Neurooncol* **113**, 1-11, doi:10.1007/s11060-013-1084-8 (2013).
19 Wlodkowic, D., Telford, W., Skommer, J. & Darzynkiewicz, Z. Apoptosis and beyond: cytometry in studies of programmed cell death. *Methods Cell Biol* **103**, 55-98, doi:10.1016/B978-0-12-385493-3.00004-8 (2011).
20 Zernecke, A. *et al.* Delivery of MicroRNA-126 by Apoptotic Bodies Induces CXCL12-Dependent Vascular Protection. *Science Signaling* **2**, ra81-ra81, doi:10.1126/scisignal.2000610 (2009).
21 Kajdos, M., Janas, L., Kolasa-Zwierzchowska, D., Wilczynski, J. R. & Stetkiewicz, T. Microvesicles as a potential biomarker of neoplastic diseases and their role in development and progression of neoplasm. *Prz Menopauzalny* **14**, 283-291, doi:10.5114/pm.2015.56540 (2015).
22 Kalra, H., Drummen, G. P. & Mathivanan, S. Focus on Extracellular Vesicles: Introducing the Next Small Big Thing. *Int J Mol Sci* **17**, 170, doi:10.3390/ijms17020170 (2016).
23 Morel, O. *et al.* Procoagulant microparticles: disrupting the vascular homeostasis equation? *Arterioscler Thromb Vasc Biol* **26**, 2594-2604, doi:10.1161/01.ATV.0000246775.14471.26 (2006).
24 Katsuda, T., Kosaka, N. & Ochiya, T. The roles of extracellular vesicles in cancer biology: toward the development of novel cancer biomarkers. *Proteomics* **14**, 412-425, doi:10.1002/pmic.201300389 (2014).
25 Thery, C., Zitvogel, L. & Amigorena, S. Exosomes: composition, biogenesis and function. *Nat Rev Immunol* **2**, 569-579, doi:10.1038/nri855 (2002).
26 Mathivanan, S., Ji, H. & Simpson, R. J. Exosomes: extracellular organelles important in intercellular communication. *J Proteomics* **73**, 1907-1920, doi:10.1016/j.jprot.2010.06.006 (2010).
27 Mittelbrunn, M. *et al.* Unidirectional transfer of microRNA-loaded exosomes from T cells to antigen-presenting cells. *Nat Commun* **2**, 282, doi:10.1038/ncomms1285 (2011).

28 Chen, W. X. *et al.* Exosomes from drug-resistant breast cancer cells transmit chemoresistance by a horizontal transfer of microRNAs. *PLoS One* **9**, e95240, doi:10.1371/journal.pone.0095240 (2014).
29 Fabbri, M. *et al.* MicroRNAs bind to Toll-like receptors to induce prometastatic inflammatory response. *Proceedings of the National Academy of Sciences of the United States of America* **109**, E2110-2116, doi:10.1073/pnas.1209414109 (2012).
30 Fang, T. *et al.* Tumor-derived exosomal miR-1247-3p induces cancer-associated fibroblast activation to foster lung metastasis of liver cancer. *Nat Commun* **9**, 191, doi:10.1038/s41467-017-02583-0 (2018).
31 Costa-Silva, B. *et al.* Pancreatic cancer exosomes initiate pre-metastatic niche formation in the liver. *Nat Cell Biol* **17**, 816-826, doi:10.1038/ncb3169 (2015).
32 Cheng, L., Zhao, W. & Hill, A. F. Exosomes and their role in the intercellular trafficking of normal and disease associated prion proteins. *Mol Aspects Med* **60**, 62-68, doi:10.1016/j.mam.2017.11.011 (2018).
33 Saman, S. *et al.* Exosome-associated tau is secreted in tauopathy models and is selectively phosphorylated in cerebrospinal fluid in early Alzheimer disease. *J Biol Chem* **287**, 3842-3849, doi:10.1074/jbc.M111.277061 (2012).
34 Choi, D. S., Kim, D. K., Kim, Y. K. & Gho, Y. S. Proteomics of extracellular vesicles: Exosomes and ectosomes. *Mass Spectrom Rev* **34**, 474-490, doi:10.1002/mas.21420 (2015).
35 Cocucci, E. & Meldolesi, J. Ectosomes and exosomes: shedding the confusion between extracellular vesicles. *Trends Cell Biol* **25**, 364-372, doi:10.1016/j.tcb.2015.01.004 (2015).
36 Fadeel, B. & Xue, D. The ins and outs of phospholipid asymmetry in the plasma membrane: roles in health and disease. *Crit Rev Biochem Mol Biol* **44**, 264-277, doi:10.1080/10409230903193307 (2009).
37 Nabhan, J. F., Hu, R., Oh, R. S., Cohen, S. N. & Lu, Q. Formation and release of arrestin domain-containing protein 1-mediated microvesicles (ARMMs) at plasma membrane by recruitment of TSG101 protein. *Proceedings of the National Academy of Sciences of the United States of America* **109**, 4146-4151, doi:10.1073/pnas.1200448109 (2012).
38 Tkach, M., Kowal, J. & Thery, C. Why the need and how to approach the functional diversity of extracellular vesicles. *Philos Trans R Soc Lond B Biol Sci* **373**, doi:10.1098/rstb.2016.0479 (2018).
39 Hanson, P. I. & Cashikar, A. Multivesicular body morphogenesis. *Annu Rev Cell Dev Biol* **28**, 337-362, doi:10.1146/annurev-cellbio-092910-154152 (2012).
40 Bhome, R. *et al.* Exosomal microRNAs (exomiRs): Small molecules with a big role in cancer. *Cancer Lett* **420**, 228-235, doi:10.1016/j.canlet.2018.02.002 (2018).
41 Kahlert, C. *et al.* Identification of double-stranded genomic DNA spanning all chromosomes with mutated KRAS and p53 DNA in the serum exosomes of

patients with pancreatic cancer. *J Biol Chem* **289**, 3869-3875, doi:10.1074/jbc.C113.532267 (2014).

42 Kalluri, R. & LeBleu, V. S. Discovery of Double-Stranded Genomic DNA in Circulating Exosomes. *Cold Spring Harb Symp Quant Biol* **81**, 275-280, doi:10.1101/sqb.2016.81.030932 (2016).

43 Cai, J. *et al.* Extracellular vesicle-mediated transfer of donor genomic DNA to recipient cells is a novel mechanism for genetic influence between cells. *J Mol Cell Biol* **5**, 227-238, doi:10.1093/jmcb/mjt011 (2013).

44 Skotland, T., Sandvig, K. & Llorente, A. Lipids in exosomes: Current knowledge and the way forward. *Prog Lipid Res* **66**, 30-41, doi:10.1016/j.plipres.2017.03.001 (2017).

45 Ghossoub, R. *et al.* Syntenin-ALIX exosome biogenesis and budding into multivesicular bodies are controlled by ARF6 and PLD2. *Nat Commun* **5**, 3477, doi:10.1038/ncomms4477 (2014).

46 Hessvik, N. P. *et al.* PIKfyve inhibition increases exosome release and induces secretory autophagy. *Cell Mol Life Sci* **73**, 4717-4737, doi:10.1007/s00018-016-2309-8 (2016).

47 Phuyal, S. *et al.* The ether lipid precursor hexadecylglycerol stimulates the release and changes the composition of exosomes derived from PC-3 cells. *J Biol Chem* **290**, 4225-4237, doi:10.1074/jbc.M114.593962 (2015).

48 Ristorcelli, E., Beraud, E., Mathieu, S., Lombardo, D. & Verine, A. Essential role of Notch signaling in apoptosis of human pancreatic tumoral cells mediated by exosomal nanoparticles. *Int J Cancer* **125**, 1016-1026, doi:10.1002/ijc.24375 (2009).

49 Beloribi, S. *et al.* Exosomal lipids impact notch signaling and induce death of human pancreatic tumoral SOJ-6 cells. *PLoS One* **7**, e47480, doi:10.1371/journal.pone.0047480 (2012).

50 Del Boccio, P. *et al.* A hyphenated microLC-Q-TOF-MS platform for exosomal lipidomics investigations: application to RCC urinary exosomes. *Electrophoresis* **33**, 689-696, doi:10.1002/elps.201100375 (2012).

51 Gross, J. C., Chaudhary, V., Bartscherer, K. & Boutros, M. Active Wnt proteins are secreted on exosomes. *Nat Cell Biol* **14**, 1036-1045, doi:10.1038/ncb2574 (2012).

52 Li, P., Kaslan, M., Lee, S. H., Yao, J. & Gao, Z. Progress in Exosome Isolation Techniques. *Theranostics* **7**, 789-804, doi:10.7150/thno.18133 (2017).

53 Momen-Heravi, F. *et al.* Current methods for the isolation of extracellular vesicles. *Biol Chem* **394**, 1253-1262, doi:10.1515/hsz-2013-0141 (2013).

54 Thery, C., Amigorena, S., Raposo, G. & Clayton, A. Isolation and characterization of exosomes from cell culture supernatants and biological fluids. *Current protocols in cell biology* **Chapter 3**, Unit 3.22, doi:10.1002/0471143030.cb0322s30 (2006).

55 Greening, D. W., Xu, R., Ji, H., Tauro, B. J. & Simpson, R. J. in *Proteomic Profiling: Methods and Protocols* (ed Anton Posch) 179-209 (Springer New York, 2015).

56 Yakimchuk, K. Exosomes: isolation methods and specific markers. *Materials and Methods* **5**, doi:10.13070/mm.en.5.1450 (2015).
57 Liu, F. *et al.* The Exosome Total Isolation Chip. *ACS Nano* **11**, 10712-10723, doi:10.1021/acsnano.7b04878 (2017).
58 Woo, H. K. *et al.* Exodisc for Rapid, Size-Selective, and Efficient Isolation and Analysis of Nanoscale Extracellular Vesicles from Biological Samples. *ACS Nano* **11**, 1360-1370, doi:10.1021/acsnano.6b06131 (2017).
59 Taylor, D. D. & Shah, S. Methods of isolating extracellular vesicles impact down-stream analyses of their cargoes. *Methods* **87**, 3-10, doi:10.1016/j.ymeth.2015.02.019 (2015).
60 Peterson, M. F., Otoc, N., Sethi, J. K., Gupta, A. & Antes, T. J. Integrated systems for exosome investigation. *Methods* **87**, 31-45, doi:https://doi.org/10.1016/j.ymeth.2015.04.015 (2015).
61 Zeringer, E., Barta, T., Li, M. & Vlassov, A. V. Strategies for isolation of exosomes. *Cold Spring Harb Protoc* **2015**, 319-323, doi:10.1101/pdb.top074476 (2015).
62 Szatanek, R., Baran, J., Siedlar, M. & Baj-Krzyworzeka, M. Isolation of extracellular vesicles: Determining the correct approach (Review). *Int J Mol Med* **36**, 11-17, doi:10.3892/ijmm.2015.2194 (2015).
63 Helwa, I. *et al.* A Comparative Study of Serum Exosome Isolation Using Differential Ultracentrifugation and Three Commercial Reagents. *PLoS One* **12**, e0170628, doi:10.1371/journal.pone.0170628 (2017).
64 Kowal, J. *et al.* Proteomic comparison defines novel markers to characterize heterogeneous populations of extracellular vesicle subtypes. *Proc Natl Acad Sci U S A* **113**, E968-977, doi:10.1073/pnas.1521230113 (2016).
65 Haraszti, R. A. *et al.* High-resolution proteomic and lipidomic analysis of exosomes and microvesicles from different cell sources. *J Extracell Vesicles* **5**, 32570, doi:10.3402/jev.v5.32570 (2016).
66 Kang, H., Kim, J. & Park, J. Methods to isolate extracellular vesicles for diagnosis. *Micro and Nano Systems Letters* **5**, 15, doi:10.1186/s40486-017-0049-7 (2017).
67 Stranska, R. *et al.* Comparison of membrane affinity-based method with size-exclusion chromatography for isolation of exosome-like vesicles from human plasma. *Journal of Translational Medicine* **16**, 1, doi:10.1186/s12967-017-1374-6 (2018).
68 Böing, A. N. *et al.* Single-step isolation of extracellular vesicles by size-exclusion chromatography. *Journal of Extracellular Vesicles* **3**, 10.3402/jev.v3403.23430, doi:10.3402/jev.v3.23430 (2014).
69 Sajeesh, P. & Sen, A. K. Particle separation and sorting in microfluidic devices: a review. *Microfluidics and Nanofluidics* **17**, 1-52, doi:10.1007/s10404-013-1291-9 (2013).

70 Wu, M. *et al.* Isolation of exosomes from whole blood by integrating acoustics and microfluidics. *Proceedings of the National Academy of Sciences of the United States of America* **114**, 10584-10589, doi:10.1073/pnas.1709210114 (2017).
71 Liu, C. *et al.* Field-Free Isolation of Exosomes from Extracellular Vesicles by Microfluidic Viscoelastic Flows. *ACS Nano* **11**, 6968-6976, doi:10.1021/acsnano.7b02277 (2017).
72 Wagner, M., Holzschuh, S., Traeger, A., Fahr, A. & Schubert, U. S. Asymmetric flow field-flow fractionation in the field of nanomedicine. *Anal Chem* **86**, 5201-5210, doi:10.1021/ac501664t (2014).
73 Fraunhofer, W. & Winter, G. The use of asymmetrical flow field-flow fractionation in pharmaceutics and biopharmaceutics. *Eur J Pharm Biopharm* **58**, 369-383, doi:10.1016/j.ejpb.2004.03.034 (2004).
74 Petersen, K. E. *et al.* A review of exosome separation techniques and characterization of B16-F10 mouse melanoma exosomes with AF4-UV-MALS-DLS-TEM. *Anal Bioanal Chem* **406**, 7855-7866, doi:10.1007/s00216-014-8040-0 (2014).
75 Wahlund, K. G. & Giddings, J. C. Properties of an asymmetrical flow field-flow fractionation channel having one permeable wall. *Analytical Chemistry* **59**, 1332-1339, doi:10.1021/ac00136a016 (1987).
76 Sitar, S. *et al.* Size characterization and quantification of exosomes by asymmetrical-flow field-flow fractionation. *Anal Chem* **87**, 9225-9233, doi:10.1021/acs.analchem.5b01636 (2015).
77 Zhang, H. *et al.* Identification of distinct nanoparticles and subsets of extracellular vesicles by asymmetric flow field-flow fractionation. *Nat Cell Biol* **20**, 332-343, doi:10.1038/s41556-018-0040-4 (2018).
78 Rupert, D. L. M., Claudio, V., Lasser, C. & Bally, M. Methods for the physical characterization and quantification of extracellular vesicles in biological samples. *Biochim Biophys Acta* **1861**, 3164-3179, doi:10.1016/j.bbagen.2016.07.028 (2017).
79 Witwer, K. W. *et al.* Standardization of sample collection, isolation and analysis methods in extracellular vesicle research. *J Extracell Vesicles* **2**, doi:10.3402/jev.v2i0.20360 (2013).
80 Szatanek, R. *et al.* The Methods of Choice for Extracellular Vesicles (EVs) Characterization. *Int J Mol Sci* **18**, doi:10.3390/ijms18061153 (2017).
81 Stetefeld, J., McKenna, S. A. & Patel, T. R. Dynamic light scattering: a practical guide and applications in biomedical sciences. *Biophys Rev* **8**, 409-427, doi:10.1007/s12551-016-0218-6 (2016).
82 Montis, C. *et al.* Size distribution of extracellular vesicles by optical correlation techniques. *Colloids Surf B Biointerfaces* **158**, 331-338, doi:10.1016/j.colsurfb.2017.06.047 (2017).

83 Dragovic, R. A. *et al.* Sizing and phenotyping of cellular vesicles using Nanoparticle Tracking Analysis. *Nanomedicine* **7**, 780-788, doi:10.1016/j.nano.2011.04.003 (2011).
84 Shpacovitch, V. & Hergenroder, R. Optical and surface plasmonic approaches to characterize extracellular vesicles. A review. *Anal Chim Acta* **1005**, 1-15, doi:10.1016/j.aca.2017.11.066 (2018).
85 Momen-Heravi, F. *et al.* Alternative methods for characterization of extracellular vesicles. *Front Physiol* **3**, 354, doi:10.3389/fphys.2012.00354 (2012).
86 Weatherall, E. & Willmott, G. R. Applications of tunable resistive pulse sensing. *Analyst* **140**, 3318-3334, doi:10.1039/c4an02270j (2015).
87 Maas, S. L., De Vrij, J. & Broekman, M. L. Quantification and size-profiling of extracellular vesicles using tunable resistive pulse sensing. *J Vis Exp*, e51623, doi:10.3791/51623 (2014).
88 Vogel, R. *et al.* A standardized method to determine the concentration of extracellular vesicles using tunable resistive pulse sensing. *J Extracell Vesicles* **5**, 31242, doi:10.3402/jev.v5.31242 (2016).
89 Ko, J., Carpenter, E. & Issadore, D. Detection and isolation of circulating exosomes and microvesicles for cancer monitoring and diagnostics using micro-/nano-based devices. *Analyst* **141**, 450-460, doi:10.1039/c5an01610j (2016).
90 Schmid, F.-X. Biological Macromolecules: UV-visible Spectrophotometry. *eLS*, doi:doi:10.1038/npg.els.0003142 (2001).
91 Gallagher, S. Quantitation of nucleic acids with absorption spectroscopy. *Current protocols in protein science* **Appendix 4**, Appendix 4K, doi:10.1002/0471140864.psa04ks13 (2001).
92 Aitken, A. & Learmonth, M. P. in *The Protein Protocols Handbook* (ed John M. Walker) 3-6 (Humana Press, 2002).
93 Ng, Y. H. *et al.* Endometrial Exosomes/Microvesicles in the Uterine Microenvironment: A New Paradigm for Embryo-Endometrial Cross Talk at Implantation. *PLoS ONE* **8**, e58502, doi:10.1371/journal.pone.0058502 (2013).
94 Montecalvo, A., Larregina, A. T. & Morelli, A. E. Methods of analysis of dendritic cell-derived exosome-shuttle microRNA and its horizontal propagation between dendritic cells. *Methods Mol Biol* **1024**, 19-40, doi:10.1007/978-1-62703-453-1_3 (2013).
95 van der Pol, E. *et al.* Optical and non-optical methods for detection and characterization of microparticles and exosomes. *J Thromb Haemost* **8**, 2596-2607, doi:10.1111/j.1538-7836.2010.04074.x (2010).
96 Jalili, N. & Laxminarayana, K. A review of atomic force microscopy imaging systems: application to molecular metrology and biological sciences. *Mechatronics* **14**, 907-945, doi:10.1016/j.mechatronics.2004.04.005 (2004).

97 Glish, G. L. & Vachet, R. W. The basics of mass spectrometry in the twenty-first century. *Nat Rev Drug Discov* **2**, 140-150, doi:10.1038/nrd1011 (2003).
98 Zhang, X. *et al.* Multi-dimensional liquid chromatography in proteomics--a review. *Anal Chim Acta* **664**, 101-113, doi:10.1016/j.aca.2010.02.001 (2010).
99 Pocsfalvi, G. *et al.* Mass spectrometry of extracellular vesicles. *Mass Spectrom Rev* **35**, 3-21, doi:10.1002/mas.21457 (2016).
100 Schey, K. L., Luther, J. M. & Rose, K. L. Proteomics characterization of exosome cargo. *Methods* **87**, 75-82, doi:10.1016/j.ymeth.2015.03.018 (2015).
101 Thammana, M. A review on high performance liquid chromatography (HPLC). *Research & Reviews: Journal of Pharmaceutical Analysis* **5**, 22-28 (2016).
102 Nadler, W. M. *et al.* MALDI versus ESI: The Impact of the Ion Source on Peptide Identification. *J Proteome Res* **16**, 1207-1215, doi:10.1021/acs.jproteome.6b00805 (2017).
103 El-Aneed, A., Cohen, A. & Banoub, J. Mass Spectrometry, Review of the Basics: Electrospray, MALDI, and Commonly Used Mass Analyzers. *Applied Spectroscopy Reviews* **44**, 210-230, doi:10.1080/05704920902717872 (2009).
104 Jennings, K. R. & Dolnikowski, G. G. in *Methods in Enzymology* Vol. 193 37-61 (Academic Press, 1990).
105 Hu, A., Noble, W. S. & Wolf-Yadlin, A. Technical advances in proteomics: new developments in data-independent acquisition. *F1000Res* **5**, doi:10.12688/f1000research.7042.1 (2016).
106 Aebersold, R. & Mann, M. Mass-spectrometric exploration of proteome structure and function. *Nature* **537**, 347-355, doi:10.1038/nature19949 (2016).
107 Liebler, D. C. Shotgun mass spec goes independent. *Nature Methods* **1**, 16, doi:10.1038/nmeth1004-16 (2004).
108 Doerr, A. DIA mass spectrometry. *Nature Methods* **12**, 35-35, doi:10.1038/nmeth.3234 (2015).
109 Gillet, L. C. *et al.* Targeted data extraction of the MS/MS spectra generated by data-independent acquisition: a new concept for consistent and accurate proteome analysis. *Molecular & cellular proteomics : MCP* **11**, O111 016717, doi:10.1074/mcp.O111.016717 (2012).
110 Frederick, K. & Ciborowski, P. in *Proteomic Profiling and Analytical Chemistry* 161-173 (2016).
111 Schubert, O. T. *et al.* Building high-quality assay libraries for targeted analysis of SWATH MS data. *Nat Protoc* **10**, 426-441, doi:10.1038/nprot.2015.015 (2015).
112 Washburn, M. P., Wolters, D. & Yates Iii, J. R. Large-scale analysis of the yeast proteome by multidimensional protein identification technology. *Nature Biotechnology* **19**, 242, doi:10.1038/85686
https://www.nature.com/articles/nbt0301_242#supplementary-information (2001).

113 Washburn, M. P., Wolters, D. & Yates, J. R., 3rd. Large-scale analysis of the yeast proteome by multidimensional protein identification technology. *Nat Biotechnol* **19**, 242-247, doi:10.1038/85686 (2001).
114 Wang, Z., Hill, S., Luther, J. M., Hachey, D. L. & Schey, K. L. Proteomic analysis of urine exosomes by multidimensional protein identification technology (MudPIT). *Proteomics* **12**, 329-338, doi:10.1002/pmic.201100477 (2012).
115 Raj, D. A., Fiume, I., Capasso, G. & Pocsfalvi, G. A multiplex quantitative proteomics strategy for protein biomarker studies in urinary exosomes. *Kidney Int* **81**, 1263-1272, doi:10.1038/ki.2012.25 (2012).
116 Demory Beckler, M. *et al.* Proteomic analysis of exosomes from mutant KRAS colon cancer cells identifies intercellular transfer of mutant KRAS. *Molecular & cellular proteomics : MCP* **12**, 343-355, doi:10.1074/mcp.M112.022806 (2013).
117 Dozio, V. & Sanchez, J. C. Characterisation of extracellular vesicle-subsets derived from brain endothelial cells and analysis of their protein cargo modulation after TNF exposure. *J Extracell Vesicles* **6**, 1302705, doi:10.1080/20013078.2017.1302705 (2017).
118 Xie, S., Moya, C., Bilgin, B., Jayaraman, A. & Walton, S. P. Emerging Affinity-Based Techniques in Proteomics. *Expert review of proteomics* **6**, 573-583, doi:10.1586/epr.09.74 (2009).
119 McKinnon, K. M. Flow Cytometry: An Overview. *Curr Protoc Immunol* **120**, 5 1 1-5 1 11, doi:10.1002/cpim.40 (2018).
120 van der Vlist, E. J., Nolte-'t Hoen, E. N., Stoorvogel, W., Arkesteijn, G. J. & Wauben, M. H. Fluorescent labeling of nano-sized vesicles released by cells and subsequent quantitative and qualitative analysis by high-resolution flow cytometry. *Nat Protoc* **7**, 1311-1326, doi:10.1038/nprot.2012.065 (2012).
121 van der Pol, E., van Gemert, M. J., Sturk, A., Nieuwland, R. & van Leeuwen, T. G. Single vs. swarm detection of microparticles and exosomes by flow cytometry. *J Thromb Haemost* **10**, 919-930, doi:10.1111/j.1538-7836.2012.04683.x (2012).
122 Nolte-'t Hoen, E. N. *et al.* Quantitative and qualitative flow cytometric analysis of nanosized cell-derived membrane vesicles. *Nanomedicine* **8**, 712-720, doi:10.1016/j.nano.2011.09.006 (2012).
123 Lof, L. *et al.* Detecting individual extracellular vesicles using a multicolor in situ proximity ligation assay with flow cytometric readout. *Sci Rep* **6**, 34358, doi:10.1038/srep34358 (2016).
124 He, M., Crow, J., Roth, M., Zeng, Y. & Godwin, A. K. Integrated immunoisolation and protein analysis of circulating exosomes using microfluidic technology. *Lab Chip* **14**, 3773-3780, doi:10.1039/c4lc00662c (2014).
125 Liga, A., Vliegenthart, A. D., Oosthuyzen, W., Dear, J. W. & Kersaudy-Kerhoas, M. Exosome isolation: a microfluidic road-map. *Lab Chip* **15**, 2388-2394, doi:10.1039/c5lc00240k (2015).

126 Zhao, Z., Yang, Y., Zeng, Y. & He, M. A microfluidic ExoSearch chip for multiplexed exosome detection towards blood-based ovarian cancer diagnosis. *Lab Chip* **16**, 489-496, doi:10.1039/c5lc01117e (2016).
127 Zhang, P., He, M. & Zeng, Y. Ultrasensitive microfluidic analysis of circulating exosomes using a nanostructured graphene oxide/polydopamine coating. *Lab Chip* **16**, 3033-3042, doi:10.1039/c6lc00279j (2016).
128 Webber, J. *et al.* Proteomics analysis of cancer exosomes using a novel modified aptamer-based array (SOMAscan) platform. *Molecular & cellular proteomics : MCP* **13**, 1050-1064, doi:10.1074/mcp.M113.032136 (2014).
129 Gold, L. *et al.* Aptamer-based multiplexed proteomic technology for biomarker discovery. *PLoS One* **5**, e15004, doi:10.1371/journal.pone.0015004 (2010).
130 Im, H. *et al.* Label-free detection and molecular profiling of exosomes with a nano-plasmonic sensor. *Nat Biotechnol* **32**, 490-495, doi:10.1038/nbt.2886 (2014).
131 Park, J. *et al.* Analyses of Intravesicular Exosomal Proteins Using a Nano-Plasmonic System. *ACS Photonics* **5**, 487-494, doi:10.1021/acsphotonics.7b00992 (2018).
132 He, M. & Zeng, Y. Microfluidic Exosome Analysis toward Liquid Biopsy for Cancer. *J Lab Autom* **21**, 599-608, doi:10.1177/2211068216651035 (2016).
133 Clancy, K. F. A. & Nicolau, D. V. in *SPIE BiOS.* 13 (SPIE).
134 Bergeron, S., Laforte, V., Lo, P. S., Li, H. & Juncker, D. Evaluating mixtures of 14 hygroscopic additives to improve antibody microarray performance. *Anal Bioanal Chem* **407**, 8451-8462, doi:10.1007/s00216-015-8992-8 (2015).
135 Schäferling, M. K., D. in *Protein Microarray Technology* (2004).
136 Seurynck-Servoss, S. L. Surface chemistries for antibody microarrays. *Frontiers in Bioscience* **12**, doi:10.2741/2362 (2007).
137 Pollard, H. B. *et al.* Protein microarray platforms for clinical proteomics. *Proteomics Clin Appl* **1**, 934-952, doi:10.1002/prca.200700154 (2007).
138 Angenendt, P., Glökler, J., Murphy, D., Lehrach, H. & Cahill, D. J. Toward optimized antibody microarrays: a comparison of current microarray support materials. *Analytical Biochemistry* **309**, 253-260, doi:https://doi.org/10.1016/S0003-2697(02)00257-9 (2002).
139 Baek, R., Sondergaard, E. K., Varming, K. & Jorgensen, M. M. The impact of various preanalytical treatments on the phenotype of small extracellular vesicles in blood analyzed by protein microarray. *J Immunol Methods* **438**, 11-20, doi:10.1016/j.jim.2016.08.007 (2016).
140 Lotvall, J. *et al.* Minimal experimental requirements for definition of extracellular vesicles and their functions: a position statement from the International Society for Extracellular Vesicles. *J Extracell Vesicles* **3**, 26913, doi:10.3402/jev.v3.26913 (2014).
141 Garnier, D., Magnus, N., Meehan, B., Kislinger, T. & Rak, J. Qualitative changes in the proteome of extracellular vesicles accompanying cancer cell transition to

mesenchymal state. *Exp Cell Res* **319**, 2747-2757, doi:10.1016/j.yexcr.2013.08.003 (2013).
142 Zhang, Y. L., X.; Xu, X.; Luo, W.-J. Construction of a high-EGFR expression cell line and its biological properties comparing with A431 cell. *African Journal of Biotechnolog* **9**, 4674-4680, doi:10.5897/AJB10.143 (2010).
143 Almonte, L., Lopez-Elvira, E. & Baro, A. M. Surface-charge differentiation of streptavidin and avidin by atomic force microscopy-force spectroscopy. *Chemphyschem : a European journal of chemical physics and physical chemistry* **15**, 2768-2773, doi:10.1002/cphc.201402234 (2014).
144 Lane, R. E., Korbie, D., Anderson, W., Vaidyanathan, R. & Trau, M. Analysis of exosome purification methods using a model liposome system and tunable-resistive pulse sensing. *Sci Rep* **5**, 7639, doi:10.1038/srep07639 (2015).
145 Waters, J. C. Accuracy and precision in quantitative fluorescence microscopy. *J Cell Biol* **185**, 1135-1148, doi:10.1083/jcb.200903097 (2009).
146 Zoller, M. CD44: can a cancer-initiating cell profit from an abundantly expressed molecule? *Nature reviews. Cancer* **11**, 254-267, doi:10.1038/nrc3023 (2011).
147 Mizrak, D., Brittan, M. & Alison, M. CD133: molecule of the moment. *The Journal of pathology* **214**, 3-9, doi:10.1002/path.2283 (2008).
148 Rachid, M. *et al.* CD44 and EpCAM: Cancer-Initiating Cell Markers. *Current Molecular Medicine* **8**, 784-804, doi:http://dx.doi.org/10.2174/156652408786733667 (2008).
149 Orian-Rousseau, V. CD44, a therapeutic target for metastasising tumours. *Eur J Cancer* **46**, 1271-1277, doi:10.1016/j.ejca.2010.02.024 (2010).
150 Ponta, H., Sherman, L. & Herrlich, P. A. CD44: from adhesion molecules to signalling regulators. *Nat Rev Mol Cell Biol* **4**, 33-45, doi:10.1038/nrm1004 (2003).
151 Grosse-Gehling, P. *et al.* CD133 as a biomarker for putative cancer stem cells in solid tumours: limitations, problems and challenges. *The Journal of pathology* **229**, 355-378, doi:10.1002/path.4086 (2013).
152 Wu, Y. & Wu, P. Y. CD133 as a marker for cancer stem cells: progresses and concerns. *Stem Cells Dev* **18**, 1127-1134, doi:10.1089/scd.2008.0338 (2009).
153 Schnell, U., Cirulli, V. & Giepmans, B. N. EpCAM: structure and function in health and disease. *Biochim Biophys Acta* **1828**, 1989-2001, doi:10.1016/j.bbamem.2013.04.018 (2013).
154 Hamidi, H. & Ivaska, J. Every step of the way: integrins in cancer progression and metastasis. *Nature reviews. Cancer*, doi:10.1038/s41568-018-0038-z (2018).
155 Hynes, R. O. Integrins: bidirectional, allosteric signaling machines. *Cell* **110**, 673-687 (2002).
156 Alberts, B. *et al.* in *Molecular Biology of the Cell* (Garland Science, 2002).
157 Murphy, G. The ADAMs: signalling scissors in the tumour microenvironment. *Nature reviews. Cancer* **8**, 929-941, doi:10.1038/nrc2459 (2008).

158 Mochizuki, S. & Okada, Y. ADAMs in cancer cell proliferation and progression. *Cancer Sci* **98**, 621-628, doi:10.1111/j.1349-7006.2007.00434.x (2007).
159 Blobel, C. P. ADAMs: key components in EGFR signalling and development. *Nat Rev Mol Cell Biol* **6**, 32-43, doi:10.1038/nrm1548 (2005).
160 Wetzel, S., Seipold, L. & Saftig, P. The metalloproteinase ADAM10: A useful therapeutic target? *Biochim Biophys Acta* **1864**, 2071-2081, doi:10.1016/j.bbamcr.2017.06.005 (2017).
161 Francisco, L. M., Sage, P. T. & Sharpe, A. H. The PD-1 pathway in tolerance and autoimmunity. *Immunological reviews* **236**, 219-242, doi:10.1111/j.1600-065X.2010.00923.x (2010).
162 Chen, L. & Han, X. Anti-PD-1/PD-L1 therapy of human cancer: past, present, and future. *J Clin Invest* **125**, 3384-3391, doi:10.1172/JCI80011 (2015).
163 Topalian, S. L. *et al.* Safety, Activity, and Immune Correlates of Anti–PD-1 Antibody in Cancer. *New England Journal of Medicine* **366**, 2443-2454, doi:10.1056/NEJMoa1200690 (2012).
164 Scurci, I., Martins, E. & Hartley, O. CCR5: Established paradigms and new frontiers for a 'celebrity' chemokine receptor. *Cytokine* **109**, 81-93, doi:10.1016/j.cyto.2018.02.018 (2018).
165 Oppermann, M. Chemokine receptor CCR5: insights into structure, function, and regulation. *Cell Signal* **16**, 1201-1210, doi:10.1016/j.cellsig.2004.04.007 (2004).
166 Velasco-Velazquez, M., Xolalpa, W. & Pestell, R. G. The potential to target CCL5/CCR5 in breast cancer. *Expert Opin Ther Targets* **18**, 1265-1275, doi:10.1517/14728222.2014.949238 (2014).
167 Chuang, J. Y. *et al.* CCL5/CCR5 axis promotes the motility of human oral cancer cells. *J Cell Physiol* **220**, 418-426, doi:10.1002/jcp.21783 (2009).
168 Ciardiello, F. & Tortora, G. Epidermal growth factor receptor (EGFR) as a target in cancer therapy: understanding the role of receptor expression and other molecular determinants that could influence the response to anti-EGFR drugs. *European Journal of Cancer* **39**, 1348-1354, doi:10.1016/S0959-8049(03)00235-1 (2003).
169 Herbst, R. S. Review of epidermal growth factor receptor biology. *International Journal of Radiation Oncology*Biology*Physics* **59**, S21-S26, doi:10.1016/j.ijrobp.2003.11.041 (2004).
170 Charrin, S., Jouannet, S., Boucheix, C. & Rubinstein, E. Tetraspanins at a glance. *J Cell Sci* **127**, 3641-3648, doi:10.1242/jcs.154906 (2014).
171 Feng, J. *et al.* Tetraspanin CD82: a suppressor of solid tumors and a modulator of membrane heterogeneity. *Cancer Metastasis Rev* **34**, 619-633, doi:10.1007/s10555-015-9585-x (2015).
172 Palazzolo, G. *et al.* Proteomic Analysis of Exosome-like Vesicles Derived from Breast Cancer Cells. *Anticancer Research* **32**, 847-860 (2012).

173 Wu, X. *et al.* A breast cancer cell microarray (CMA) as a rapid method to characterize candidate biomarkers. *Cancer Biol Ther* **15**, 1593-1599, doi:10.4161/15384047.2014.961886 (2014).
174 Imai, K., Ichibangase, T., Saitoh, R. & Hoshikawa, Y. A proteomics study on human breast cancer cell lines by fluorogenic derivatization-liquid chromatography/tandem mass spectrometry. *Biomed Chromatogr* **22**, 1304-1314, doi:10.1002/bmc.1102 (2008).
175 Moss, M. L., Stoeck, A., Yan, W. & Dempsey, P. J. ADAM10 as a Target for Anti-Cancer Therapy. *Current Pharmaceutical Biotechnology* **9**, 2-8 (2008).
176 Klinke, D. J., Kulkarni, Y. M., Wu, Y. & Byrne-Hoffman, C. Inferring alterations in cell-to-cell communication in HER2+ breast cancer using secretome profiling of three cell models. *Biotechnology and bioengineering* **111**, 1853-1863, doi:10.1002/bit.25238 (2014).
177 Kulkarni, Y. M., Suarez, V. & Klinke, D. J. Inferring predominant pathways in cellular models of breast cancer using limited sample proteomic profiling. *BMC Cancer* **10**, 291, doi:10.1186/1471-2407-10-291 (2010).
178 J., P. A., F., S. E., G., C. D., D., S. R. & G., P. M. Quantitative proteome analysis of breast cancer cell lines using 18O-labeling and an accurate mass and time tag strategy. *PROTEOMICS* **6**, 2903-2915, doi:doi:10.1002/pmic.200500582 (2006).
179 Holliday, D. L. & Speirs, V. Choosing the right cell line for breast cancer research. *Breast Cancer Research* **13**, 215, doi:10.1186/bcr2889 (2011).
180 Lanning, N. J. *et al.* Metabolic profiling of triple-negative breast cancer cells reveals metabolic vulnerabilities. *Cancer Metab* **5**, 6, doi:10.1186/s40170-017-0168-x (2017).
181 Liu, P. C. C. *et al.* Identification of ADAM10 as a major source of HER2 ectodomain sheddase activity in HER2 overexpressing breast cancer cells. *Cancer Biology & Therapy* **5**, 657-664, doi:10.4161/cbt.5.6.2708 (2014).
182 Velasco-Velazquez, M. *et al.* CCR5 antagonist blocks metastasis of basal breast cancer cells. *Cancer Res* **72**, 3839-3850, doi:10.1158/0008-5472.CAN-11-3917 (2012).
183 Li, D. M. & Feng, Y. M. Signaling mechanism of cell adhesion molecules in breast cancer metastasis: potential therapeutic targets. *Breast Cancer Res Treat* **128**, 7-21, doi:10.1007/s10549-011-1499-x (2011).
184 Lautenschlaeger, T. *et al.* In vitro study of combined cilengitide and radiation treatment in breast cancer cell lines. *Radiation Oncology (London, England)* **8**, 246-246, doi:10.1186/1748-717X-8-246 (2013).
185 Weaver, V. M. *et al.* Reversion of the Malignant Phenotype of Human Breast Cells in Three-Dimensional Culture and In Vivo by Integrin Blocking Antibodies. *The Journal of Cell Biology* **137**, 231-245, doi:10.1083/jcb.137.1.231 (1997).
186 Lu, S., Simin, K., Khan, A. & Mercurio, A. M. Analysis of integrin beta4 expression in human breast cancer: association with basal-like tumors and prognostic

significance. *Clin Cancer Res* **14**, 1050-1058, doi:10.1158/1078-0432.CCR-07-4116 (2008).

187 Saunus, J. M. *et al.* Multidimensional phenotyping of breast cancer cell lines to guide preclinical research. *Breast Cancer Res Treat* **167**, 289-301, doi:10.1007/s10549-017-4496-x (2018).

188 Subik, K. *et al.* The Expression Patterns of ER, PR, HER2, CK5/6, EGFR, Ki-67 and AR by Immunohistochemical Analysis in Breast Cancer Cell Lines. *Breast cancer : basic and clinical research* **4**, 35-41 (2010).

189 Pla-Roca, M. *et al.* Antibody colocalization microarray: a scalable technology for multiplex protein analysis in complex samples. *Molecular & cellular proteomics : MCP* **11**, M111 011460, doi:10.1074/mcp.M111.011460 (2012).

190 Jorgensen, M. M., Baek, R. & Varming, K. Potentials and capabilities of the Extracellular Vesicle (EV) Array. *J Extracell Vesicles* **4**, 26048, doi:10.3402/jev.v4.26048 (2015).

191 Avens, H. J. & Bowman, C. N. Development of Fluorescent Polymerization-based Signal Amplification for Sensitive and Non-enzymatic Biodetection in Antibody Microarrays. *Acta biomaterialia* **6**, 83-89, doi:10.1016/j.actbio.2009.06.008 (2010).

192 Cao, X., Ye, Y. & Liu, S. Gold nanoparticle-based signal amplification for biosensing. *Analytical Biochemistry* **417**, 1-16, doi:https://doi.org/10.1016/j.ab.2011.05.027 (2011).

193 Schweitzer, B. *et al.* Multiplexed protein profiling on microarrays by rolling-circle amplification. *Nature Biotechnology* **20**, 359, doi:10.1038/nbt0402-359 https://www.nature.com/articles/nbt0402-359#supplementary-information (2002).

194 Niemeyer, C. M., Adler, M. & Wacker, R. Immuno-PCR: high sensitivity detection of proteins by nucleic acid amplification. *Trends in Biotechnology* **23**, 208-216, doi:https://doi.org/10.1016/j.tibtech.2005.02.006 (2005).

195 Dirks, R. M. & Pierce, N. A. Triggered amplification by hybridization chain reaction. *Proceedings of the National Academy of Sciences of the United States of America* **101**, 15275-15278, doi:10.1073/pnas.0407024101 (2004).

196 Muller, U. R. Protein detection using biobarcodes. *Molecular BioSystems* **2**, 470-476, doi:10.1039/B608442G (2006).

197 Li, J. *et al.* Characterization of Human Cancer Cell Lines by Reverse-Phase Protein Arrays. *Cancer cell* **31**, 225-239, doi:10.1016/j.ccell.2017.01.005 (2017).